

MASTER OF SCIENCE THESIS

Observing through the water surface with a green-wavelength terrestrial laser scanner

I.L.E. DE LANGE

NOVEMBER 2016



DELFT UNIVERSITY OF TECHNOLOGY

MASTER THESIS

Observing through the water surface with a green-wavelength terrestrial laser scanner

An engineering approach

Author:

I.L.E. de Lange
4012674

Thesis committee:

prof. dr. M. Menenti
dr. R.C. Lindenberg
drs. W.F. Gard

Delft University of Technology
Faculty of Civil Engineering and Geosciences
Department of Geoscience and Remote Sensing
Section of Optical and Laser Remote Sensing

November 24, 2016

Acknowledgements

I would like to express my gratitude to my thesis committee during the realisation of this graduation project. I would like to acknowledge my daily supervisor Roderik Lindenbergh whom I thank for his sympathy, continuous support and inexhaustible feedback, my second supervisor Wolfgang Gard whom I thank for his enthusiasm and ideas and last but not least my graduation professor Massimo Menti whom I thank for his valuable proposals and insights.

Also I would like to thank the following employees of the Water laboratory: the coordinator Sander de Vree for arranging a space in the Water laboratory on short notice and technician Jaap van Duin for practical help during the lab experiments. In addition I would like to thank my fellow Master of Science student Niels Treffers for helping me build the set up for the laboratory experiments.

Last I would like to thank all of my loved ones that stood by me during the graduation work. Outstandingly I would like to thank my life partner and best friend for his encouragement and compassion. Every cloud has its silver lining and you have truly been my silver lining throughout this phase. Additionally, thanks to you too Tony. To make a long story short, this phase has had its highs and lows and by trial and error I have discovered more than I could ever imagine.

Isabelle Laura Elisabeth de Lange

Abstract

Laser scanning technique is an upcoming technique for many engineering purposes. Terrestrial laser scanners have become widely accessible for companies, universities and research centres in the last decade. A green-wavelength terrestrial laser scanning device is available for scan projects at the Delft University of Technology. Green-wavelength terrestrial laser scanners have successfully been used in many scan projects. Specifically, because its laser light is green and able to scan through the water surface, the scanner may also be used in through water scan applications. In this graduation thesis the possibilities and limitations of a green-wavelength terrestrial laser scanner in underwater scan applications are explored. Recommendations of the laboratory experiments will lead to experimental set ups of field experiments. The latter will provide recommendations for future research goals in the field.

In this research project various targets have been scanned through the water. Basic laboratory experiments have been set up to discover the required and preferred scan settings. Various scan targets have been scanned both dry and under water to determine the scan prospects. Also a design for the field experiments was created based on the experiments that simulated outdoor environments. The underwater targets were chosen specifically for their presence in the outdoor environment. Two case studies were set up that represented real life situations. The first case study concerned the scanning of mooring poles for marine structure inspection purposes. The second case study was set up for both bathymetry and ecological studies as it consisted of mapping the bottom of a water body and the underwater vegetation.

Even though the terrestrial laser scanner in question, the Leica C10 ScanStation, is not especially designed for underwater scan applications, the scanner is able to detect underwater objects. The main limitation is induced by the laser scanning device itself. For the most part, scans of underwater targets by a terrestrial laser scanner require a downward scan angle. The field of view limitation that applies to the vertical downward scan angle of the Leica C10 makes adjustment to the experimental set up necessary.

The scan possibilities are defined by three dominating factors: the scan target, the water conditions and the power and wavelength of the light that the laser scanning device emits. Experience learns that under certain water conditions some scan targets will provide sufficient returns and others may not. As the characteristics of the laser scanning device are fixed, the combination of the reflectance spectra of the target and water depth and turbidity will determine whether the scan is successful.

Before scanning in the field the surroundings and target should be investigated thoroughly before conducting the experiment. After the environment is explored and the project goals are clear it is advised to make an informed choice for the type of laser scanning device and to draw an experimental design. One of the deliverables of this thesis is a 'how to scan with the Leica C10' manual that is attached as an appendix. With this manual a new user should be able to operate the Leica C10 in a variety of scan projects.

A mind map is created to support the conclusions of this research project. The mind map summarises all of the findings and can be used as a guideline for further research studies.

Table of Contents

Acknowledgements	i
Abstract	ii
List of Figures	vi
List of Tables	ix
List of Symbols	x
1 Introduction	1
1.1 Background	1
1.1.1 A brief history of laser scanning	1
1.1.2 Laser scanning usage nowadays	2
1.2 Objectives	3
1.2.1 Target scheme	3
1.2.2 Scope and keywords	4
1.2.3 Research questions	4
1.3 Thesis outline	5
2 Theory behind Laser Scanning	6
2.1 Physics of light	6
2.1.1 Electromagnetic spectrum	6
2.1.2 Index of refraction	7
2.1.3 Snell’s law	7
2.1.4 Reflectance spectra and reflecting surfaces	9
2.2 Conditions of the media	10
2.2.1 Atmospheric conditions	10
2.2.2 Water flow conditions	11
2.2.3 Water clarity conditions	12
2.3 Bathymetric laser mapping	14
2.3.1 Differences between airborne and terrestrial bathymetric scanning	14
2.3.2 Similarities between airborne and terrestrial bathymetric scanning	15
2.4 Principle of terrestrial laser scanning	16
2.4.1 Time of flight principle	16
2.4.2 Range formula	16
2.4.3 Features of the return signal	17
2.4.4 The edge effect	17
3 Methodology	18
3.1 Terrestrial laser scanner Leica ScanStation C10	18
3.1.1 Technical specifications of the Leica C10	19
3.1.2 Foreordained scan settings	20
3.2 Experimental design	21
3.2.1 Design of laboratory experiments	21
3.2.2 Design of field experiments	22
3.2.3 Parameters of interest	22

3.3	Modifications to the return signal	22
3.3.1	Extraction and preprocessing of the data	22
3.3.2	Coordinate system transformation	23
3.3.3	Correction for refraction	24
3.4	Assessment of the data	25
3.4.1	Basic statistical evaluation	25
3.4.2	Terminology: accuracy versus precision	26
3.4.3	Assessment of point accuracy	26
3.4.4	Assessment of point precision	27
3.4.5	Assessment of point density	27
4	Basic Laboratory Experiments	28
4.1	Experimental arrangements	28
4.1.1	Location and surroundings	28
4.1.2	Lab equipment list	29
4.1.3	Experimental set up	30
4.2	Experiments to explore the settings	31
4.2.1	Effects of the resolution setting	31
4.2.2	Repeat scan assessment per quadrant	32
4.2.3	Influence of the horizontal distance	32
4.3	Experiments with different materials, shapes and colours	34
4.3.1	Coloured glass marbles	35
4.3.2	Dimpled titanium golf balls	36
4.3.3	Green rubber tile	38
4.3.4	Coloured concrete cubes	39
4.3.5	Concrete buddha sculpture	39
4.4	Experiments simulating the outdoor environment	41
4.4.1	Wooden measuring pole with varying water level	41
4.4.2	Wooden measuring pole with varying water turbidity	43
4.4.3	Metamorphic rocks	46
4.4.4	Beach sand with varying water level	48
4.4.5	Water plants	51
4.5	Review of the return signal	53
4.5.1	Comparison of intensity outcomes	53
4.5.2	Power of the return signal	55
4.5.3	Working example: recorded versus computed signal	57
4.6	Initial conclusions and further scan recommendations	60
4.6.1	Findings from the basic experiments	60
4.6.2	Practical findings	60
5	Case Study I: Wood Samples in Lab	62
5.1	Experimental set up and description of wood samples	62
5.1.1	Features of the wood samples	63
5.1.2	Common damage to wood in a marine environment	64
5.2	Detailed scans of the individual wood samples	66
5.2.1	Wood sample A: Basralocus	66
5.2.2	Wood sample B: Azobe	66
5.2.3	Wood sample C: Spruce	67
5.2.4	Wood sample D: Eucalyptus	68
5.3	Wood experiments under water	68
5.3.1	Prospect of the underwater wood scans	69
5.3.2	Results of the underwater wood experiments	69
5.4	Scan recommendations for marine wood inspection	70

6 Case Study II: Coastal Dune Pools	72
6.1 Dune pool I	72
6.1.1 Location, surroundings and outdoor environment	72
6.1.2 Experimental field set up	73
6.1.3 Scan results of dune pool I	73
6.2 Dune pool II	75
6.2.1 Location, surroundings and outdoor environment	75
6.2.2 Experimental field set up	75
6.2.3 Scan results of dune pool II	76
6.3 Findings and recommendations	77
Conclusions and Recommendations	78
Bibliography	84
Appendices	I
Appendix A Manual 'how to scan with the Leica C10'	I
Appendix B Overview of the laboratory experiments	VIII
Appendix C Software, tools and scripts	XI

List of Figures

1.1	Sweepnik in action [19]	1
1.2	The steering mirrors of Sweepnik [19]	1
1.3	Principle of airborne bathymetric laser scanning [46]	2
1.4	Chemical site, the Netherlands [1]	2
1.5	Power line mast, Krakow, Poland [1]	2
1.6	Town hall, Klodzko, Poland [1]	3
1.7	Railway, Stomniki, Poland [1]	3
2.1	Visible light spectrum as part of the electromagnetic spectrum [32]	6
2.2	Transmission of green light propagating from air into water	8
2.3	Snell's law with $n_{air} = 1.0002782$ and $n_{water} = 1.335$ for different angles of incidence	8
2.4	Reflectance spectra for materials [34]	9
2.5	Reflectance curves for colours [48]	9
2.6	Specular reflection of light [13]	9
2.7	Diffuse reflection of light [13]	9
2.8	Ripples on a puddle of water created by wind [12]	10
2.9	Laminar and turbulent flow patterns [29]	11
2.10	Suspended sediments in Lake Superior nearby Minnesota, United States of America [20]	12
2.11	Schematic Secchi disk depth [44]	13
2.12	Secchi disk in clear/algae water [42]	13
2.13	EAARL lidar system [43]	15
2.14	Bathymetry of Florida Keys [43]	15
2.15	Time of flight pulse characteristics, modified from Vosselman and Maas [46]	16
2.16	Edge effect and resolution setting [10]	17
2.17	Result of edge effect [10]	17
3.1	Leica C10 on top of Leica tripod [22]	18
3.2	Leica C10 trunk in Mekelpark	18
3.3	Dimensions of the Leica C10 [22]	19
3.4	Field of view of the Leica C10 [22]	19
3.5	Dimensions of the Intex pool	21
3.6	Geometry scheme of laboratory experimental set up	21
3.7	Polar coordinate system [40]	23
3.8	Cilindrical coordinate system [40]	23
3.9	Geometry of the correction for refraction [37]	24
3.10	Portrayal of accuracy, precision and combinations of both	26
4.1	Faculty sign	28
4.2	First floor entrance to the Water Laboratory	28
4.3	Experimental lab set up - eye level	30
4.4	Experimental lab set up - top view	30
4.5	Hach 2100N Turbidimeter	30
4.6	Point clouds of the four quadrants	31
4.7	Bar plot of densities for low/high resolution	31
4.8	Bar plot of the number of points per cell versus the horizontal distance	33
4.9	Point cloud views of duct tape	33

4.10	Plot of point density versus horizontal distance	33
4.11	Plot of the point density versus the horizontal distance for various cell sizes	34
4.12	The coloured glass marbles during scanning	35
4.13	Two points clouds of the marbles; top dry scan, bottom wet	35
4.14	Bar plot of intensity values marbles	36
4.15	Bar plot of point densities marbles	36
4.16	Photo of the golf balls	36
4.17	Point cloud of the golf balls	36
4.18	Box plot of intensity values golf balls	37
4.19	Plot of range vs intensity golf balls	37
4.20	Photo of tile	38
4.21	Tile in screen Leica	38
4.22	Point cloud of tile	38
4.23	Box plot of intensity values tile	38
4.24	Photo of the seven coloured concrete cubes	39
4.25	Photo of buddha	39
4.26	Point cloud buddha	39
4.27	Point cloud buddha, side	39
4.28	Bar plot of intensity values buddha	40
4.29	Box plot of point densities buddha	40
4.30	Point cloud of the dry buddha	40
4.31	Point cloud of the wet buddha	40
4.32	Pole before/after correction	41
4.33	Bar plot of point densities wooden pole	41
4.34	Bar plot of intensity values - dry pole	42
4.35	Bar plot of intensity values - wet pole	42
4.36	Returns of the wet part of the pole for different water depths	42
4.37	Bar plot of the intensity values of the wooden pole for different turbidity values	43
4.38	Scatter plot of the intensity values versus the height and point cloud of the wooden pole	44
4.39	Scatter plot of the intensity values versus the range through the water	45
4.40	Scatter plot of the intensity values versus the range through the water - binned	46
4.41	Photo of the metamorphic rocks	46
4.42	Point cloud of metamorphic rocks	46
4.43	Point cloud of the rocks under water	47
4.44	Point cloud of the dry rocks	47
4.45	Surface roughness rocks $k = 0.01$	47
4.46	Surface roughness rocks $k = 0.1$	47
4.47	Photo of beach sand, depth 5 <i>cm</i>	48
4.48	Point cloud of beach sand, depth 10 <i>cm</i>	48
4.49	Scatter plot beach sand, depth 40 <i>cm</i>	48
4.50	Scatter plot beach sand, depth 20 <i>cm</i>	48
4.51	Scatter plot beach sand, depth 10 <i>cm</i>	49
4.52	Scatter plot beach sand, depth 5 <i>cm</i>	49
4.53	Scatter plot beach sand, Δh_{d20-d5}	49
4.54	Scatter plot beach sand, Δh_{d10-d5}	49
4.55	Mesh plot of beach sand including water surface, depth 5 <i>cm</i>	50
4.56	Scatter plot of the intensity values versus the range through water for different depths	50
4.57	The two water plants	51
4.58	Leaves of Anubias	51
4.59	Leaves of Echinodorus	51
4.60	Most common leaf shapes [47]	51
4.61	Point clouds of the two waterplants	52
4.62	Bar plot of intensity values water plants	52
4.63	Bar plot of the intensity values for all of the experiments with tap water	53
4.64	Bar plot of the intensity values for all of the experiments with mixture water	54
4.65	Scatter plot of beach sand return intensity versus computed return signal power	57
4.66	Bar plot of residuals return signal of beach sand	58

4.67	Scatter plot of buddha return intensity versus computed return signal power	58
4.68	Scatter plot of pole return intensity versus computed return signal power	58
4.69	Scatter plot of water plants return intensity versus computed return signal power	59
5.1	Placement of the wood samples in the quadrants	62
5.2	Experimental set up wood - dry	63
5.3	Experimental set up wood - wet	63
5.4	Origins of the four kinds of wood	64
5.5	Damage profile of wood in marine environment, modified from Lopez-Anido et al [24]	64
5.6	Shipworm manifestation in wood [31]	65
5.7	Wood sample A	65
5.8	Point cloud of intensity values wood sample A: Basralocus	66
5.9	Wood sample B: Azobe	67
5.10	Point cloud of relief on wood sample B	67
5.11	Wood sample C: Spruce	67
5.12	Point cloud of wood sample C	67
5.13	Wood sample D: Eucalyptus	68
5.14	Point cloud of wood sample D	68
5.15	Point cloud of intensity values wood sample A: Basralocus - underwater result	70
5.16	Schematic view of Leica C10 on harbour site	71
6.1	Aerial photographs of dune pool I	73
6.2	Picture of dune pool I	73
6.3	Scan set up of dune pool I	73
6.4	Point cloud intensity values of dune pool I	74
6.5	Aerial photographs of dune pool II	75
6.6	Picture of dune pool II	76
6.7	Scan set up of dune pool II	76
6.8	Intensity point cloud of dune pool II	76
6.9	RRB image of dune pool II	76

List of Tables

2.1	Indices of refraction of air [6] and fresh water [9] at $\lambda = 532nm$	7
2.2	Properties of airborne lidar EAARL [25] and terrestrial laser scanner Leica C10 [22] . .	14
3.1	Specifications of the Leica C10 [22]	19
3.2	Foremost examples of experimental set ups from literature [15] [26] [27] [37] [38] [41] . .	20
3.3	Basic statistical measures and their Matlab operator	25
3.4	Different measures of point density	27
4.1	Turbidity (NTU) measures of water samples	30
4.2	Point densities of point clouds with low respectively high resolution	31
4.3	Repeat scan error values (RSEV) per quadrant for all high resolution point clouds . . .	32
4.4	Scan characteristics of the segmented duct tape point clouds	32
4.5	Overview of the targets with different materials, shapes and colours	34
4.6	Point densities of the golf balls	37
4.7	Point densities of the rubber tile	38
4.8	Overview of the targets from the outdoor environment	41
4.9	Characteristics of the two water plants	51
4.10	Decrease intensity values - wet to dry	54
5.1	Characteristics of the four wood samples	63
5.2	Relative point densities of underwater scans wood samples	69

List of Symbols

α	$^{\circ}$	angle of incidence
β	$^{\circ}$	angle of refraction
θ	$^{\circ}$	angular coordinate cylindrical coordinate system
λ	m	wavelength
μ	$kg/(m \cdot s)$	dynamic viscosity
μ	–	arithmetic mean
μ	m^{-1}	attenuation coefficient
ν	m^2/s	kinematic viscosity
ρ	kg/m^3	density
ρ	–	radial coordinate cylindrical coordinate system
σ	–	standard deviation
τ	s	time of flight
A	m	amplitude
A	$^{\circ}$	solar altitude
A_R	m	amplitude of transmitted signal
A_{SD}	m	apparent Secchi disk depth
A_T	m	amplitude of return signal
c	m/s	speed of light in vacuum ($2.99792458 \cdot 10^8$ m/s)
C	m	circumference
d	m	water depth
D	m	diameter
\hat{e}	–	residuals between two datasets
E	J	energy
f	Hz	frequency
GA	m^2	ground area
h	m	height
i	$^{\circ}$	angle of incidence
i	–	intensity
k	–	factor
L	m	path length
LA	m^2	leaf area
LAI	–	leaf area index
m	–	median
n	–	index of refraction
n_{air}	–	refractive index of air
n_{water}	–	refractive index of water
N	–	number of measurements
O	–	origin
p	Pa	pressure
P	–	point in coordinate system
P	–	power return signal

r	—	radius
r	°	angle of refraction
r	—	radial coordinate cylindrical coordinate system
R	m	range
R_{air}	m	range in air
R_{water}	m	range in water
Re	—	Reynolds number
S	PSU	salinity
t	s	time
t_p	s	pulse width
t_r	s	pulse rise time
t_{rep}	s	pulse repetition time
T	°C	temperature
T	—	transmittance
v	m/s	speed of light in medium
v	m/s	flow velocity
w	m/s	surface wind speed
x	—	coordinate Cartesian coordinate system
x_{off}	m	horizontal offset
y	—	coordinate Cartesian coordinate system
z	—	coordinate Cartesian/cylindrical coordinate system
z_{off}	m	vertical offset
z_{SD}	m	Secchi disk depth

Chapter 1

Introduction

To measure is to know. This often quoted saying plays an important role in the world, especially in the world of technology. Observing the environment remotely has become one of the key elements in this world. Remote sensing can be done by various techniques, depending on the demands and the application in question. Laser scanning is one remote sensing technique. Laser scanning technique has rapidly evolved in the last century and it is nowadays used for a lot of different applications. Laser scanning through the water surface is one of these applications and the objective of this Master thesis.

1.1 Background

In this graduation project a terrestrial laser scanner is used to observe the underwater topography, also known as bathymetry, as well as objects that lie partly or fully under water. In this section the laser scanning technique and its origin are described shortly.

1.1.1 A brief history of laser scanning

It was Albert Einstein who set the theoretical principles of laser in 1917. It was not until the 1950s that the acronym LASER (Light Amplification by Stimulated Emission of Radiation) was introduced by Gordon Gould. Who officially invented the laser is still unresolved.

In 1969 physicist Otto Robert Frisch together with academics John Rushbrooke and Graham Street founded the first laser scanner in the Cavendish Laboratories, which was part of the Physics department of the University of Cambridge in the United Kingdom. In this laboratory a prototype of a machine was built that was able to follow lines on photographs automatically using a laser beam steered by two mirrors; the upper mirror controlled the horizontal position of the beam while the lower mirror controlled the vertical position of the beam. The name of the machine was Sweepnik [19]. Figure 1.1 shows the machine during scanning and figure 1.2 displays the principle of the two mirrors.



Figure 1.1: Sweepnik in action [19]

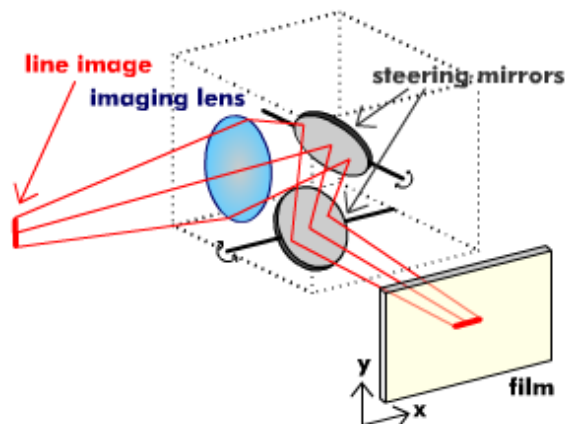


Figure 1.2: The steering mirrors of Sweepnik [19]

In the 1970s the National Aeronautics and Space Administration (NASA) developed laser technology prototypes for airborne and spaceborne applications. The developed system was able to obtain the range to a target by illuminating the target with a laser signal and analysing the reflected light. Beside the range, the system could measure the chemical properties of the air based on differential absorption technique, and the velocity of the target using Doppler shift. In the 1980s the first laser altimetry systems were deployed for the study areas of atmosphere, oceanography and topography. NASA called the system Light Detection And Ranging or Laser Imaging Detection and Ranging (LIDAR) yet in the military the system is commonly referred to as Laser Illuminated Detection And Ranging.

1.1.2 Laser scanning usage nowadays

The first laser scanning systems have been the basis for the laser scanning techniques that exist nowadays. As laser scanning is a wide term, it is usually specified by the platform type of the scan. In general the division is made between airborne and terrestrial laser scanning.

Airborne laser scanning is presently a widely used technique for acquiring digital elevation models of the topography of the landscape [46]. The height models are created by scanning from an airplane or helicopter with an onboard GNSS (Global Navigation Satellite System), for example GPS, and Inertial Measurement Unit so its position and movement is known. Airborne laser scanning can also be applied to scan the underwater topography, also known as bathymetry. For this, two lasers are typically operated simultaneously: one laser with red light and the other with green or blue light. The red light will be reflected from the water surface. The green or blue laser light however can break through the water surface. The ray of blue or green light will be reflected at the bottom of a waterbody if the signal is not completely absorbed and scattered within the water. By combining the data from both laser scanners, the distances between laser device, water surface and bottom can be determined.

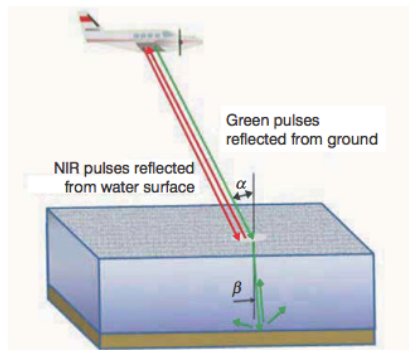


Figure 1.3: Principle of airborne bathymetric laser scanning [46]

Terrestrial laser scanners can be used for many applications. For example in civil engineering projects laser scanners are used to generate a 3-dimensional, in short 3D, picture of complex structures like industrial installations and archeological sites. Terrestrial laser scanners are also used to determine whether a building or other structure has moved over a period of time by comparing two 3D scans. Figures 1.6, 1.7, 1.4 and 1.5 display some resulting scans of terrestrial laser scanning applications.

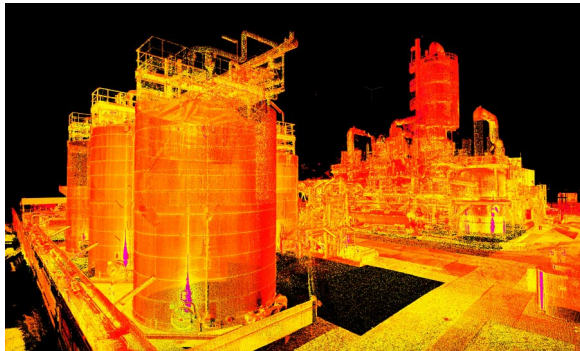


Figure 1.4: Chemical site, the Netherlands [1]

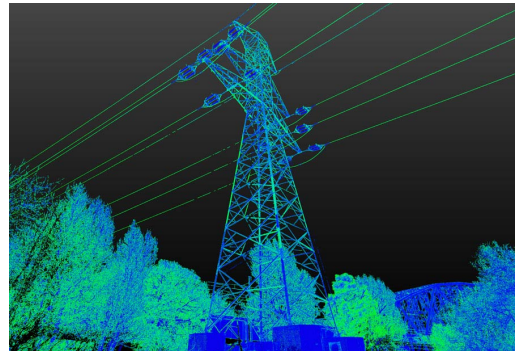


Figure 1.5: Power line mast, Krakow, Poland [1]

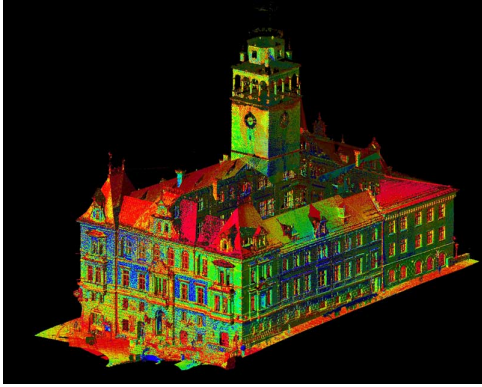


Figure 1.6: Town hall, Klodzko, Poland [1]

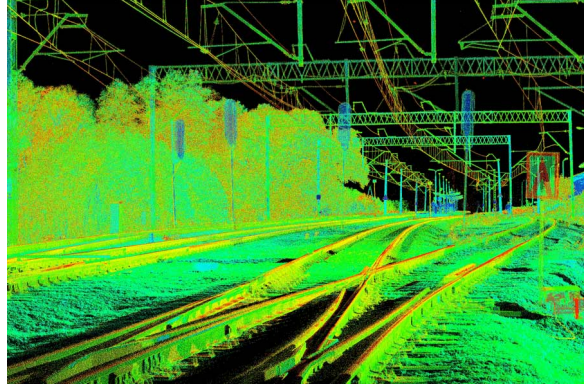


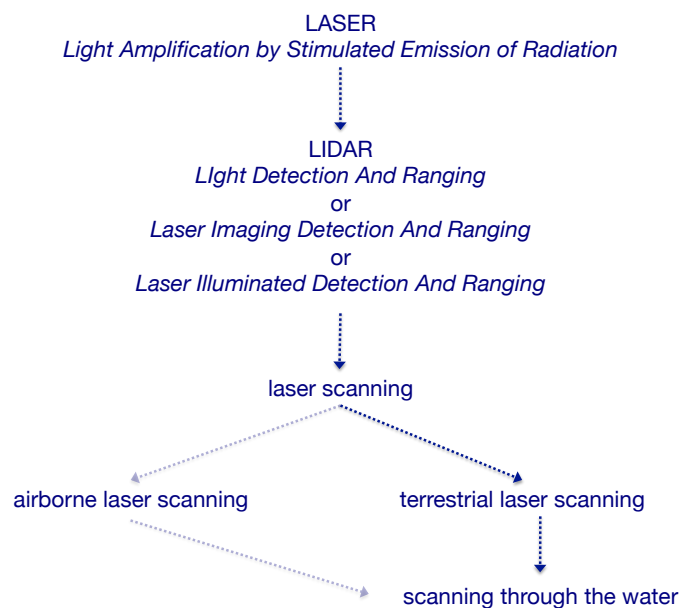
Figure 1.7: Railway, Stomniki, Poland [1]

In this research a terrestrial laser scanner is used for through water scans of underwater targets. The choice of the wavelength of the light depends on the absorption and reflection of the wavelength in water. In other words, the scanner needs to be able to penetrate the water surface and for this a green-wavelength laser scanner is chosen. The beam of the laser scanner will be refracted at the air-water boundary leading to a deformed image. Therefore a correction for refraction needs to be applied. How far, or deep, the laser scanner can see through the water and what the conditions of both scanner settings, medium and target are, need to be explored. The first already known rule of thumb is that green laser light is able to penetrate the water surface three times as far as one can see - in case the bottom of the water body can not be seen with bare eyes.

1.2 Objectives

1.2.1 Target scheme

The objective of the research is first represented as a schematic representation known as a target scheme. It contains all the techniques as described in the previous section. A lot of research concerning bathymetric scanning through the water surface has been done in the field of airborne laser scanning. Scanning through the water surface with a terrestrial laser scanner however is an upcoming technique. The field of airborne bathymetric laser scanning can provide insights that can be used for through water scan experiments with a terrestrial laser scanner.



1.2.2 Scope and keywords

The scope of this graduation project is to explore the possibilities and limitations of scanning through the water surface with a terrestrial green-wavelength laser scanner. The terrestrial laser scanner used in this research is the Leica C10 ScanStation. The project aims to explore the settings needed when scanning with the Leica C10 laser scanner through the water surface. After these basic experiments, the laser will be used in two case studies where the obtained findings from the laboratory experiments will be applied to the field experiments.

The topic as well as the research question consists of several technical keywords. The keywords that shape this graduation work are:

- terrestrial laser scanning
- green-wavelength
- scanning objects through water

1.2.3 Research questions

The purpose of this graduation research project is to explore the possibilities and limitations of the Leica C10 terrestrial laser scanner when observing through the water surface.

The subquestions form the specification of the main research question. The subquestions concerning the basic experiments are related to the scanning conditions. There are three different angles concerning the scanning conditions that will be considered in the subquestions concerning the basic experiments. These three are:

- the terrestrial laser scanner, which is the Leica C10 ScanStation
- the media: air and water
- the scan target

The subquestions for the basis experiments are all related to at least one of these three angles. The subquestions are:

- Regarding the measurement geometry and including the travel distance of the laser light from origin to target, what height and scan angle of the Leica C10 laser scanner device are required?*
- What resolution scan settings, leading to a certain point density, of the Leica C10 laser scanner, are preferred?*
- What is the influence of the travel distance, both through air and water, on the return signal?*
- How does the return signal change in relation to an increase in water depth?*
- What influence have the characteristics of the medium water, like salt content, turbidity, contamination, on the scan results?*
- What influence have the characteristics of the object, like material, shape, colour, smoothness, on the results?*
- How does the raw data need to be processed and corrected for refraction?*

After the basic experiments, two case studies will be undertaken, the first in laboratory settings simulating outdoors environment and the second case study will be in the field. The subquestions for the first case study, wood samples in laboratory setting, are:

- What resolution is needed to detect the damages present on the wood samples?*
- Is there a difference between the wood samples in the through water scan results?*
- What influence has the turbidity of the water on the resulting wood scans?*

- xi. *Simulating the water of a harbour, is the laser scanner able to see whether the mooring pole is damaged?*

The following subquestions have been formulated for the second case study, the coastal dune pools:

- xii. *Which environmental conditions should be taken into account beforehand?*
- xiii. *Can the laser scanner detect the bathymetry of a pool?*
- xiv. *Can the laser scanner distinguish the various types of vegetation present in the dune pools?*

1.3 Thesis outline

In this graduation research project several underwater targets will be scanned with a green-wavelength terrestrial laser scanner. In this first chapter some background of the laser scanning technique and the research questions are provided. Chapter two will continue with the theory behind laser scanning technique including the physics of light, and describe the atmospheric and water conditions as well as the principle of terrestrial laser scanning. In chapter three the methods including foreordained scan settings, the experimental design, modifications to the return signal and assessment criteria are outlined. The laser scans have been performed guided by this methodological chapter and the results are reported in chapters four up to and including six. Chapter four comprises the basic experiments in laboratory settings while chapter five gives the first case study concerning wood samples that have been examined in the same laboratory setting. In chapter six the field experiment, which is the second case study, is covered. The field experiment of this graduation project consists of the scanning of two coastal beach pools that are both located in the dunes of the Netherlands. The findings and answers to all of the research questions are gathered in the Conclusions and Recommendations chapter. Furthermore the literature that has been referred to throughout this thesis is listed in the Bibliography. Last three appendices are formed which include the deliverable 'how to scan with the Leica C10' manual, an overview of the laboratory experiments and the software used in this project.

Chapter 2

Theory behind Laser Scanning

2.1 Physics of light

Some basic theory concerning light be clarified in this section. Albert Einstein set the first principles that lead to the discovery of the LASER (Light Amplification by Stimulated Emission of Radiation) technique, as also described in paragraph 1.1.1. Einstein did so by proposing a new theory of light: he tested the quantum theory of light and found out that light is transmitted as tiny particles via waves [13]. This discovery showed that light can be considered as a part of electromagnetic radiation.

2.1.1 Electromagnetic spectrum

A fundamental force of nature is the electromagnetic field. As the name suggests, the electromagnetic field is the combination of an electric and magnetic field, where the first is static and the latter dynamic. The electromagnetic field is a physical field through space in which objects interact. The interactions of the static electric charges and the dynamic magnetic currents are described by Maxwell's equations [13].

The electromagnetic spectrum consists of all known frequencies of electromagnetic radiation in an electromagnetic field. Laser light is part of the visible light range of this spectrum, so a laser operates in the visible light spectrum of the electromagnetic spectrum. It has been stated before that light is a wave phenomenon, so it behaves like a wave. The colour of visible light is defined by its wavelength. The wavelength is the distance over which the wave repeats, for example the distance between two tops of the wave. Visible light has wavelengths in the range of 400 to 700 nanometre [13]. Figure 2.1 displays the visible light range within the electromagnetic spectrum including the corresponding wavelengths.

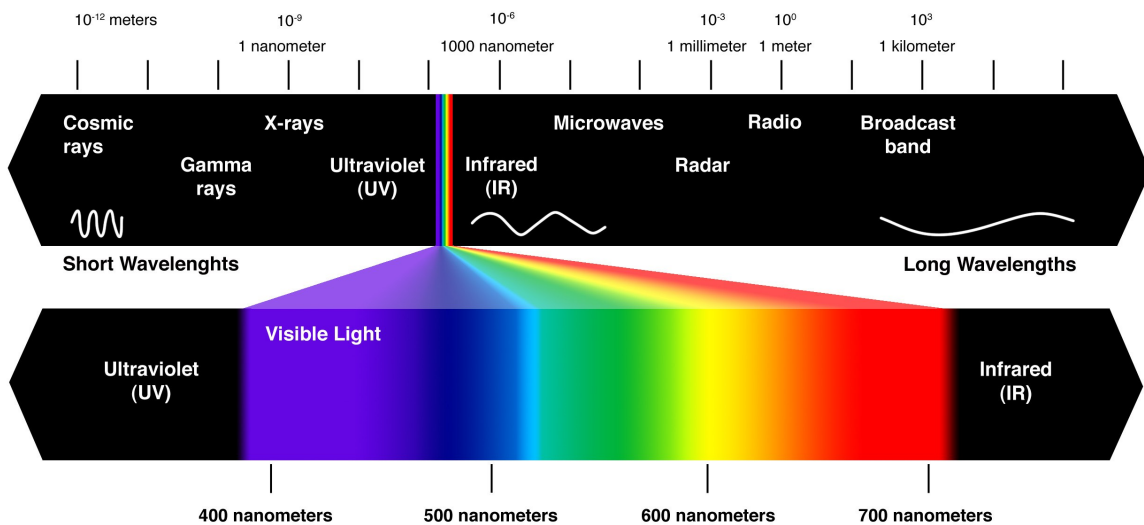


Figure 2.1: Visible light spectrum as part of the electromagnetic spectrum [32]

2.1.2 Index of refraction

Light waves travel at a speed of $2.99792458 \cdot 10^8$ metre/second, usually rounded off to $3.00 \cdot 10^8$ m/s , in vacuum. This speed of light, c , is used to determine the index of refraction. The index of refraction is the ratio of the speed of light in vacuum to the speed of light in a medium or substance:

$$n = \frac{c}{v} \quad (2.1)$$

where n is the dimensionless index of refraction of the medium, c is the speed of light in vacuum and v is the speed of light in the medium, the latter two quantities both in unit $[m/s]$. The index of refraction of the medium vacuum is thus 1. Because light travels slower in any other media than vacuum, the index of refraction is always larger than 1 [13].

The index of refraction depends on several parameters. The most prominent parameter is the wavelength of the light. As a green-wavelength terrestrial laser scanner with a wavelength of 532 nanometre will be used, only refractive indices consistent with light that has a wavelength λ of 532 nm will be considered. For the medium air the temperature, pressure, humidity and gas contents should be taken into account. Beside the wavelength, the temperature and salinity are the most influential parameters for the refractive index of the medium water. Table 2.1 provides the refractive indices of both air and fresh water for different temperatures according to literature. What should be noted is that the refractive index of air is for so-called standard air, which is dry air at 15 °C, with a pressure p of 101.325 kPa and with 450 ppm of CO_2 content [6]. Because the refractive indices of dry air only vary with wavelength while the temperature influence on the refractive index is negligible, only the refractive index of standard air is given in table 2.1.

substance	temperature T [°C]	index of refraction n [-]
air	15	1.0002782
water	19	1.3355
	20	1.3354
	21.5	1.3352
	24	1.3350

Table 2.1: Indices of refraction of air [6] and fresh water [9] at $\lambda = 532nm$

The refractive index of air, $n_{air} = 1.0002782$, from table 2.1 will be used in the correction for refraction that needs to be applied to the returned scan data. Table 2.1 shows that the indices of refraction for rather clear, fresh water vary in the order of 10^{-4} . Moreover it has been proven in 1976 that the refractive index of water varies by ± 0.007 , which is less than 1%, for a wide range of temperatures and salinity [16]. Therefore the index of refraction for water that will be used is: $n_{water} = 1.335$. The index of refraction of water will be used for the correction for refraction throughout this research project for all waterbodies, both in the laboratory and in the field.

2.1.3 Snell's law

If light travels from one transparent medium into another transparent medium that has a different index of refraction, the ray of light will change. A part of the ray of light will be reflected at the boundary. The remaining part of the ray of light will continue but refracted, in other words changed in direction as it passes the boundary between the two media. For liquid media such as water, a part of the ray of light will also be absorbed by the water and a part of the light will be scattered within the water. The larger the path travelled, the more light is absorbed. The extent of absorption depends, apart from the path length through the media and the strength of the laser signal, on the wavelength of the laser light. Red light will be completely absorbed within a metre of clear water, while green light can penetrate through a depth of up to 100 metre of clear water before it is completely absorbed. Blue light is also able to penetrate the water surface. In airborne bathymetric laser scanning practice, depths of a maximum of 50 metre for a green-wavelength laser are the norm under favourable conditions [46]. Figure 2.2 displays the transmission of a ray of light propagating from air into water with a water depth d . The transmission of light thus comprises reflection, refraction, absorption and scattering [13].

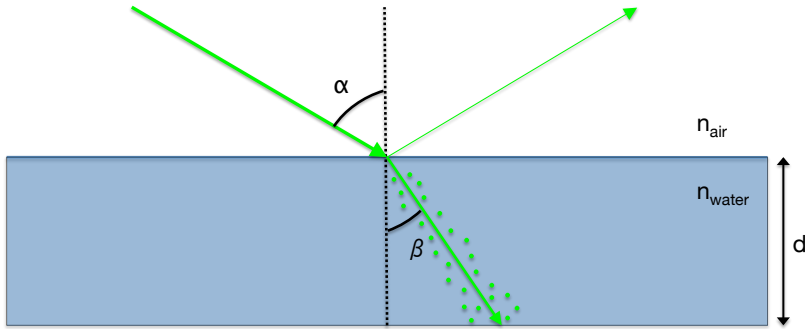


Figure 2.2: Transmission of green light propagating from air into water

The refraction of the ray of light at the boundary of two different media is described by the law of refraction, which is known as Snell's law. Willebrord Snell found the relation between the angles of incidence and refraction and the speed of light in the two media. The speed of light in two media can be rewritten into the refractive indices of two different media with the formula given in equation 2.1. Snell's law is written as:

$$n_1 \sin(\alpha) = n_2 \sin(\beta) \quad (2.2)$$

with n_1 and n_2 respectively the refractive indices of the two different media, α the angle of incidence and β the angle of refraction. Snell's law can be specified for the case a ray of light passes from air into water and is refracted at the boundary:

$$\frac{\sin(\alpha)}{\sin(\beta)} = \frac{n_{water}}{n_{air}} \quad (2.3)$$

with α and β the angle of incidence respectively refraction and n_{air} , n_{water} the refractive index of air respectively water.

The refractive indices for air and water are set to 1.0002782 [6], respectively 1.335 [9]. With these refractive indices and a known angle of incidence, the angle of refraction can be computed with some basic trigonometrics. Figure 2.3 displays the light rays from a light source, in this case the laser scanner, propagating from air into water for different angles of incidence.

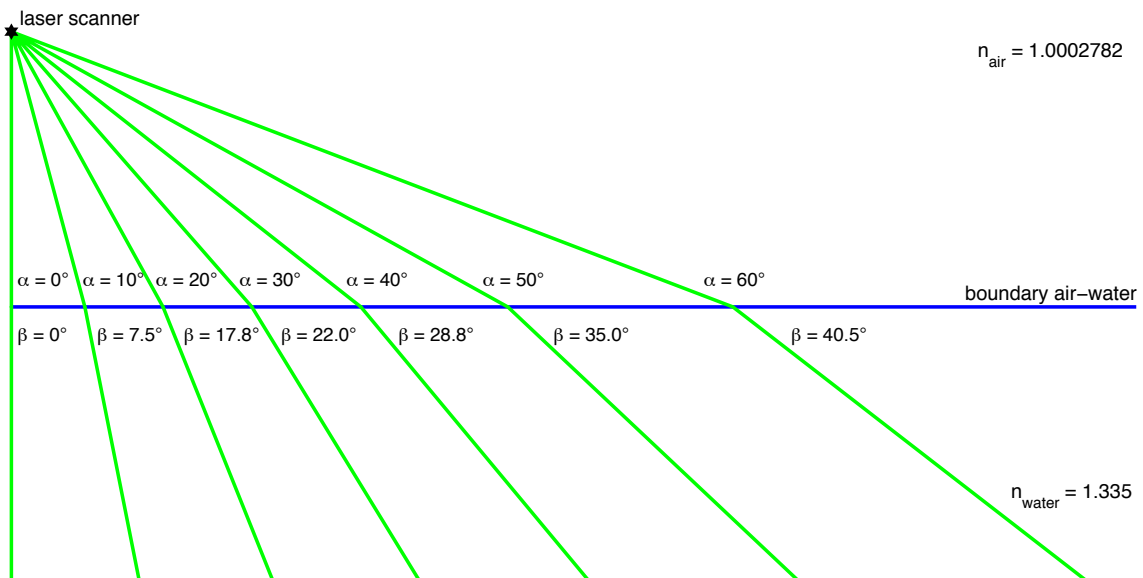


Figure 2.3: Snell's law with $n_{air} = 1.0002782$ and $n_{water} = 1.335$ for different angles of incidence

2.1.4 Reflectance spectra and reflecting surfaces

Aforesaid, the transmission of light comprises reflection, refraction or scattering, and absorption [13]. The light of the laser will partly reflect at the air water boundary as is presented in figure 2.2. The light is also reflected at the target. In figure 2.2 this is the bottom of the water body. The reflectance spectrum of the object gives the reflectance for different wavelengths, expressing the percentage of the light that is reflected. Green light with a wavelength of 532 nanometre will be used. The reflectance of various targets can be inquired for this particular wavelength.

Examples of reflectance spectra of natural materials like bark, foliage, sand, dry ground, concrete and the sea over wavelengths in the visible light range are displayed in figure 2.4. Note that there is always some natural variability. Other samples of these materials may give somewhat different spectra. The reflectance of these natural materials specific for light with a wavelength of 532 nm might be estimated from this graph.

Figure 2.5 gives examples of reflectance curves at visible wavelengths for objects ascribed by human observation with certain standard colours. Again these are examples and observations by the human eye are always subjective. The human eye is not an accurate spectrophotometer.

The bar on top of figure 2.5 represents the colour corresponding to the wavelength of light on the x-axis. The reflectance is relatively high at wavelengths of light corresponding to the standard ascribed colour. For example, an object with a standard green colour has relatively high reflectances at green wavelengths of light. The exceptions are black and white. The sum of all colours of light add up to white, so white reflects all colours equally. Black can be seen as the absence of reflectivity. An absolute black body absorbs all light.

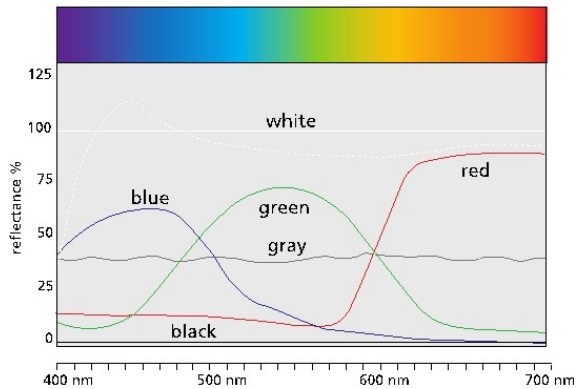
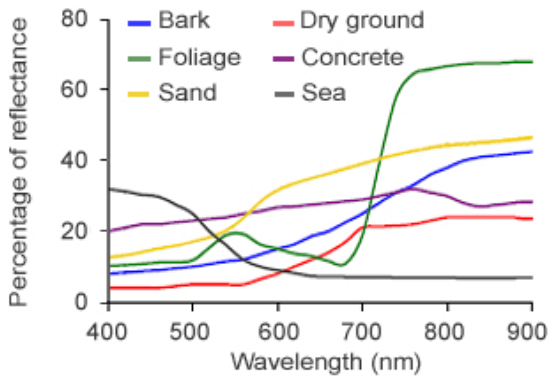


Figure 2.4: Reflectance spectra for materials [34] Figure 2.5: Reflectance curves for colours [48]

When light falls on a surface it is, to a certain extent, reflected as set by the ancient Greek law of reflection [13]. Light that falls on a smooth surface is reflected back with an angle of reflection as depicted in figure 2.6. This is called specular reflection. However, if the surface is not smooth but rough, even if it is at the microscopic level, the light is reflected back diffusely as depicted in figure 2.7. Only perfectly smooth objects like mirrors and glass reflect solely specular. There are a lot of almost smooth surfaces that have both forms of reflection. Nevertheless it can be stated that most of the surfaces are diffusely reflecting surfaces.

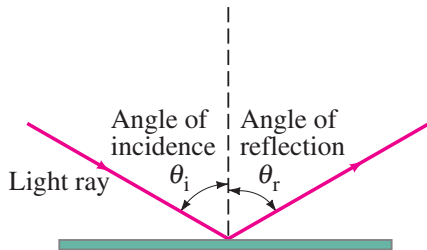


Figure 2.6: Specular reflection of light [13]

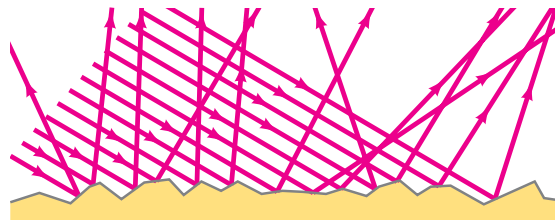


Figure 2.7: Diffuse reflection of light [13]

2.2 Conditions of the media

There are two media through which the laser light travels before it reaches the object: air and water. The conditions of these two media are important as they may influence the light emitted by the laser, leading to a change in the return signal.

2.2.1 Atmospheric conditions

The directly measurable parameters of the atmosphere, which is the medium air, that are of importance are the temperature, the pressure and the humidity. The latter parameter, humidity, influences the light through the air when the humidity is very high. In a tropical climate the humidity may influence the signal. In practice, the humidity only has an effect in case of extreme steam [35], when the air is very humid and hot. As the research location is not in the tropics but in the Netherlands and the weather will be checked beforehand, the humidity is ruled out as an influential parameter.

The temperature and pressure of air are of great importance for airborne laser scanning as there is a rather large temperature respectively pressure gradient in the vertical column [46]. In the case of terrestrial laser scanning, the distance between the scanner and the object will be in the order of metres. Therefore, the temperature respectively pressure gradient will be negligible and does not influence the laser light.

Nevertheless, the three parameters described above, the temperature, pressure and humidity, do influence the indices of refraction of air, and water as described in paragraph 2.1.2.

Another condition of the atmosphere concerns the presence of ambient light, in other words the presence or availability of light in the scan experiment environment [39]. The ambient light does have an influence on the scan results when the ambient light is not the same in one experiment comprising of different scans. When the ambient light is the same for each experiment, this factor can be scored out. Hence the experiments need to be controlled. In this research, the laboratory experiments will be in the same environment with artificial light. The field experiments will take place in a short period of time in order to have the same weather conditions, including the ambient light.

As said before, the field experiments are influenced by the weather conditions. Besides the temperature and the ambient light, the wind speed is of important. If the laser scanner is properly assembled and thus stable, the wind speed will not influence the scanning process itself. The terrestrial laser scanner used, the Leica C10, has proven to sustain rough weather conditions. What could cause problems is the wind on the water surface. The surface wind can be detected by the ripples that arise on the water surface. An example of this phenomenon is displayed in figure 2.8.



Figure 2.8: Ripples on a puddle of water created by wind [12]

The surface wind speed may create surface instability of the water surface when the wind speed becomes greater than a certain threshold. This water surface instability will cause the return signal to be distorted at the boundary between air and water. According to Smith et al, the threshold for surface wind speed is 6.0 m/s . Surface wind speeds smaller than $w = 6.0 \text{ m/s}$ have a minor effect on the surface instability and are thus acceptable [38]. Precipitation can also cause undesirable water surface instability. So for the field experiments the weather conditions should be taken into account.

2.2.2 Water flow conditions

The second medium the laser light will travel through is water. The temperature and salinity of water mainly determine the index of refraction as described in paragraph 2.1.2. Even though these two parameters influence the refraction, they have no influence on the possible distortion. The condition of the water that defines whether the return signal will be distorted or not is the flow condition. The basic experiments are set up in the lab with a still body of water. In the field experiments on the other hand, flow conditions do play a role. In order to determine whether the flow influences the outcomes, the flow needs to be classified. The classification can be made using the Reynolds number. The Reynolds number measures the degree of turbulence, or random changes in flow direction. For water bodies with a free surface and width that is much larger than the depth, the Reynolds number can be written as:

$$Re = \frac{\rho v d}{\mu} = \frac{v d}{\nu} \quad (2.4)$$

with Re the dimensionless Reynolds number, ρ the density of the fluid [kg/m^3], v the flow velocity [m/s], d the water depth [m], μ the dynamic viscosity [$kg/(m \cdot s)$] and ν the kinematic viscosity [m^2/s]. The kinematic viscosity ν is the ratio between the dynamic viscosity and the density, so $\nu = \frac{\mu}{\rho}$ [13] [29]. Laminar flow occurs at low Reynolds numbers caused by a low flow velocity, while turbulence occurs at high Reynolds numbers. The values of the Reynolds number that determine laminar or turbulence flow depend on the situation. For open water bodies, laminar flow is characterised by a Reynolds number that is much smaller than 1, while for flow through a pipe, the flow is laminar when smaller than 2300.

Laminar flow is characterised by smooth constant flow, while turbulent flow can be identified as chaotic and unpredictable with eddies, vortices and other instabilities. Between laminar and turbulent flow, there is transitional flow, which is a combination of both flow regimes. Figure 2.9 displays the two flow regimes including the transient flow between both regimes.

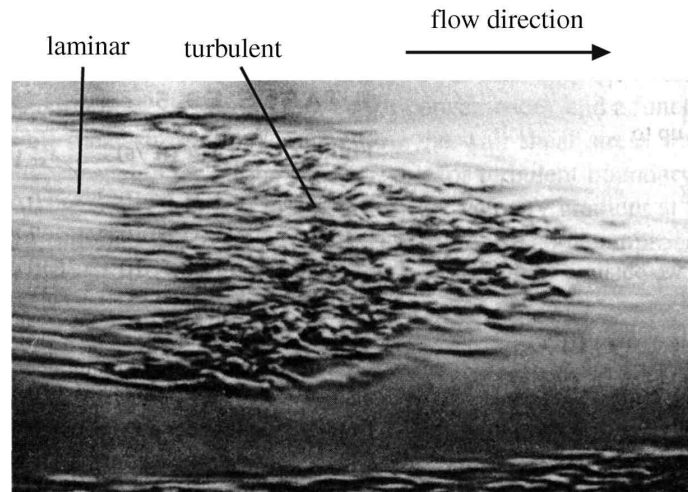


Figure 2.9: Laminar and turbulent flow patterns [29]

Turbulent flow will result in distortion of the return signal. The source of the distortion can be understood by considering the incidence angle of the laser beam. Because of the turbulence, there is not one angle of incidence at a specific location at the boundary between water and air, but many. Moreover the ray of light is scattered diffusely within the turbulent upper layer of the water. In the resulting scan point cloud the distortion can be seen as a blur at the air-water boundary and upper water layer. Also the results of the underwater targets are affected by the distortion as the signal is scattered due to turbulence water conditions and may not reach the target at all. Hence a laminar flow is desired during the field experiments. As the exact value of the Reynolds number is not of significance for this research, it suffices to determine whether the water flow is laminar or turbulent by just looking at the water body. This visual estimation will be sufficient as it can easily be checked after scanning. Additionally, the water bodies that will be scanned in this research project are almost still up to completely still water bodies so in case of water flow, it is expected to be laminar flow.

2.2.3 Water clarity conditions

Like the water flow conditions, the water clarity conditions play an important role when scanning through the water. The clarity of the water can be defined by the water quality parameter turbidity. The parameter turbidity expresses whether a water body is clear thus has a low turbidity or whether a water body has a high turbidity. A water body with a high turbidity is for example a river that has been filled with mud after a landslide, or a pond with excessive algae growth.

The turbidity is determined by the amount of Total Suspended Solids (TSS) in the water. The greater the amount of TSS, the higher the turbidity is. There are several sources of suspended solids. The most common suspended solids are from soils that are eroded or soils in sediment fluxes, like sand, clay and silt. Other sources of suspended solids are suspended algae like phytoplankton, fine organic materials, which are bits of decaying vegetation, acids, dyes and chemical precipitates, like nutrients, from industrial wastes and sewage [28] [36]. Figure 2.10 shows an example of suspended solids, in this case mostly sand, in Lake Superior, on the border of the United States of America and Canada.



Figure 2.10: Suspended sediments in Lake Superior nearby Minnesota, United States of America [20]

Measuring the turbidity in rivers and streams is important for several reasons. As the turbidity indicates the amount of TSS, the parameter is of importance for sediment load and transport studies. The turbidity is also an important parameter in diverse water quality studies. The quality of water bodies like lakes and ponds are regularly monitored. A high amount of TSS is often undesired. Especially a TSS caused by a high concentration of nutrients is a problem as over enrichment of nutrients cause deterioration of water bodies and their ecological system. Turbidity has been the key indicator for the water quality of environmental water sources. The higher the turbidity of the water body, the poorer the water quality is [36]. Another example where the turbidity is of importance concerning water quality is drinking water. Drinking water needs to be of high quality for health reasons. Additionally the drinking water needs to look appealing; drinking water of high quality that looks muddy is not desired. The turbidity of drinking water is thus frequently measured [28].

There are generally two methods of measuring the turbidity of a water body. The first one is exact while the second is approximate. The turbidity can be determined exact with a turbidimeter or spectrophotometer. The turbidimeter measures the turbidity in Turbidity Units (TU). There are several TU, mostly the turbidity is expressed in Nephelometric Turbidity Units (NTU) when using a turbidimeter or Formazin Turbidity Units (FTU) when using a spectrophotometer. The difference between the two instruments and thus the two units is that the NTU expresses the amount of light that is scattered through a sample, while the FTU expresses the amount of light that is transmitted through a sample. The latter unit is mostly used in specific absorption studies, while the turbidity expressed in NTU is common for environmental and water quality measurements [20] [36].

The turbidity scale expressed in NTU goes from 0 up to 100.000 NTU, though a turbidimeter has a range from 0 to 1000 NTU. Typical turbidity values for groundwater are 1 NTU or smaller, ecological water systems have a NTU of 1 to 10 and water bodies extremely enriched with nutrients and algae have a NTU from 10 to 50. The limit of turbidity in produced drinking water is in most developed countries 0.5 NTU. Beside most countries regard drinking water with a turbidity up to 1 NTU as safe, while advising not to drink water with a NTU exceeding 1 [28].

While the turbidimeter quantifies the turbidity in water, the second method is not exact but focussed on the water quality. The turbidity can also be measured with a Secchi disk. A secchi disk is a black-and-white disk with a diameter of generally 30 centimetre. The Secchi disk, created by Angelo Secchi in 1865, is the oldest visual optical instrument to measure the transparency of water bodies [21]. The method is not exact but used often as it is easy to operate and cheap. The largest variable is the visual performance of the observer. It works as follows: the Secchi disk is attached to a marked rope and is then lowered from a boat or dock into the water until the disk disappears. The Secchi disk is then raised very slowly until the observer is able to see the disk again. The Secchi disk depth, usually expressed in metre or centimetre, can then be read off from the marked rope where the rope intersects with the water surface. The Secchi disk depth is a function of the absorption and scattering of light by particles and suspended sediments in the water. One could state that the Secchi disk depth is simply the depth of water clarity. A large Secchi disk depth implies that the water body is rather clean, while low Secchi disk depth values indicate that the water body is very turbid. The Secchi disk depth range is a few centimetre for very turbid lakes to 70 metre for clear oceanic waters [21]. Mostly observed are Secchi disk depths between 2 and 10 metre.

A Secchi depth reading should take place preferably when the sun is high, around noon. This can be explained using figure 2.11. In figure 2.11, a beam of sunlight enters the water with an angle A , which is the solar altitude. The beam of light is refracted according to Snell's law (paragraph 2.1.3) at point of incidence C . The angle of incidence i and angle of refraction r are also displayed in figure 2.11. The Secchi disk, indicated with D , is lowered in the water at point E so that the observer can just see the disk. The path that determines the Secchi disk depth is $C-D-E$, which leads to Secchi disk depth indicated with A_{SD} . This apparant Secchi disk depth is however not the correct value. The correct value would be observed when the sun is directly overhead, in zenith as displayed in figure 2.11. If the sun is at zenith, the correct Secchi depth z_{SD} will be observed [44]. Thus a Secchi depth reading should take place between 10 a.m. and 14 p.m., which is around noon.

The Secchi depth can be used in the Beer-Lambert Law. This law relates the attenuation of light to the properties of the material through which the light is traveling. The Secchi depth is then the path length along which light is scattered and absorbed as a function of the concentration of the particles in the water. This approach is used often in scientific studies. In this research, the main importance is to determine whether the water is clear enough for laser scanning purposes. The penetration of green light from a laser scanner in water is dependent on the travelled path length through and turbidity of the water [38]. The already before mentioned rule of thumb that light, specifically green light, can penetrates the water surface three times as far as one can see still holds. The Secchi disk depth can be measured, along with the water depth. With these two values it can be estimated whether the laser light is able to reach the bottom. An example of a Secchi depth measurement with algae is displayed in figure 2.12. In this figure, the Secchi disk can be viewed in the left water column, however in the right water column the disk is blocked from view due to a high turbidity caused by algae. Obviously, the situation in the left water column is preferred for scanning purposes.

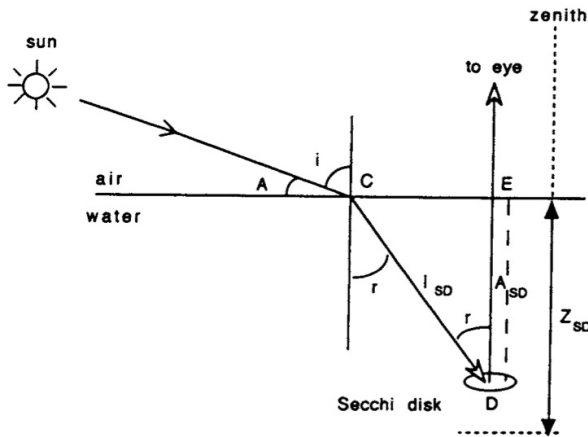


Figure 2.11: Schematic Secchi disk depth [44]

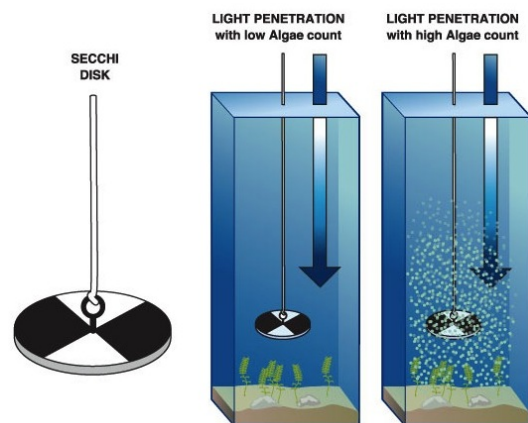


Figure 2.12: Secchi disk in clear/algae water [42]

2.3 Bathymetric laser mapping

Scanning the underwater topography, also called bathymetric laser scanning, is a technique mostly used in coastal areas and river systems. Large scale bathymetric maps are usually acquired by an airborne laser scanner. The main advantage of airborne bathymetric laser scanning in coastal areas is that the mapping is done from the air, so the water depth does not play a role as it does when the mapping is done from a vessel where there is the risk of the ship to run aground in shallow waters. Another advantage of airborne bathymetric scanning compared to conventional mapping methods is that the survey speed may be up to 20 times quicker [46]. The main disadvantage of laser bathymetric mapping is the maximum applicable water depth. As stated before in paragraph 2.1.3, airborne bathymetric laser scanning is only applicable up to depths of 50 metre [46]. For depths larger than 50 metre, SONAR is still the most used technique. SONAR, SOund Navigation And Ranging, uses sound waves where laser scanning uses light waves for underwater mapping. There are sonar systems in circulation that have a depth range of up to 5000 metre.

Bathymetric laser mapping can be done by both airborne and terrestrial laser scanners. Bathymetry maps can also be acquired by scanning from a boat. The differences and similarities between the two laser scanning systems in the context of bathymetric mapping will be discussed in this section.

2.3.1 Differences between airborne and terrestrial bathymetric scanning

In the context of bathymetric scanning, there are several differences between an airborne lidar system and a terrestrial laser scanner. The most obvious one is the scale where the two different techniques are used. Bathymetric airborne lidar is used at far larger scale than terrestrial laser scanning. Survey areas of 2 by 1 kilometre [5] respectively 1 by 5 kilometre [3] for a river environment are very common for airborne lidar bathymetry studies. Additionally, smaller survey areas are also of interest for lidar studies, for example an area of 60 by 100 metre for a channel and riparian zone [25]. Terrestrial laser scanning in a bathymetry context is mostly used at a smaller scale as the technique is even able to depict individual grains [37]. Larger surveys of for example an area of 180 square metre [14] are also performed, the disadvantage is that the terrestrial laser scanner needs to be moved several times in order to obtain the full area. In the case of moving the terrestrial laser scanner, targets need to be used in order to patch together the several scans.

The accuracy of bathymetric mapping differs for the two techniques. First one must keep in mind what is desired: a large survey area with a lower accuracy or a smaller survey area with a high accuracy. The accuracy of bathymetric terrestrial laser scanning is higher, studies show accuracies of 0.01 metre for the position [14] for bathymetric studies. The accuracy of airborne lidar is in the order of 0.1 metre [17], which is acceptable for most large scale studies.

The distance between an airborne lidar and the bathymetry is much larger than the distance between a terrestrial laser scanner and its bathymetric target. Because of this, the energy that is needed to overcome the distance and penetrate the water surface is larger for a airborne lidar than for a terrestrial laser scanner. Table 2.2 displays the properties of the often used airborne lidar system EAARL [17] [25] and the terrestrial laser scanner that is used in this research, the Leica C10 ScanStation [22]. The EAARL (Experimental Advanced Airborne Research Lidar) is an aquatic-terrestrial airborne lidar system developed by NASA (National Aeronautics and Space Administration). The EAARL is used for a wide range of aquatic environments like coral reefs, nearshore benthic habitats, coastal vegetation, and sandy beaches [43].

	airborne lidar EAARL	terrestrial laser Leica C10
maximum applicable water depth [m]	50	1
wavelength [nm]	532	532
maximum scan rate [points/s]	25	50000
pulse length [s]	$1.2 \cdot 10^{-9}$	$250 \cdot 10^{-12}$
pulse repetition frequency [kHz]	3 -10	≤ 50
pulse energy [J]	$70 \cdot 10^{-6}$	$30 \cdot 10^{-9}$

Table 2.2: Properties of airborne lidar EAARL [25] and terrestrial laser scanner Leica C10 [22]

It is obvious that bathymetric lidar is a dynamic technique while terrestrial bathymetric scanning is static. A terrestrial laser scanner has a fixed position and is fixed at both its position and level. Airborne lidar is dynamic and uses an onboard GNSS, commonly GPS, for positioning in combination with a GPS base station on the ground. Besides an onboard IMU (Inertial Measurement Unit) is needed in order to register the movements of the airplane. In other words, there is more equipment needed in the case of airborne bathymetric scanning. Also in the case of a survey done by airplane, there needs to be a survey flight planning, which includes how to fly over the project area. Plus the topography of the project area in the form of a digital elevation model is often required. The bathymetric maps are combined with the topography maps in order to obtain the correct height. Figure 2.13 depicts the aquatic-terrestrial airborne EAARL lidar system with onboard GPS and IMU systems and figure 2.14 displays one of the applications of the EAARL lidar system: the mapping of coral reef in the northern Florida Keys [43].

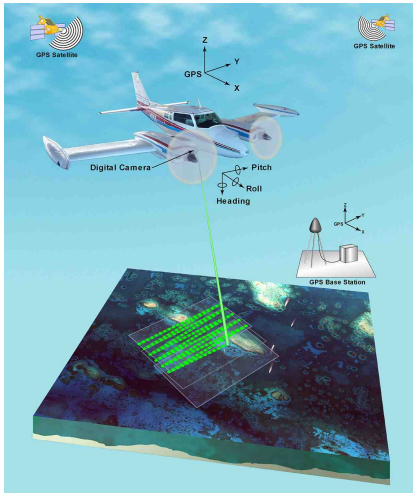


Figure 2.13: EAARL lidar system [43]

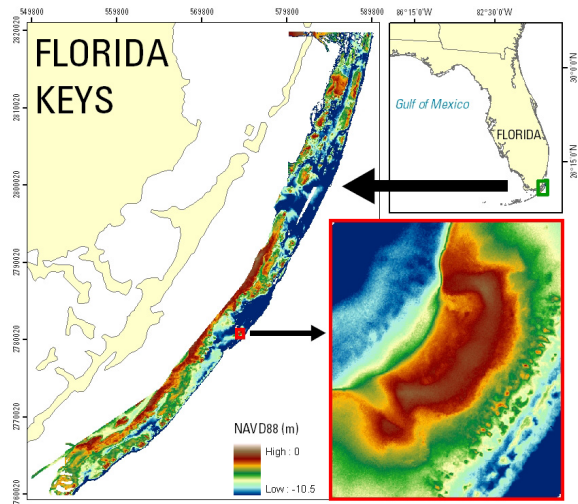


Figure 2.14: Bathymetry of Florida Keys [43]

2.3.2 Similarities between airborne and terrestrial bathymetric scanning

There are several similarities between airborne lidar and terrestrial laser scanning. First of all, both techniques normally use a green-wavelength laser with a typical wavelength of 532 nanometre for scanning of bathymetry. Also, in both cases, the project area needs to be clearly outlined before starting the survey. Beside the survey area, the position of the laser scanner should be determined, both for surveys using a fixed scanner and for surveys using a dynamic one.

Both techniques use targets in order to patch the scans together. The targets used for terrestrial laser scanning have a set position so that the different scans can be patched together. Airborne lidar also uses targets to patch the scans together. However, these targets are not the round targets with a diameter of approximately 15 centimetre [22] as used when scanning with a terrestrial laser scanner. The targets used by airborne lidar are usually ground points, also called ground truth. This known and marked position on the ground has GPS coordinates. With this ground truth and the recorded position of the airplane, the scans can be patched together.

A correction for the refraction that occurs at the water surface needs to be applied to all datasets. The correction for refraction is the same for both techniques. The only difference is that the angle of incidence is different. Data obtained by airborne lidar has an almost vertical incidence angle, while the incidence angle of a terrestrial laser scanner is oblique. Besides this correction, atmospheric conditions should be taken into account as described in section 2.2.

Finally, besides the differences like the scale and detail, mapping of the bathymetry will lead to the same product for the two techniques: a map of the bathymetry and other objects under water, and the water depth. At smaller scales the focus may be different, for example morphological or ecological studies, while bathymetric mapping at larger scales focusses mainly on the differences in the bathymetry over a period of time. The technique is rapidly evolving and it is expected that laser scanning will be adopted more and more for bathymetric purposes in the future.

2.4 Principle of terrestrial laser scanning

There are three different principles a laser scanning device may use for the determination of the range, which is the distance between the origin of the laser light and the target. The first ranging principle is triangulation. The second method to determine the range is done by determination of the phase shift, which is the phase difference between the emitted and received signal. The last principle is called time of flight: after emitting a signal the laser scanning device will wait for the return [35]. The latter principle is used by the laser scanner device in question, which is the Leica ScanStation C10.

2.4.1 Time of flight principle

The time of flight principle is a ranging principle based on the time it takes between the sent pulse and the received echo. The principle assumes that the laser beam travels in a straight line at constant velocity [37]. The laser scanner thus emits a pulse towards the target and waits for the returning echo. The pulse can be characterised as a wave with an amplitude A during time t , with a pulse width t_p , and rise time t_r . A schematic overview of the pulse is displayed in figure 2.15. The laser scanner device transmits a pulse, indicated with P , and receives an echo of the transmitted pulse, indicated with E . The transmitted pulses and echos have an amplitude A_T respectively A_R , where the underscript T stands for transmitted and R for return or received. The return pulse is always smaller than the transmitted pulse due to scattering within the media. Also, there may be multiple echos for one transmitted pulse. The time between two emitted pulses is the pulse repetition time t_{rep} . The time of flight τ is the time between the middle of the pulse rise time of the emitted pulse and the middle of the pulse rise time of the echo. Figure 2.15 gives an overview of the time of flight description [46].

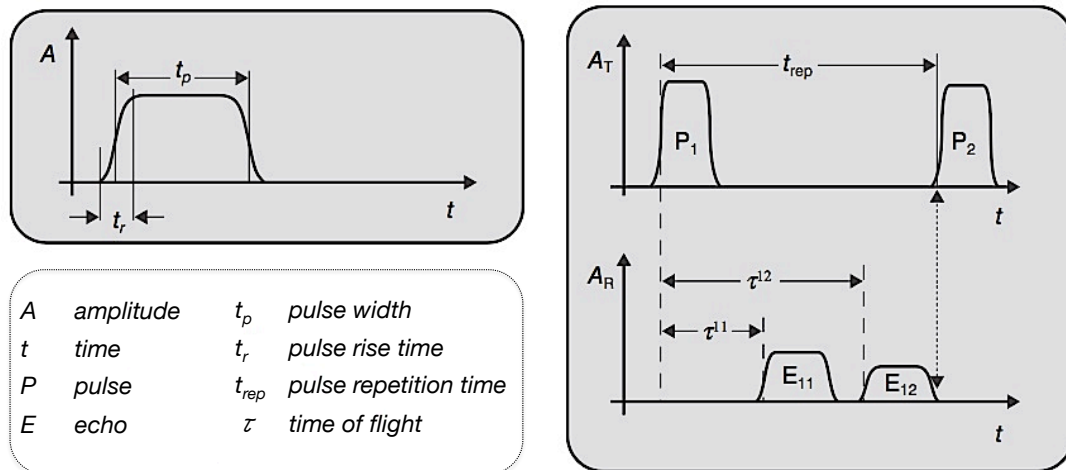


Figure 2.15: Time of flight pulse characteristics, modified from Vosselman and Maas [46]

2.4.2 Range formula

The time of flight can be used to determine the range, which is the distance between the target and the scanner. The range can be computed with the following formula:

$$R = \frac{c \tau}{n 2} \quad (2.5)$$

with R the range between the scanner and the target [m], c the speed of light, which is the speed of light in vacuum: $2.99792458 \cdot 10^8$ m/s, n the refractive index of the medium through which the laser beam is travelling, and τ the time of flight [s]. In the case of the laser beam travelling through water, the range can be divided into R_{air} and R_{water} using Snell's law as described in paragraph 2.1.2.

2.4.3 Features of the return signal

The return signal is stored in the laser scanning device. Each dataset consists of a three dimensional point cloud where each point has its coordinates, x , y , z and intensity i . The origin of the three-dimensional system, so $x = 0$, $y = 0$, $z = 0$, is the origin of the laser scanner. All of the points in the point cloud are thus relative to the origin of the laser light. The intensity can be seen as the strength of the return signal. When light travels through a medium, a part of the light will be absorbed by and scattered within the medium [13]. Scattering of light is also known as the dispersion of light. The transmission of light is displayed in figure 2.2. The part of the light that is lost in the media will thus not return to the device. The return signal is thus less strong, which is displayed in the amplitude of the echo in figure 2.15.

The intensity that is recorded in the laser scanner device is actually the measure of return signal energy [23]. This recorded return signal energy, or return power [33], is measured for each point. The scale of the recorded intensity values may differ for different types of laser scanners, the Leica C10 provides intensity values that are scaled between 0 and 1.

The intensity values of all points together form an intensity image or point cloud representing the intensity. The intensity image is often visualised with an intensity colour scale. A low intensity value indicates a low reflectance of the target on which the point is situated. So a point with a high intensity value implies that the scan target has a large reflectance for that specific wavelength of the laser light. The reflectance spectra and spectral signatures for visible light of different observed coloured objects and Earth features are given in paragraph 2.1.4. Note that in this research only green light with a wavelength of 532 nanometre is considered.

The size of a dataset depends on the size of the target and the resolution settings used within the laser scanning device. The larger the target and the higher the resolution settings, the more points in a dataset. In optics, the resolution of an image is often defined as the sharpness expressed as the number of pixels. In laser scanning, the resolution is in fact the spatial resolution and mostly defined as the number of points per measured area. The resolution can be set within the laser scanning device, ranging from low to highest resolution. Plus the Leica ScanStation C10 offers the option of setting the resolution manually by putting in the range and horizontal and vertical accuracy.

2.4.4 The edge effect

Terrestrial laser scan targets are often detailed, rather small and require high resolution settings. One of the most common effects when scanning targets is the edge effect [10] as depicted in figures 2.16 and 2.17. It is the effect that occurs at the edge of a scan target: because part of the ray of light will fall off the target, the return signal and thus the returned intensity values will be less strong at the edge. The edge effect depends on the resolution setting: in order to obtain a valid point cloud the resolution needs to be small enough as illustrated in figure 2.16. The edge effect is the reason why the edges of a target appear a bit blurry and have lower return intensity values as shown in figure 2.17.

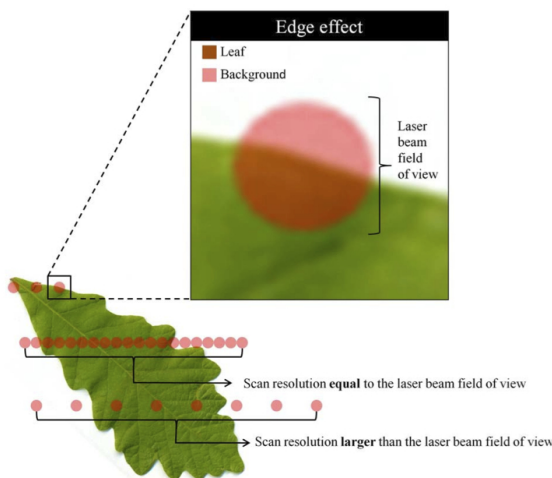


Figure 2.16: Edge effect and resolution setting [10]

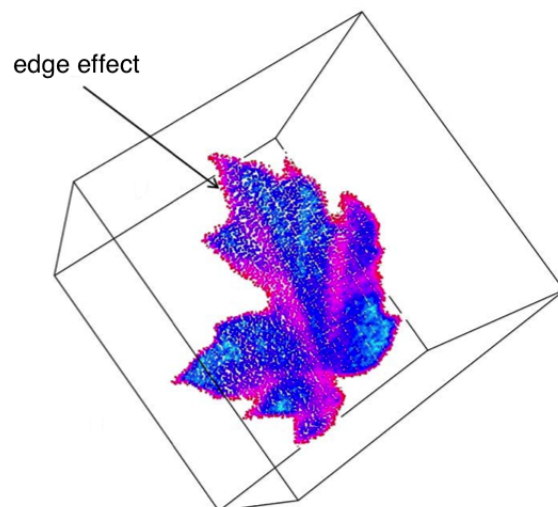


Figure 2.17: Result of edge effect [10]

Chapter 3

Methodology

The scope of this graduation project is to explore the possibilities and limitations of the Leica C10 laser scanner when observing through the water. In order to do so, basic experiments are set up which will give the preferred scan conditions before doing the outdoors field experiments. Previously gathered insights into the scanning process will be taken into account before designing the experimental set up. The methodology chapter first describes the laser scanner that will be used throughout the experiments to continue with the experimental designs of both laboratory and field experiments. Further all the parameters of interest will be summarised. The modifications that need to be done to the return signal will then be described, to wrap up with the assessment criteria that will be applied to the data.

3.1 Terrestrial laser scanner Leica ScanStation C10

The Leica ScanStation C10, shortly Leica C10, is the terrestrial laser scanner device that will be used throughout this project. The Leica C10 laser scanner in question is property of the Delft University of Technology, faculty Civil Engineering and Geosciences, department Geoscience and Remote Sensing. The Leica C10 laser scanner with the accessory Leica tripod is displayed in figure 3.1. The red trunk containing the Leica C10 is displayed in figure 3.2. The latter image is taken in the Mekelpark of the Delft University of Technology, in front of the faculty of Civil Engineering and Geosciences.



Figure 3.1: Leica C10 on top of Leica tripod [22]



Figure 3.2: Leica C10 trunk in Mekelpark

3.1.1 Technical specifications of the Leica C10

As stated before, the terrestrial laser scanner Leica C10 is a pulsed laser scanner that uses green light in the visible spectrum. The laser scanner is operational under a large spectrum of conditions: it can be used in temperatures between zero to over forty degrees Celsius and is fully operational from bright sunlight to complete darkness [22]. All of the significant specifications are given in table 3.1.

feature	unit	abbreviation	value
weight	kilogram	kg	13
depth	millimetre	mm	238
width	millimetre	mm	358
height	millimetre	mm	395
operating time (2 batteries in use simultaneously)	hour	h	> 3.5
battery charging time	hour	h	< 3.5
operating temperatures	degree Celsius	°C	0 - 40
maximum operating humidity	percentage	%	95
wavelength	nanometre	nm	532
horizontal field of view	degree	°	360
vertical field of view	degree	°	270
maximum scan rate	points/second	points/s	50000
pulse length	picosecond	ps	250
pulse repetition frequency	kilohertz	kHz	≤ 50
pulse energy	nanojoule	nJ	30
accuracy of position	millimetre	mm	6
accuracy of distance	millimetre	mm	4
accuracy of angle (horizontal and vertical)	microrad	μrad	6
modeled surface precision/noise	millimetre	mm	2
minimum range	metre	m	0.1
maximum range (albedo 0.9)	metre	m	300
maximum range (albedo 0.18)	metre	m	134

Table 3.1: Specifications of the Leica C10 [22]

Moreover, the field of view and the resolution can be set within the instrument. The field of view of the Leica C10 is displayed in figure 3.4, while figure 3.3 gives the dimensions of the device. The resolution can be set varying from a low resolution to the highest or custom resolution. The custom resolution setting will allow for the input of the range between scanner and target and the desired horizontal and vertical accuracy. The resolution determines the point density, so how many points per area the laser will scan. In order to make a scan of a target, first a scan with a low resolution and broad field of view will be made to determine the exact location of the target. The location of the target can then be locked in the settings before performing the highest or custom resolution scans.

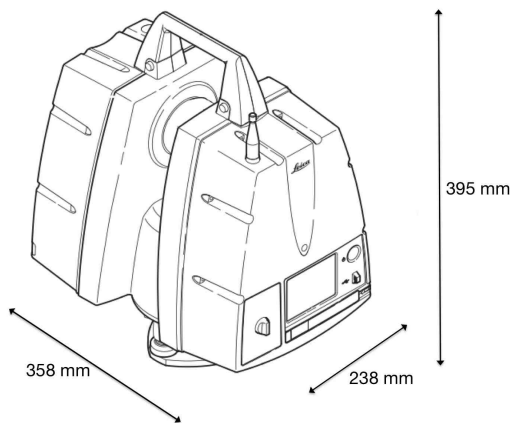


Figure 3.3: Dimensions of the Leica C10 [22]

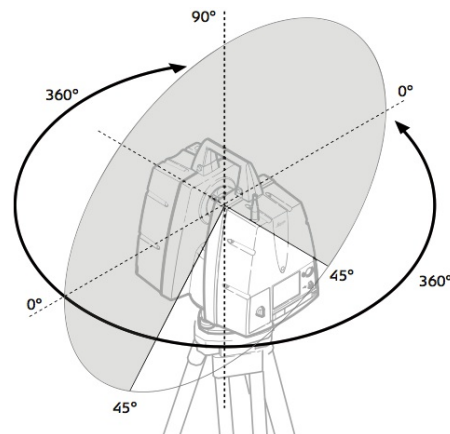


Figure 3.4: Field of view of the Leica C10 [22]

3.1.2 Foreordained scan settings

Literature in combination with previous practical scan experience have shown that some scan settings are advisable while others are impractical or rather poor. Starting with the scanning geometry, literature demonstrates the various experimental set ups that have proven to be successful. The geometry of these experimental set ups are provided in table 3.2. All of the laser scanner devices as described in table 3.2 are pulsed and work on the principle of time of flight measurement, as described in paragraph 2.4.1. What further should be noted is that the height in table 3.2 is the vertical height between the target and the origin of the laser scanner. One exception here is the experimental set up of Miura et al [27], where the height is the height between the origin of the laser scanner and the ground of the bank. In this latter case, approximately half a metre should be added up, so this will give a scanner height of 1 to 2 metre instead. The ranges given in table 3.2 are the range between the origin of the laser scanner and the target.

source	application	type of laser scanner	height [m]	range [m]
Hodge et al [15]	in-situ morphology	Leica HDS3000/ScanStation	1.5	3
Miura et al [26]	mountain channel	Leica ScanStation C10	1.207 - 2.003	< 5
Miura et al [27]	mountain channel	Leica ScanStation C10	0.5 - 1.5	< 9
Smith et al [37]	gravel beds	Leica Total Station 1200	1.8	3.4
Smith et al [37]	lab: water tank	Leica ScanStation	1.8	2
Smith et al [38]	lab: flow velocity	Leica ScanStation C10	1.4	2.7
Smith et al [38]	lab: TSS	Leica ScanStation C10	1.93	2.11
Smith et al [38]	boulder bank	Leica ScanStation C10	4 - 5	16.8 - 17.3
Streicher et al [41]	in-situ water waves	SICK LMS511	1.2	< 25

Table 3.2: Foremost examples of experimental set ups from literature [15] [26] [27] [37] [38] [41]

The scanner height can be deduced from table 3.2: that is, roughly between 1 and 2 metre above the target. Further, Miura et al [27] concluded that the best results were obtained with the scanner at 1.5 metre from the bank ground, so approximately 2 metre above the target. When setting the scanner height, one must also include the workability. Therefore, a scanner height of approximately 1.75 metre above the target is preferred.

The range between the scanner and the target can vary depending on the type and location of the experiment. In general, field experiments tend to have a larger range than laboratory experiments. The closer the range, the larger the possible scan detail. The minimum range for the Leica C10 is 0.1 metre as described in table 3.1. With the scanner at 1.75 metre above the target, and taking into account the field of view of the Leica C10 as displayed in figure 3.4, the minimum range is easily obtained by some basic trigonometrics. If the height is 1.75 metre, and the scan angle is 45° downward, a 45-45-90 isosceles triangle can be envisioned. The minimum range is then, rounded to two decimals, 2.47 metre.

In the experiments of Smith et al [38], who also used the Leica C10, the resolution settings were set to custom. For a close range between 4 and 5 metre, the accuracy of 2 millimetre for both horizontal and vertical accuracy (see also table 3.1) was set. The standard settings of the highest resolution in the Leica C10 are a range of 100 metre and an accuracy of 2 centimetre. At close range it is thus advisable to use custom settings and put in the maximum range of the experimental set up, and the desired accuracy. The minimum horizontal and vertical accuracy that can be set is 1 millimetre for close range.

The foreordained scan settings are: a scanner height of approximately 1.75 metre, a close range between 2.5 and 5 metre and custom resolution settings. The scanner geometry, mainly the range, may vary for laboratory and field experiments. The highest accuracy that can be set in the custom resolution settings will be used. One side note is that with such a high resolution it takes a while to do one scan, so the target needs to be locked first as described in paragraph 3.1.1. Lastly, the Leica C10 is able to make a RGB (Red, Green, Blue) picture of the target. This RGB picture will be taken for each different scan setting once and not for each separate scan as this will consume too much time.

3.2 Experimental design

There will be an experimental design for each different scan situation. First of all, the laboratory experiments will have a set up. The laboratory experiments will include all of the basic experiments as described in chapter 4 and the first case study concerning the wood samples as outlined in chapter 5. Lab cards have been created which help organising the lab experiments, an example of a lab card can be found in Appendix B. The laboratory experiments will also generate a 'how to scan with the Leica C10' manual, which can be found in Appendix A. After the laboratory scan results have been examined, field experiments can be planned and executed. The field experiments are not in a controlled environment so the experimental set up differs strongly from the controlled lab experimental set up.

3.2.1 Design of laboratory experiments

The main elements of the laboratory experiments are: the Leica C10 laser scanner, a basin like a pool with water and the scan target. The Leica C10 laser scanner is described in section 3.1. The basin needs to be able to provide a water depth of maximum 50 centimetre, as previous experiments have shown this is the maximum water depth of clear water the laser can observe through. The basin that will be used is a pool of the brand Intex, which is a pool that can be easily set up as a result of the outside metal frame. The outside dimensions of the pool are: length 269 centimetre, width 201 centimetre, height 60 centimetre. The inside measures are: length 220 centimetre, width 150 centimetre and height 60 centimetre. With a maximum water depth of 51 centimetre, the pool can contain up to 1662 litre. The schematics of the pool are displayed in figure 3.5.

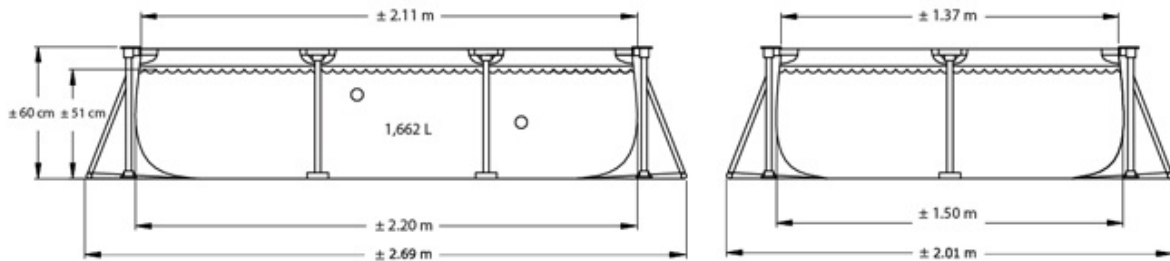


Figure 3.5: Dimensions of the Intex pool

Further, the geometry settings as determined in paragraph 3.1.2 are a scanner height h of approximately 1.75 metre and a minimum range R of 2.47 metre. Figure 3.6 depicts the geometry scheme of the laboratory experimental set up. What should be noted is that the wall of the pool has a height of 60 centimetre. As a result, 60 centimetre of the pool can not be viewed by the scanner. This will be taken into account when dividing the pool in four quadrants. These quadrants will be indicated by taping on the floor of the pool. The quadrants will contain different targets during the experiments.

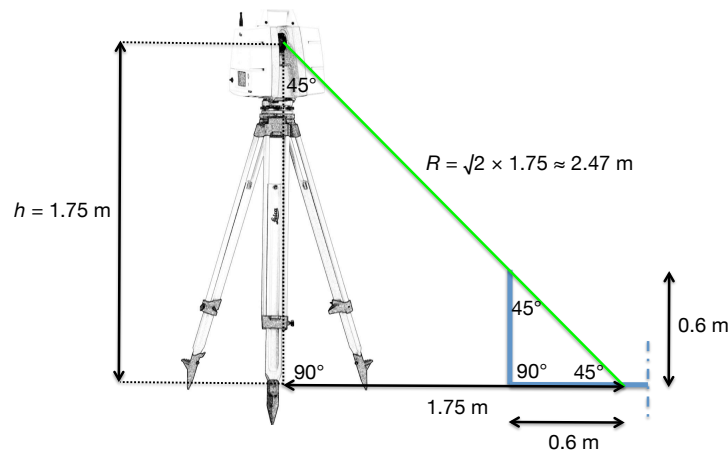


Figure 3.6: Geometry scheme of laboratory experimental set up

3.2.2 Design of field experiments

The height of the origin of the laser scanner to the ground and thus the target depends on the surroundings. The horizontal distance between the origin of the laser scanner and the target will be larger than the distance of the laboratory experiments. Combining the vertical and horizontal distance will lead to the range. The range of the laboratory experiments was between 2.47 and 4 metre, while the range of the field experiments will be larger, say between 3 and 10 metre. Also the scan targets will in general be larger so for the workability this implies that it will take much longer to make a detailed scan. Moreover, the environment is not controlled like in the lab. The weather conditions as described in paragraph 2.2.1 need to be taken into account. Of main importance are the lighting: is it cloudy or is there direct sunlight, and the wind conditions: are there ripples on the water surface. Ideally a water body without flow, as described in 2.2.2, will be chosen for the field experiments. Also there should be no precipitation on the field scan day. The turbidity as outlined in paragraph 2.2.3 should also be measured or estimated. In the lab the turbidity can be measured with a turbiditymeter, however in the field a Secchi disk is needed. Only if the Secchi disk depth is larger than the depth scanning is possible.

3.2.3 Parameters of interest

There are several parameters of interest that will influence the scan results. The scanner geometry is already described in the previous paragraphs. Further the water depth of all experiments should be measured manually with a measuring rod. The water surface is visible on the resulting point clouds, though for validation and also correction of refraction the water depth should be measured too. The next list of parameters summarises all the parameters that should be taken into account; these have been mentioned previously.

- scanner geometry: scan angle, angle of incidence, angle of refraction, height, distance, range
- resolution: low for first quick scan; custom for detailed scan
- atmospheric conditions: type of ambient light, surface wind, precipitation
- water conditions: turbidity, flow
- target properties: shape, material, size, colour (reflectivity), smoothness/roughness

3.3 Modifications to the return signal

3.3.1 Extraction and preprocessing of the data

After scanning, the data in the form of a point cloud is stored in the Leica C10. One scan project in the device contains multiple point clouds as for each scan one point cloud is saved. The data can be exported from the laser scanner with an USB stick. The USB should have sufficient capacity, depending on the size of the scan projects. A capacity of 8 GB or more is preferred. The raw data on the USB then needs to be preprocessed. The preprocessing is done with Cyclone, which is 3D Point Cloud Processing Software from the same manufacturer as the laser scanner, that is Leica Geosystems HDS [22]. The details of the preprocessing with Cyclone can be found in Appendix A. The preprocessing is essentially converting the raw point cloud, which has the format '.bin', to another format, that is '.ptx'. The unit of the location data is in metres and the recorded intensity values are the actual intensity values. The intensity range is between 0 and 1.

The conversion to '.ptx' is necessary as the new format allows other software like Matlab and CloudCompare to read the data. After this conversion, the data will be exported from Cyclone to the USB. One converted '.ptx.' file contains all the point clouds of the scan project. Each point cloud has coordinates x , y , z , intensity i and colours $R G B$, in full *Red, Green, Blue*, in the case also an image has been taken by the laser scanner. The scan project containing the separate point clouds can be viewed and modified with the open source software CloudCompare [8]. An area of interest from the point cloud can be visually downsampled by segmentation or filtering by (intensity) value in CloudCompare. The creation of these downsampled subsets will increase the workability of the processing in both CloudCompare and Matlab as it reduces the processing time.

3.3.2 Coordinate system transformation

After the preprocessing, the return signal will consist of a three-dimensional point cloud with coordinates in a Cartesian coordinate system where each point has its own coordinates: x , y and z . The Cartesian coordinate system, introduced by René Descartes [40], is the most used coordinate system. However, other coordinate systems exist which may be applied for specific applications. For instance, the laser scanning device itself operates from a spherical coordinate system: the horizontal and vertical scan angles set the field of view.

The extracted data thus has coordinates in a Cartesian coordinate system. The polar coordinate system, introduced by Newton [40], is more convenient for the modification to the return signal in terms of the correction for refraction [37]. The polar coordinate system, displayed in figure 3.7, is a two-dimensional coordinate system. The pole, or origin O , as displayed in figure 3.7, would be the laser scanner in this case, scanning one point P . The point P is represented by the polar coordinates r and θ instead of Cartesian coordinates x and y . The polar coordinate r , the radial coordinate, is in the polar coordinate system often described as the distance or range, while the angular coordinate, θ , is described as the azimuth, or simply the angle.

The polar coordinate system becomes the cylindrical coordinate system in the case of a three-dimensional system. Just like the polar coordinate system, the cylindrical system comprises the radial coordinate r , which is the horizontal distance in the x , y plane, and the angular coordinate θ . The third coordinate is the height, z . Figure 3.8 displays the cylindrical coordinate system.

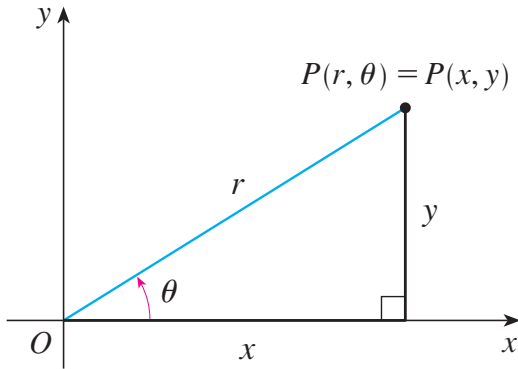


Figure 3.7: Polar coordinate system [40]

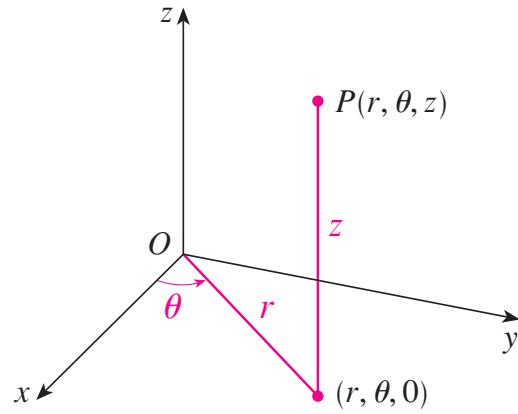


Figure 3.8: Cylindrical coordinate system [40]

Cartesian coordinates, x , y and z can be rewritten into cylindrical coordinates r , θ , z , following from figures 3.7 and 3.8 using some basic trigonometry. To convert from Cartesian to cylindrical coordinates:

$$r^2 = x^2 + y^2 \quad \tan(\theta) = \frac{y}{x} \quad z = z \quad (3.1)$$

The other way around, so to convert cylindrical coordinates into Cartesian coordinates, the following holds:

$$x = r \cos(\theta) \quad y = r \sin(\theta) \quad z = z \quad (3.2)$$

The extracted data consists of point clouds with coordinates in a Cartesian coordinate system. The correction for refraction as described by Smith [37] is in a polar, or cylindrical, coordinate system. Hence the data first needs to be converted into polar or cylindrical coordinates before applying the correction for refraction. After the correction for refraction, the corrected data can be converted back to Cartesian coordinates. This last conversion is mainly for visualisation purposes.

3.3.3 Correction for refraction

The correction for refraction that needs to be applied to the retrieved point cloud is outlined by Smith [37]. The correction for refraction is described for data in polar coordinates for a two dimensional system. The terrestrial laser scanner is placed in the origin, point $(0, 0)$ in the case of a 2D illustration and $(0, 0, 0)$ in 3D, and a correction for refraction is made. Figure 3.9 illustrates the 2D situation with x and z coordinates. It should be noted that this correction needs to be made for each point individually.

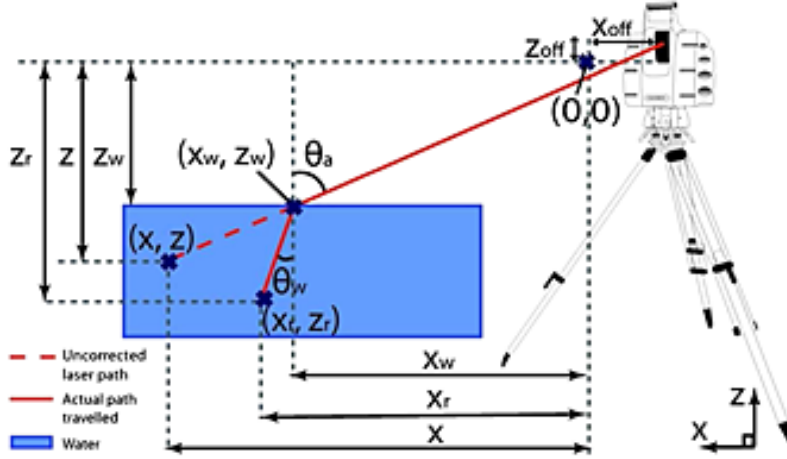


Figure 3.9: Geometry of the correction for refraction [37]

In figure 3.9, the height, z , and x axis are depicted, the y coordinate is zero as the figure represents a cross section. Further, the laser scanner does not recognise where the signal interacts with the water so the laser beam will travel in a direct line to point (x, z) . However, the actual path travelled through the water will be refracted at the water surface, point (x_w, z_w) . The actual point (x_r, z_r) is the point after the correction for refraction. Figure 3.9 also includes the incidence angle θ_a and the angle of refraction θ_b . The angles, as shown in figure 2.2, will be indicated with α and β for the incidence respectively refractive angle.

Last the origin, which is the origin of the laser beam, is moved with parameters x_{off}, z_{off} . This is the so-called offset, which is a slight move from the origin due to technical imperfections of the laser scanner itself. The offset is usually really small, in the order of millimetres. It turns out that in the case of correction for refraction, the offsets have a very small effect and can be set to zero. The correction for refraction is most sensitive to the refractive indices and the water level [37]. The water level can be distinguished and derived from the point cloud itself, yet a more accurate method is to measure it with a measuring rod during the experiments.

Hence the water level z_w is assumed to be known as it is measured during the experiments. Subsequently the other coordinate where the laser beam breaks through the water surface needs to be calculated. The correction for refraction as described by Smith [37] is in polar, or cylindrical coordinates. The height coordinate, z , is the same for both a Cartesian and cylindrical coordinate system. The correction for refraction as given by Smith [37] is a correction for the range, or horizontal distance, as can be seen from figure 3.8 where r is the range in the horizontal x, y plane. The range coordinate r is often written as ρ and this symbol will be used further on for the range coordinate. Because figure 3.9 is two-dimensional, the x coordinates as given in this figure are in fact range coordinates, ρ . Following paragraph 3.4.2, $\rho = \sqrt{x^2 + y^2}$. First x and y need to be converted to ρ . Then, implementing the polar coordinates in the formula given by Smith [37] and cancelling out the offsets as they are set to be zero, the following holds in order to find the corrected point (ρ_r, z_r) .

First the actual incidence angle is given by:

$$\alpha = \tan^{-1} \left(\frac{\rho + x_{off}}{z + z_{off}} \right) = \tan^{-1} \left(\frac{\rho}{z} \right) \quad (3.3)$$

with α the incidence angle, ρ the range coordinate, z the height coordinate and x_{off} and z_{off} the horizontal respectively vertical offset, which both are set to be zero.

Further the location of the water surface, (ρ_w, z_w) needs to be computed. z_w is assumed to be known so ρ_w can be computed:

$$\rho_w = z_w \tan(\alpha) \quad (3.4)$$

with ρ_w the range coordinate of the water level, z_w the height coordinate of the water level and α the incidence angle. Finally the corrected point (ρ_r, z_r) can be computed with:

$$\rho_r = \frac{\rho - \rho_w}{n^2} + \rho_w \quad (3.5)$$

$$z_r = \frac{\cos(\beta)(\rho - \rho_w)}{n \sin(\alpha)} + z_w \quad (3.6)$$

with ρ_r the range coordinate of the corrected point, ρ the coordinate of the point in question, ρ_w the range coordinate of the water level, z_r the height coordinate of the corrected point, z_w the height coordinate of the water level, α the incidence angle, β the refractive angle and n the refractive index. The refractive index in this case is:

$$n = \frac{n_{water}}{n_{air}} \quad (3.7)$$

with n_{water} the refractive index for water, which is set to 1.335, and n_{air} the refractive index of air, which is set to 1.0002782. The refractive indices can be found in paragraph 2.1.2.

The correction for refraction for the range coordinate ρ needs to be applied to each point individually as each point has a different and unique set of x, y, z coordinates and thus a unique range coordinate ρ . After the correction for refraction, the data can be converted back to Cartesian coordinates if necessary with the formula given in paragraph 3.4.2.

Finally, of importance is that the range coordinate ρ should not be confused with the actual range R as described in paragraph 2.4.2 and depicted in figure 3.6. The range R is the actual range between the laser scanner device and the target, while the range coordinate ρ a coordinate is in the polar and cylindrical coordinate system as depicted in figures 3.7 and 3.8. ρ could also be described as the horizontal range. The actual range R in the cylindrical coordinate system as displayed in figure 3.8 would be between the origin O and the point P .

3.4 Assessment of the data

The corrected return data can be evaluated in many different ways. First of all, the data can be assessed with basic statistics. Further, the three evaluation criteria are the point accuracy, the point precision and the point density. The assessment criteria are described in this section.

3.4.1 Basic statistical evaluation

The corrected datasets contain an intensity i for each x, y, z point. The intensity of each object and colour is different as the reflectivity of different objects and colours is different as explained in paragraph 2.1.4. For each scan and specifically each target within the scan, basic statistics can be derived. The basic statistics will provide a feel for the data. The basic statistics that can be calculated for various experiments are listed in table 3.3.

statistic measure	symbol/abbreviation	Matlab operator
minimum value	min	min
maximum value	max	max
arithmetic mean	μ	$mean$
standard deviation	σ	std
median	m	$median$
root mean squared error	$RMSE$	rms
residuals	$\hat{\epsilon}$	-

Table 3.3: Basic statistical measures and their Matlab operator

The arithmetic mean, or simply the mean, is the mean value of a dataset. If a dataset consists of N measurements $x_1 \dots x_N$, the mean μ is computed with:

$$\mu = \frac{x_1 + x_2 + \dots + x_N}{N} \quad (3.8)$$

The standard deviation gives the amount of variation of the dataset from the mean value. Again, with a dataset of N measurements $x_1 \dots x_N$ and the mean μ , the standard deviation σ is:

$$\sigma = \sqrt{\frac{\sum_{i=1}^N (x_i - \mu)^2}{N}} \quad (3.9)$$

The median is the middle value of the dataset, so if the dataset is ordered from the lowest value to the highest value, the median is the middle value. If the dataset has an even number of values, the median is the mean of the two middle values. In the case of a normal distribution of data, the median is the same as the mean.

The root mean squared error, shortly RMSE, is actually a measure of accuracy as it gives the difference between an observed and a simulated dataset. In the case of a high RMSE, the observed and simulated datasets do not fit. A rather low RMSE implies that the observed and simulated datasets form a good match. The RMSE can be used for example to determine the difference between the coordinates of the measured water surface level and the water surface level as viewed in the scan. Likewise the RMSE can be used to determine the difference between a dry reference scan of an object like the bottom of the pool and a scan of the bottom with water on top. For two datasets both consisting of N measurements, where the observed data is y and the simulated data is \hat{y} , the RMSE can be computed with:

$$RMSE = \sqrt{\frac{\sum_{i=1}^N (\hat{y}_i - y_i)^2}{N}} \quad (3.10)$$

The difference between the observed data y and the modeled data \hat{y} is called the residuals: $\hat{e} = \hat{y} - y$. The smaller the residual values are, the more the two datasets coincide.

3.4.2 Terminology: accuracy versus precision

The terms accuracy and precision are often confused. Though both terms are used frequently, they can not be interchanged. The accuracy is usually defined as the closeness to the true value, so how close the data, or the mean of the data, is to the true value. The precision is often defined as the spread in outcomes, or the repeatability. The accuracy and precision are illustrated in figure 3.10.

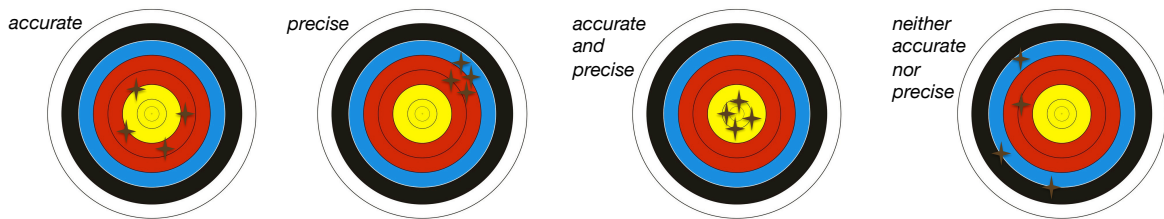


Figure 3.10: Portrayal of accuracy, precision and combinations of both

3.4.3 Assessment of point accuracy

As the term indicates, the point accuracy gives the accuracy of the points in a dataset. The point accuracy can only be assessed if there is both a dry reference scan and an underwater scan of the same target. The point accuracy can be determined by looking at the difference between a point from the underwater point cloud and its nearest neighbour in the dry reference point cloud [38]. The dry reference cloud will then function as the so-called ground truth. The point accuracy can be used to determine whether the location of the bottom of the pool is accurate when scanning through water compared to the dry reference scan.

3.4.4 Assessment of point precision

The point precision can be quantified using the repeat scan error value [15] [38]. The repeat scan error value, shortly RSEV, is defined as the maximum three-dimensional distance between repeat measurements of the same point [38]. The RSEV can be determined when one specific scan is repeated multiple times as it gives the error between two scans. The scans that are compared must have exactly the same scan settings so the same locked scan area and the same resolution setting. If a scan is repeated twice, the RSEV between the two datasets i and j can be computed with:

$$RSEV = \max \left[\sqrt{(x_i - x_j)^2 + (y_i - y_j)^2 + (z_i - z_j)^2} \right] \quad (3.11)$$

with RSEV the repeat scan error value, x_i and x_j the x coordinates of the two datasets, y_i and y_j the y coordinates of the two datasets and z_i and z_j the z coordinates of the two datasets.

The RSEV can be computed for each pair of scans, given that the scan settings are the same. So in the case there are three scans of the same area, let's say scan i , j and k , there are three pairs: $i-j$, $i-k$ and $j-k$. As the RSEV is in fact an error, it holds that the lower the RSEV is, the higher the precision of the pair of scans.

3.4.5 Assessment of point density

Overall, there are two ways to determine the point density of a dataset in the form of a point cloud: absolute or relative. The absolute density can be determined when the surface area is known or measured. The number of return points in that area can be retrieved from the point cloud and the point density can then be computed as the number of points per area: *points/m²*, or *points/cm²* for smaller objects. This method will work rather well for easily measurable areas, like a part of the bottom of the pool, or the area of the vertical measuring pole. The latter is of interest because the measuring pole, consisting of a homogeneous piece of wood, is partly submerged in the water. It is expected that the point density under water will be smaller than the point density above the water surface due to a loss of signal when scanning under water.

The point density can also be a relative measure. There are multiple methods to determine the relative point density. One method is to express the density in a percentage of returns in the dry reference scan [38]. Hence a dry reference scan is needed and the number of returns at a specific area are set to 100%. The number of returns in the underwater scan of that same specific area is then the relative point density, expressed in percentage. Another relative method is to express the density in a percentage of returns where a density of 100% is the expected returns from the scan settings of the point spacing.

An other often used method for the relative point density is using the nearest neighbours (NN) measure. The nearest neighbours measure will, as the name implies, use the nearest neighbours of a specific point to determine the point density. There are two rather straightforward methods using the nearest neighbours measure. The first one is called precise: the point density is estimated by counting the number of neighbours N for each point. For the precise method, a search radius r needs to be set, all neighbour points that fall inside the radius around the selected point will then be counted. The second method is called the approximate method: the density is estimated by determining the distance to the nearest neighbour. The distance to the nearest neighbours can also result in a relative surface density, where the number of neighbours within radius r are divided by the neighbourhood surface. The neighbourhood surface is simply πr^2 , with r the radius.

Table 3.4 provides an overview of the different ways the point density can be estimated.

measure	description	output (unit)
absolute	points divided by measured area	<i>points/m²</i> or <i>points/cm²</i>
relative	percentage of returns compared to dry reference scan	%
relative	percentage of returns compared to expected returns	%
relative	nearest neighbours measure: precise method	number of neighbours N
relative	nearest neighbours measure: approximate method	distance [m] to nearest neighbour
relative	nearest neighbours measure: approximate method	neighbourhood surface: $N/\pi R^2$

Table 3.4: Different measures of point density

Chapter 4

Basic Laboratory Experiments

This chapter consists of the basic experiments that have been done in a controlled environment, that is a laboratory. First the arrangements of the experiment will be described, followed by the experiments that have been done to explore the settings. After that the experiments with different materials, shapes and colours will be discussed to continue with experiments that simulate an outdoor environment. The power of the signal is examined to finish with conclusions and recommendations that can be used in the field experiments. What should be noted is that both the laboratory experiments as described in this chapter and in the next took place at the same location and have the same experimental set up.

4.1 Experimental arrangements

4.1.1 Location and surroundings

The laboratory experiments took place at the Water Laboratory, also known as Lab Hydraulic Engineering or Stevin III lab, at the Faculty of Civil Engineering and Geosciences at Delft University of Technology. The 5000 square metre surface area of the lab offers equipment to operate a wide variety of both hydraulic engineering and water quality experiments. Figures 4.1 and 4.2 display the location of this lab.



Figure 4.1: Faculty sign



Figure 4.2: First floor entrance to the Water Laboratory

The experiments were done in a controlled environment, which means that all of the dimensions and characteristics of the media, environment and targets are known. The two storeys high ceiling is equipped with artificial light, though there is also some day light coming in from the top of the walls. The floor on which the experiment has been set up was hard, smooth and nearly level. Due to the heavy equipment and use of chemicals in the water lab, safety rules applied, which included the use of safety shoes with steel toes.

4.1.2 Lab equipment list

The following equipment, materials and substances have been used in the laboratory experiments:

- laser scanning equipment:
 - Leica tripod
 - tripod star (because of smooth floor)
 - tribrach for initial levelling of the tripod
 - Leica C10 ScanStation in its red trunk
 - Leica measuring rod
 - 4 Leica C10 batteries (2 in use, 2 reserve)
 - Leica battery charger
- USB stick, size 16 GB
- laptop with Cyclone software (Delft University of Technology laptop TUD251188)
- notebook, labcards and pencil
- Intex pool (dimensions 220x150x60 *cm*)
- basic tools:
 - measuring pole, homemade from piece of wood and marked
 - measuring rod
 - duct tape and double-sided tape
 - water resistant markers
 - towels
- water:
 - approximately 1750 litre clean water from clean water supply
 - approximately 1170 litre Schie water from Schie water pipe
 - hosepipes
 - water pump
- scan target materials:
 - 9 coloured glass marbles
 - 15 dimpled titanium golf balls
 - 1 green rubber tile
 - 1 concrete buddha sculpture
 - 7 coloured concrete cubes
 - 2 types of water plants
 - bucket of rocks (available in water lab)
 - bucket of beach sand (available in water lab)
 - 4 wood samples of different wood (provided by section Structural and Building Engineering)
- safety shoes with steel toes (provided by the staff of the lab)

4.1.3 Experimental set up

The experimental design of all of the laboratory experiments has been described and depicted in section 3.2, especially paragraph 3.3.1. The experimental set up for the lab experiments is shown in figures 4.3 and 4.4.



Figure 4.3: Experimental lab set up - eye level

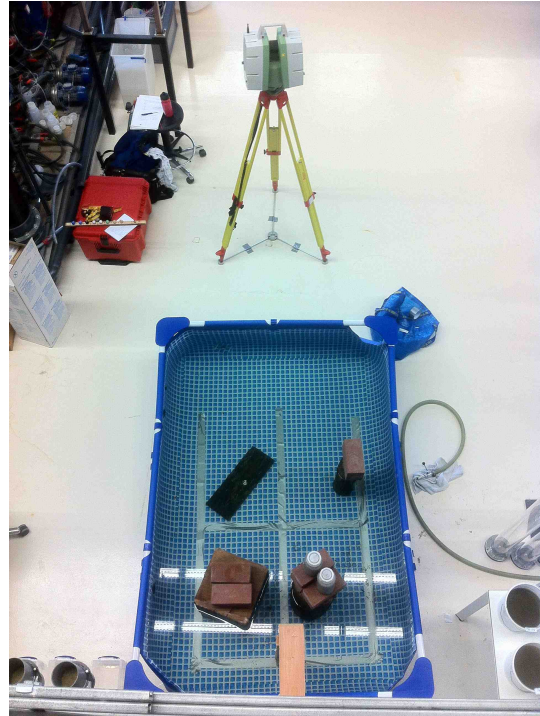


Figure 4.4: Experimental lab set up - top view

Furthermore, the height of the origin of the laser scanner to the ground has been measured with the accessory Leica measuring rod. This height should be approximately 1.75 metre according to the experimental design. The true height is almost 1.75 metre: the measuring rod read out 1.748 metre. Concluding, figure 3.6 including distances and scan angles, provides an accurate overview of the scanning geometry. The four quadrants that have been taped on the pool floor have a width of 45.5 centimetre. The two quadrants furthest away from the laser scanner have a length of 70 centimetre, while the two closest have a length of 50 centimetre. The quadrants are visible in figure 4.4.

Throughout the lab experiments, two types of water have been used: clean drinking water and water from the river the Schie. These two types have also been added together in order to obtain two mixtures of water: 50% clean water and 50% Schiewater; 75% clean water and 25% Schie water. The turbidity expressed in NTU of the four water samples has been measured with a turbidimeter, that is the Hach 2100N Turbidimeter that was available in the Water Laboratory. Figure 4.5 displays the Hach 2100N Turbidimeter and table 4.1 displays the turbidity measures of the four water samples.



Figure 4.5: Hach 2100N Turbidimeter

water sample	turbidity [NTU]
clean water	0.3
75% clean 25% Schiewater	1.3
50% clean 50% Schiewater	1.4
Schiewater	2.0

Table 4.1: Turbidity (NTU) measures of water samples

4.2 Experiments to explore the settings

The first set of experiments are scans of the pool without any water. In this section, first the effects of the resolution setting will be examined, to follow with the repeat scan assessment of the point clouds per quadrant and last the influences of the horizontal distance on the number of points and the point density will be evaluated. The tools used for the processing of the data are given in Appendix C.

4.2.1 Effects of the resolution setting

The dry pool has been scanned with both low and high resolution settings. To determine the difference between both settings, one point cloud of each setting, cloud 3 for low resolution and cloud 5 for high resolution, is selected. The bottom of the pool had been divided into quadrants and these have been selected by segmentation in point clouds 3 respectively 5. Quadrant 1 and 2 have the same area, that is 3185 cm^2 , and quadrant 3 and 4 have the same area, that is 2275 cm^2 . The four segmented quadrants of point cloud 5 with corresponding number are displayed in figure 4.6. The point densities of each quadrant for both clouds have been plotted next to each other in figure 4.7. As can be seen, the resolution setting has a major influence on the number of points and thus the point density. If the number of points of a quadrant of cloud 5 would be 100%, then a quadrant of cloud 3 contains only 6% of the points. This 6% also holds for the point density: the point density of a quadrant of cloud 5 is $16\frac{2}{3}$ as dense as that of cloud 3.

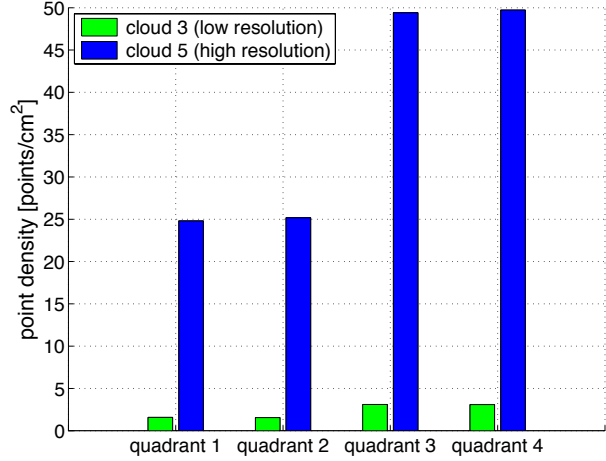
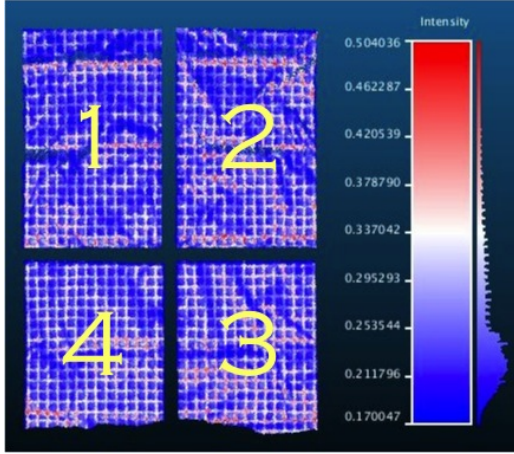


Figure 4.6: Point clouds of the four quadrants Figure 4.7: Bar plot of densities for low/high resolution

The other characteristics, and principally the nearest neighbour (NN) distances, of the two compared point clouds are given in table 4.2. The bottom of the pool comprises all four quadrants as well as the duct tape boundaries between them, with a total area of 13780 cm^2 . The nearest neighbour distances as well as the standard deviation is smaller for the high resolution setting: the mean nearest neighbour distance is a factor 3.5 respectively 3.3 smaller for quadrants 1 and 2 respectively 3 and 4.

	point cloud 3 (low resolution)					point cloud 5 (high resolution)				
	<i>bottom</i>	<i>q1</i>	<i>q2</i>	<i>q3</i>	<i>q4</i>	<i>bottom</i>	<i>q1</i>	<i>q2</i>	<i>q3</i>	<i>q4</i>
number of points	29267	5023	4936	7061	7042	478152	79005	80156	112398	113123
point density [$points/cm^2$]	2.12	1.58	1.55	3.10	3.10	34.70	24.81	25.17	49.41	49.72
min NN distance [mm]	3.63	4.80	4.86	3.67	3.63	0.89	1.17	1.16	0.89	0.89
max NN distance [mm]	16.82	16.71	16.82	10.45	8.24	8.15	11.41	7.99	5.59	4.99
mean NN distance [mm]	5.51	6.27	6.30	4.87	4.86	1.63	1.78	1.79	1.47	1.46
median NN distance [mm]	5.36	6.11	6.13	4.77	4.78	1.55	1.69	1.69	1.39	1.39
std NN distance [mm]	1.08	0.97	0.98	0.68	0.63	0.43	0.40	0.40	0.36	0.36

Table 4.2: Point densities of point clouds with low respectively high resolution

So with a low resolution only 6% of the points will return compared to a high resolution setting. For a first scan to lock the target this low resolution scan is effective as the scan is fast, however for a detailed scan high or custom resolution settings are essential.

4.2.2 Repeat scan assessment per quadrant

The point precision is obtained by comparing the repeat scan error value (RSEV) for different combinations of point clouds per quadrant. The description and formula of the RSEV are given in paragraph 3.4.4. Before the RSEV can be computed, the three point clouds need to be aligned in both .txt files: the index of one point in the first cloud needs to coincide with the index of that same point in the second cloud. This can be done by computing the closest point set for a point cloud referenced with a second point cloud. For each set of two clouds, the point cloud that is smallest will be taken as comparison and then the closest distance set for the second point cloud is computed. After the closest distance set computation is done, all point clouds have the same number of points and the same indices for corresponding points. Then for each quadrant and each pair of clouds the RSEV can be computed and these are given in table 4.3.

	<i>quadrant 1</i>	<i>quadrant 2</i>	<i>quadrant 3</i>	<i>quadrant 4</i>	mean value
<i>RSEV cloud 5 - 6 [m]</i>	0.0165	0.0138	0.0055	0.0048	0.0101
<i>RSEV cloud 5 - 7 [m]</i>	0.0075	0.0106	0.0061	0.0068	0.0077
<i>RSEV cloud 6 - 7 [m]</i>	0.0132	0.0140	0.0060	0.0050	0.0095
mean value	0.0124	0.0128	0.0059	0.0055	0.0091

Table 4.3: Repeat scan error values (RSEV) per quadrant for all high resolution point clouds

As the coordinates of the points $x y z$ are in metre, so are the RSEV as given in table 4.3. Of the three pairs of clouds, the mean RSEV of cloud 5 and 7 is the smallest and thus this cloud pair is the best with regard to the repeat scan assessment. However, all three pairs have rather smaller mean RSEV, where the mean is 9.1 millimetre. In other words, if the same scan target, which is the dry scan of the pool, will be repeated, the repeat error is expected to be maximum 9.1 millimetre. When looking at the RSEV of the quadrants, it becomes clear that the quadrants that are closer to the laser scanner, that are quadrant 3 and 4, have a smaller RSEV. The difference between quadrants 1 and 2 and quadrants 3 and 4 is the same: 4 millimetre.

For a dry repeat scan, the RSEV are small, with mean values of 9.1 millimetre. The RSEV is expected to be larger when scanning under water, as there are more influencing factors like loss of signal and variable water conditions.

4.2.3 Influence of the horizontal distance

In order to examine the influence of the horizontal distance on the number of return points and the point density, the duct tape in the middle of the pool is selected by segmentation from the three high resolution point clouds. The characteristics of the three point clouds containing the duct tape are given in table 4.4. The horizontal range from the laser scanner to a point is computed for each point separately. The total duct tape has a width of 5 centimetre, and a length of 130 centimetre so an area of 650 cm^2 . This area has been used to compute the point density.

<i>duct tape</i>	point cloud 5	point cloud 6	point cloud 7
number of points	21604	21291	20772
point density [$\text{points}/\text{cm}^2$]	33.24	32.76	31.96
minimum horizontal range [m]	1.8120	1.8131	1.8127
maximum horizontal range [m]	3.0961	3.0970	3.0982

Table 4.4: Scan characteristics of the segmented duct tape point clouds

Next each point cloud is divided into cells of 5 by 5 centimetre. There exist 26 cells over the 130 centimetre long duct tape. The number of points that fall into each cell are plotted versus the horizontal distance, or the horizontal range, in figure 4.8. The middle of the cell is taken for the visualisation, so for example all the points that fall in the cell with range between 1.8 and 1.85 metre, have been represented at the middle value, which is 1.825 metre, in figure 4.8. Further the mean value of the three point clouds has been added in figure 4.8.

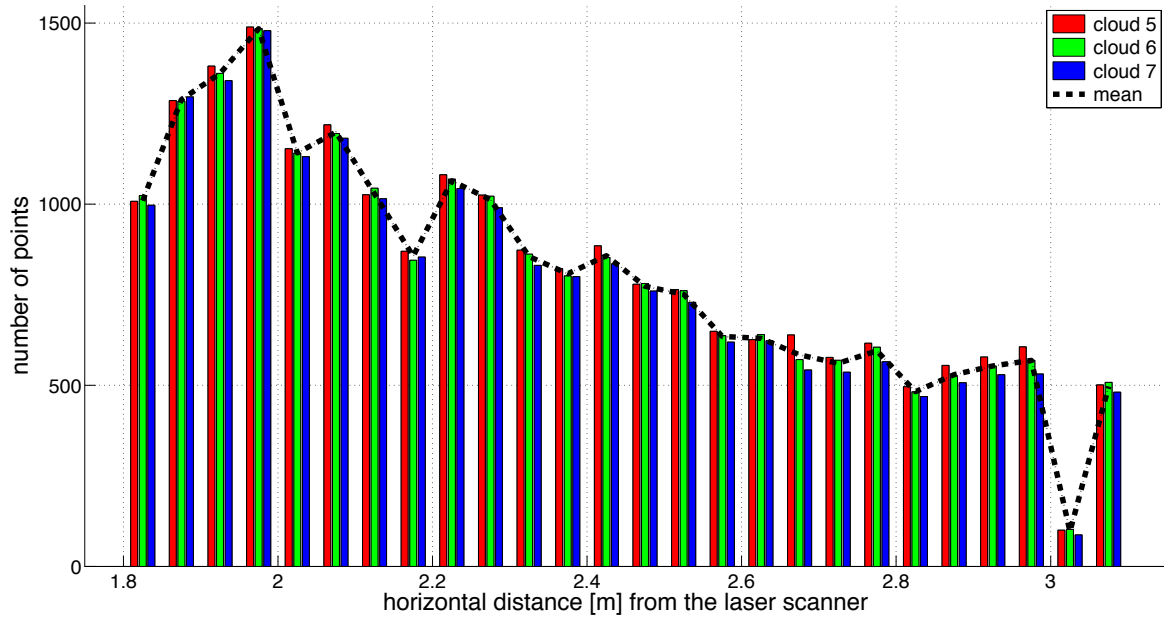


Figure 4.8: Bar plot of the number of points per cell versus the horizontal distance

Overall the number of points decreases with an increase in horizontal range. There do exist some peculiarities. Most of the sudden drops can be explained by the fact that the duct tape and the bottom of the empty pool were not horizontal or flat but rather bumpy. This means that the incidence angle, which is the angle between the laser beam and the duct tape, will vary not only with an increasing horizontal distance but also at the same distance due to this bumpiness. Moreover, where the duct tape lies in the shadow, there will be no return points. The bumpiness is expected to be reduced or to have disappeared when scanning under water because of the weight of the water on the bottom of the pool. Figure 4.9 gives two point cloud views of the duct tape where the bumpiness is visible. The location of the last sudden drop in figure 4.8, around 3 metre from the laser scanner, is the foremost example of the shadow effect as there are almost no return points at this location.

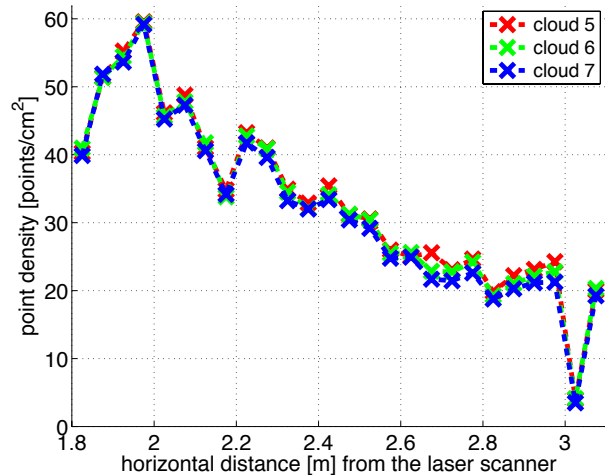
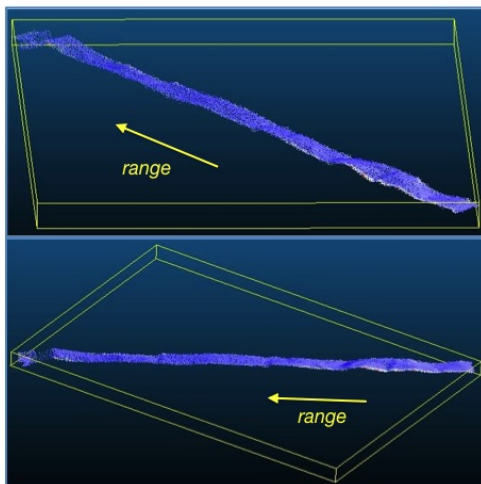


Figure 4.9: Point cloud views of duct tape Figure 4.10: Plot of point density versus horizontal distance

The point density versus the horizontal distance is plotted in figure 4.10. The point density curves of the three point clouds concur well. It can be concluded that the values between 1.8 and 2.4 metre from the laser scanner have a point density that is higher than the average over the whole area, while the point density of points between 2.4 and 3.1 metre is smaller.

What should be noted is that the horizontal distance is rather small, that is from 1.8 to 3.1 metre. If a larger horizontal distance, lets say 1 to 20 metre, would be examined, the resulting point density versus horizontal distance curve is expected to be smoother.

The influence of the cell size on the resulting point density curves is plotted in figure 4.11. Here the point densities of the three point clouds have been averaged for four different cell sizes. The largest cell size, that is the cyan curve, does not have the oscillation that the curves with the smaller cell sizes possess. The cyan curve actually represents the overall trend: with an increase in horizontal distance, the point density will reduce.

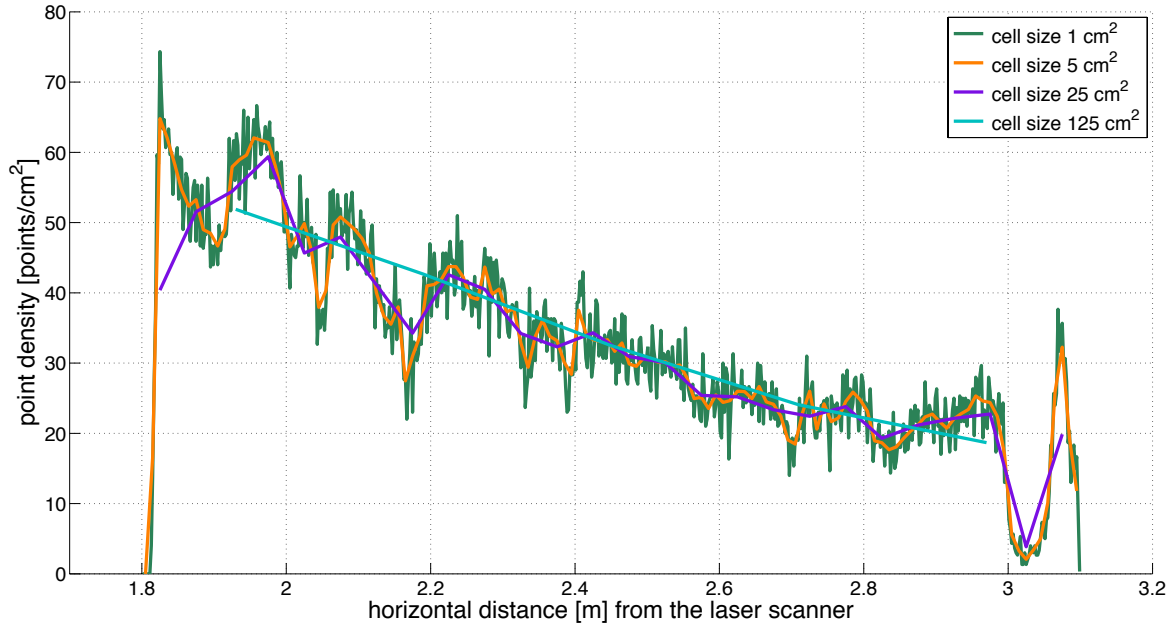


Figure 4.11: Plot of the point density versus the horizontal distance for various cell sizes

4.3 Experiments with different materials, shapes and colours

In this section several objects made of different materials and with several shapes and observed colours have been scanned with custom resolution settings: that is a range of maximum 4 metre and a horizontal and vertical resolution of 1 millimetre. Five different objects have been used, these are listed in table 4.5. The experiments with the coloured glass marbles, the rubber tile and the concrete buddha sculpture have been done both dry and under water while the scans of the dimpled titanium golf balls and the coloured concrete cubes only have been performed under water. Each different experiment will be assessed differently with the assessment criteria as given in section 3.4.

#	target	material	observed colour	shape
9	marbles	glass	blue, black, white, green, yellow	circular
15	golf balls	titanium	white	circular with dimples
1	tile	rubber	green	square; coarse surface
7	cubes	concrete	red, orange, blue, black	cubical
1	buddha	concrete with cord	grey	sculpture

Table 4.5: Overview of the targets with different materials, shapes and colours

The targets in this section will be scanned with a green-wavelength laser scanner. Both the fore-ordained reflectance of these targets according to paragraph 2.1.4 and return intensity values are based on measurements with laser light that has a wavelength of 532 nanometre. In other words, the green 532 nm reflectance of these targets is measured by the laser scanner and expressed in return intensity. The experiments in this section will be discussed in the order of the scan targets in table 4.5.

4.3.1 Coloured glass marbles

Round, with a shiny surface and of different observed colour, that is why the coloured glass marbles have been selected. Eight glass marbles with a circumference of 8.2 centimetre and one smaller marble with a circumference of 5.7 centimetre have been used. The eight larger, shiny marbles have different observed colours: two blue, one black, two white, one green and two yellow marbles. The smallest marble is a more matte black marble with yellow markings on it. Figure 4.12 displays the marbles during the dry scanning. The green laser light is also visible in this picture.

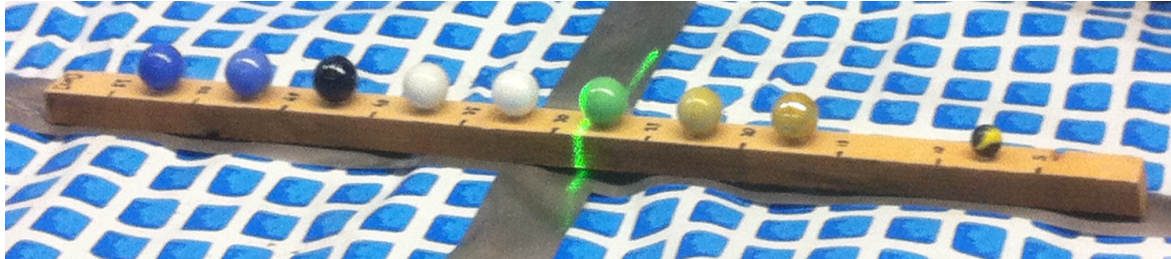


Figure 4.12: The coloured glass marbles during scanning

Both dry and wet scans have been repeated three times. The wet scans were performed under 40 centimetre deep tap water with a turbidity of 0.3 *NTU*. The return parameters of interest are the intensity values and the point densities of the dry versus the wet scans. In figure 4.13 two point clouds of the scans are depicted; on top one of the dry scans and bottom one of the wet scans. The smallest marble, which is located most right, is not visible in the wet scan: there are some return points of the yellow markings but the shape can not be derived from the cloud. In the dry scan the scanner is able to distinguish the observed yellow from the observed black colour of the marble as the set point spacing is much smaller than the marble itself. If the marble would have the same size as the point spacing, it would be impossible to detect differences of the marble as there would be only one laser point on the marble.

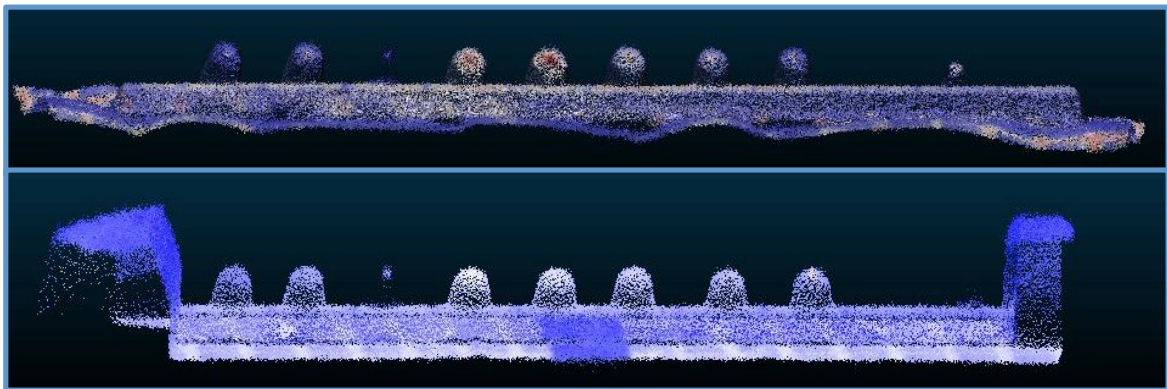


Figure 4.13: Two points clouds of the marbles; top dry scan, bottom wet

From the point cloud in figure 4.13 can directly be observed that the marbles in the wet scan appear to be not round but oval. The black marble, which is the third marble from the left, has only a few return points for both dry and wet scans. The points that have returned on the black marble are due to the shiny surface that all eight marbles possess, however the black colour behind that shiny surface absorbs most of the green laser light so does not reflect back. This corresponds to the illustration of the reflectance spectrum of a standard black object as given in figure 2.5. In this figure the example black object has a reflectance of only a few percent for a wavelength of 532 nanometre.

Furthermore, the returned intensity values concur qualitatively with the reflectance values for a wavelength of 532 *nm* as given in figure 2.5: the observed white marble indeed has the largest intensity values, followed by observed green, yellow, blue and finally black.

With the exception of the smallest marble, each marble is segmented individually from the point cloud, leading to eight marbles per point cloud. There are three dry and three wet point clouds and the intensity values of each marble are averaged over the corresponding data obtained from three clouds, either dry or wet. The resulting mean intensity values for each marble for the wet and dry situation are displayed in figure 4.14. The mean intensity values are overall lower for the wet scans. When putting the marbles under water, they appeared to be less shiny than above the water surface. Because of this effect, the intensity was expected to decrease.

The point densities of the eight larger marbles are computed for each marble for each cloud separately and then averaged to obtain the mean point density over three clouds for each marble and each situation. Figure 4.15 shows the point densities for each marble for the dry and wet scans. The black marble had almost no return points and this is visible in the point density bar plot. The point density decreases when scanning under water due to absorption and scattering. The observed white and green marbles have the highest number of returns and thus the highest point densities. The reflectance of the observed white and green marbles is higher than that of the other marbles at 532 nanometre.

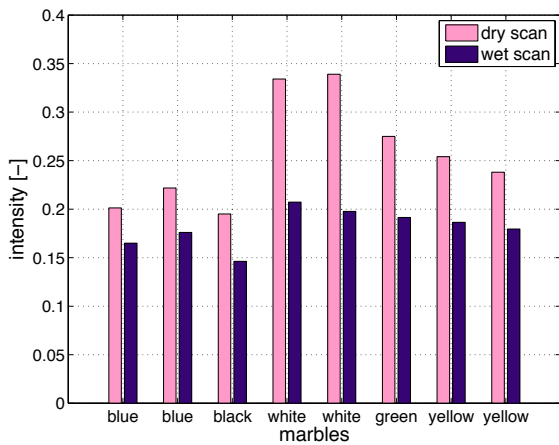


Figure 4.14: Bar plot of intensity values marbles

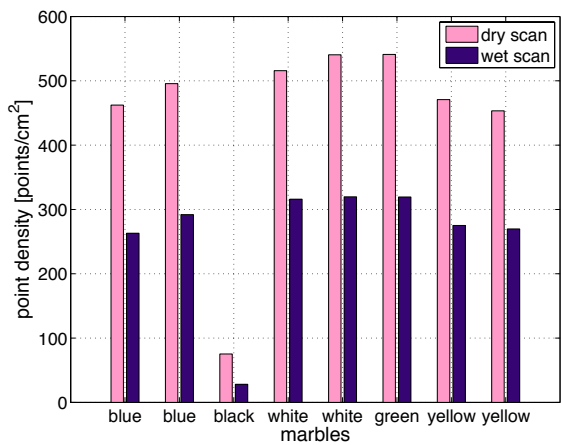


Figure 4.15: Bar plot of point densities marbles

4.3.2 Dimpled titanium golf balls

Fifteen white dimpled titanium golf balls with a circumference of 13 centimetre, neglecting the dimples, have been used in this experiment. The golf balls from figure 4.16 have been scanned under water, in tap water with a turbidity of 0.3 *NTU* and a depth of 40 centimetre, on two separate scan days. The point cloud with the intensity values of the golf balls as shown in figure 4.17 has been corrected for refraction and is then segmented from the bottom of the pool. From figure 4.17 can be seen that the intensity values are largest at the center of each golf ball, to decrease to the edges. This is the edge effect as described in paragraph 2.4.4.



Figure 4.16: Photo of the golf balls

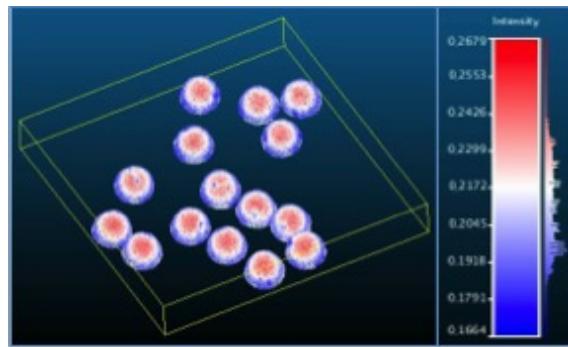


Figure 4.17: Point cloud of the golf balls

The fifteen golf balls have been scanned three times on each scan day, resulting in six point clouds. The second scan day, the golf balls had been in the water for three days and small air bubbles had formed in the dimples. The point densities have been computed for all six point clouds. The point densities for all golf balls and averaged for one golf ball per cloud are given in table 4.6. The golf balls with the small air bubbles in the dimples, which are balls in cloud 21, 22 and 23, have significant smaller point densities. If the point density of one golf ball in cloud 16, 17 and 19 would be 100%, a golf ball with air bubbles would only reach a relative point density of 60%.

<i>golf balls</i>		point density [$points/cm^2$]	
		all 15 golf balls	averaged; 1 golf ball
normal wet scans	cloud 16	1682.65	112.18
	cloud 17	1659.06	110.60
	cloud 19	1669.49	111.30
wet scans with air bubbles	cloud 21	1027.04	68.47
	cloud 22	1008.66	67.24
	cloud 23	1002.93	66.86

Table 4.6: Point densities of the golf balls

The air bubbles cause a part of the laser light to be scattered, or simply lost, in the air bubble causing less return points. At microscopic level, the air bubbles are in fact a third medium. The laser light, starting at the origin of the laser scanner, first travels through air, to be refracted at the air water boundary and then travels through the water to the target. When the laser light reaches an air bubble, the laser light will be refracted again at the water air bubble boundary, to finally reach the target: the golf ball. The dimples are not flat but rounded, leading to diffuse reflection as depicted in figure 2.7, where some of the return rays do not come back as they get reflected within the dimple. This effect is stronger when there are air bubbles present. The third medium causes also a decrease in the power of the signal, which is in fact expressed as the intensity. The intensity values, as given in figure 4.18 are approximately 0.05 smaller for the golf balls with air bubbles. Besides, the clouds with air bubbles have more outliers. Evidently the air bubbles cause the signal to scatter and lose some of its strength at the return of the laser scanning device. The atmospheric and water conditions as well as the lighting was the same at both scan days, thus the air bubbles themselves cause the decrease in intensity values. When examining only the intensity values of the dimples, the intensity values in the dimples decrease with an average of 20% where there are air bubbles located in the dimples.

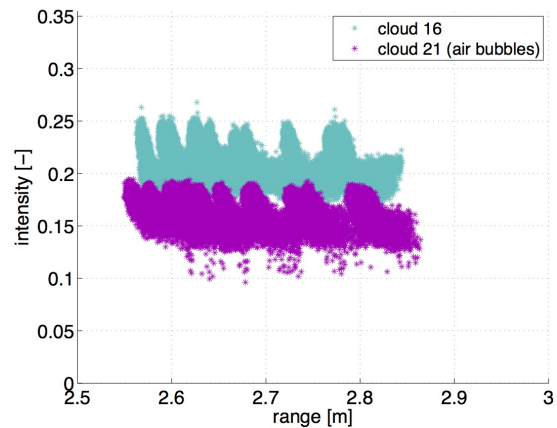
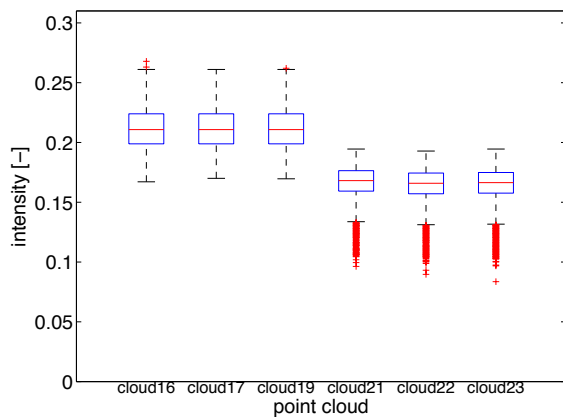


Figure 4.18: Box plot of intensity values golf balls

Figure 4.19: Plot of range vs intensity golf balls

The range versus the intensity is plotted in figure 4.19 for one of the clouds without the air bubbles, which is cloud 16, and one cloud with air bubbles, cloud 21. The other four clouds are not displayed as they correspond rather well with either cloud 16 or cloud 21. The graph follows roughly the same pattern for both clouds. The intensity values decrease slightly with an increase in the range, where the range is the distance between the origin of the laser scanner and a point. The intensity values were significantly smaller for the cloud with air bubbles, however the pattern of intensity versus the range is the same.

4.3.3 Green rubber tile

A green rubber tile was chosen because it is expected to reflect better than for example a red tile at a wavelength of 532 nm . The rubber tile has a coarse surface as is visible in figure 4.20. The tile has been scanned both dry and under water to compare the return signal. The wet scans were performed with a water mixture of 75% clean water and 25% Schiewater, so a turbidity of 1.3 NTU , and a water depth of 40 centimetre. Figure 4.21 displays the result of the dry scan of the rubber tile in the screen of the Leica C10 during scanning. The corresponding point cloud of this scan, displaying the intensity values, is depicted in figure 4.22. The wet point clouds have first been corrected for refraction and all of the point clouds have been segmented from the flooring beneath it to obtain solely the tile for comparing the dry and wet situation.

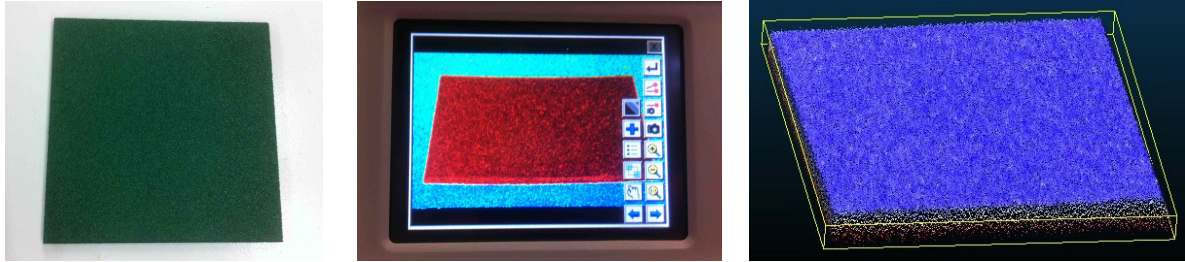
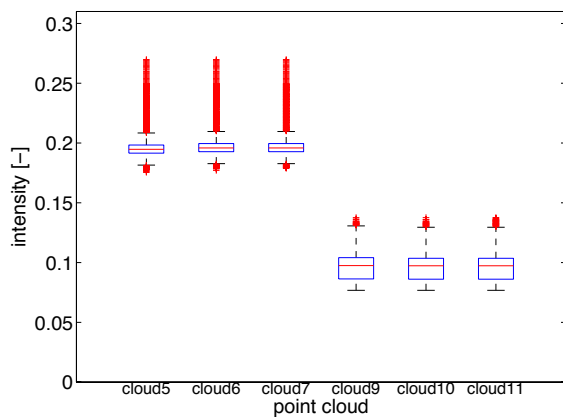


Figure 4.20: Photo of tile Figure 4.21: Tile in screen Leica Figure 4.22: Point cloud of tile

The intensity values of the rubber tile are displayed in figure 4.23, where cloud 5, 6 and 7 are the dry and cloud 9, 10 and 11 are the wet scans. The large amount of outliers can be explained by looking at the point cloud in figure 4.22. Only the front and parts of the left and right sides are visible for the laser scanner, the back side is in the shadow of the tile thus gives no return value. The higher intensity values from the sides of the tile are the outliers as displayed in figure 4.23. These outliers are possibly caused by the backscatter from the white flooring. When scanning through the water this effect did not occur and it was not visible in the resulting point clouds, causing less outliers in figure 4.23.

Further the mean intensity values of the wet tile were lower than the mean intensity values of the dry tile. The reason for this decrease is, beside the signal losses in the water, that the tile became saturated with water. The tile absorbed water and reflected less in this state. By eye this effect could be noticed by the change in colour as the tile appeared to be darker. The absorption effect can be distinguished from the signal loss in the water by scanning the tile in wet state without the media water. This experiment has not been performed however.



<i>rubber tile</i>		point density [$points/cm^2$]
dry	cloud 5	163.58
	cloud 6	163.44
	cloud 7	163.37
wet	cloud 9	51.97
	cloud 10	45.53
	cloud 11	47.42

Table 4.7: Point densities of the rubber tile

Figure 4.23: Box plot of intensity values tile

The point densities for the six point clouds are given in table 4.7. If the point density of the dry tile is set to 100%, the wet tile would only have a relative point density of 30%. This is mostly due to the effect of the turbid water, where part of the signal was lost. The other cause was thus that the tile absorbed water and reflected less in wet state than was the case when the tile was dry.

4.3.4 Coloured concrete cubes

Seven concrete cubes with different colours observed by human eye are scanned. Of the seven cubes, two are red, two blue, two black and one is yellow/orange. The edge length of the red, orange and blue cubes is 2.5 and the edge length of the black cubes 1.8 centimetre. Figure 4.24 pictures the cubes.



Figure 4.24: Photo of the seven coloured concrete cubes

The cubes were scanned under tap water with a turbidity of 0.3 *NTU* and a depth of 40 centimetre. Of the seven cubes, only the yellow/orange one was fully visible in the three resulting point clouds. This cube thus had the largest reflectance for green laser light with a wavelength of 532 nanometre. The two blue cubes had only a couple of return points but a shape could not be detected. The red and the black cubes were not visible at all, there was a hole in the cloud where these four cubes were located. That the two black cubes would not be visible was to be expected based on the example reflectance curve in figure 2.5. However the lack of points for the red and blue cubes was not expected as the experiment with the blue marbles in paragraph 4.3.1 did give back returns. The water depth and water and atmospheric conditions were the same for both the experiments with the cubes and the marbles. The observed colours did differ of course, as this observation of colour is by human eye and thus not exact. However there were no return points for the red and blue cubes while it is expected that a glass marble of the same colour would give returns. It can thus be concluded that the material plays an important role when scanning through water with a green-wavelength laser scanner. The marbles are made of glass and had very reflective surfaces, while the cubes are made of concrete and had matte surfaces. The laser light was mostly to fully absorbed by all of the cubes except the yellow/orange one. The cubes have only been scanned under water. If the experiment would be done dry it is expected to have sufficient return points for all.

The intensity value of the yellow/orange cube has been averaged for each point cloud, leading to three values: 0.1301, 0.1296 and 0.1307. These intensity values are really close to each other so there is not much difference between the three scans. There were some outliers and these were at the same location as was the case with the rubber tile, that is the sides had lower intensity values than the top.

4.3.5 Concrete buddha sculpture

A sculpture in the form of a buddha has been used to determine whether the laser scanner can distinguish the details of such a sculpture. The buddha sculpture is made of smooth concrete and has a cord on top. Figure 4.25 displays a photo of the buddha sculpture and the point cloud of the dry scan is displayed in figures 4.26 and 4.27.

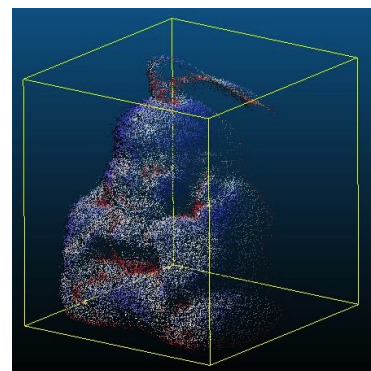
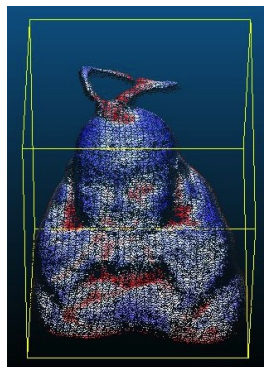


Figure 4.25: Photo of buddha Figure 4.26: Point cloud buddha Figure 4.27: Point cloud buddha, side

The point clouds of the dry scan as depicted in figures 4.26 and 4.27 show the carving and cord rather well. The photograph of the buddha displays some white chalk markings and at these locations the intensity values are higher than at the darker parts of the concrete buddha sculpture. Laser scanning is often used for the scanning of detailed historical objects and the dry experiment shows that the Leica C10 laser scanner is also able to detect these details when scanning through air.

The buddha has also been placed under water with a depth of 40 centimetre. The water consisted of a water mixture of 75% tap and 25% Schiewater and had a turbidity of 1.3 *NTU*. Based on figure 2.4, the reflectance of concrete is approximately 25% for a wavelength of 532 *nm*. The dry scan provided satisfying results concerning the shape of the sculpture, however when scanning the buddha under water the results were less promising. The buddha has been scanned three times under water. After the correction for refraction the buddha has been segmented from the point cloud. The intensity values of the four clouds, one dry and three wet, are given in the bar plot in figure 4.28. As the intensity values vary due to the white chalk, the minimum and maximum intensities have also been plotted besides the mean intensity. The intensity values of the dry cloud, which is cloud 2, had overall higher intensity values than the three wet clouds. This is again because the intensity values represent the power of the return signal and part of this is lost when scanning through the turbid water. The three wet scans concur rather well.

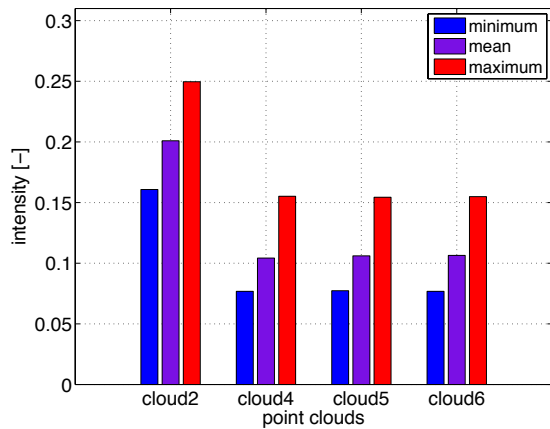


Figure 4.28: Bar plot of intensity values buddha

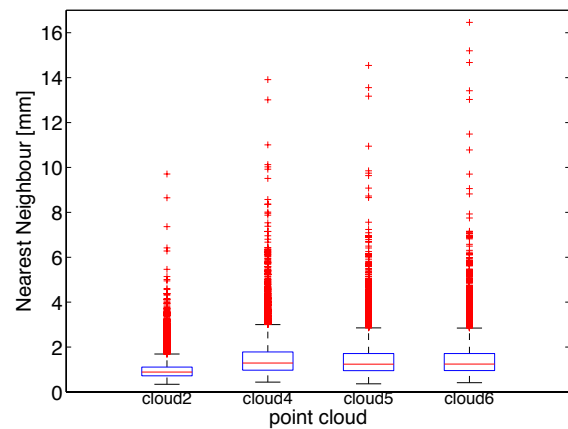


Figure 4.29: Box plot of point densities buddha

The point density, expressed as the nearest neighbour distances, are plotted in figure 4.29. Not surprisingly, the dry scan has smaller NN values. There are rather a lot of outliers and these are because of the cord on top. The mean nearest neighbour values of the wet scans compared to the dry one do not differ much, leading to the conclusion that the point density of the wet buddha is sufficient so the buddha can also be detected under water. However, if the number of points of the dry buddha are set to 100 %, the number of return points of the buddha under water is only 30%. Not all the details can thus be recognised, as can be seen when comparing figure 4.31 with figure 4.30.

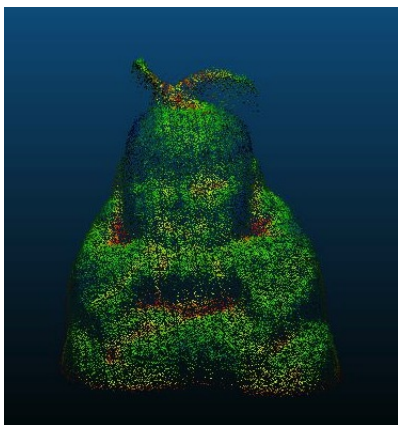


Figure 4.30: Point cloud of the dry buddha

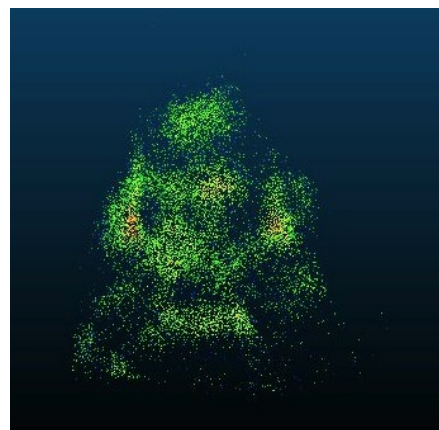


Figure 4.31: Point cloud of the wet buddha

4.4 Experiments simulating the outdoor environment

The experiments in this section simulate the outdoor environment. The different scan targets from table 4.8 are all natural objects: objects that can be found in nature or in the outdoor built environment. The experiment with the rocks has been done both dry and under water while the experiments with the water plants and the sand only have been performed under water. The measuring pole has been partly submerged in the water. The sand scans have been done with varying water levels and the experiments with the wooden measuring pole have been performed with varying water levels and varying turbidity.

#	target	material	observed colour	shape
1	measuring pole	wood	brown	rectangular
28	rocks	metamorphic rock: slate	grey	irregular; angular
-	beach sand	shell sand	beige	granular sand with seashells
1	Anubias	water plant	green	multiple stems, cordate leaves
1	Echinodorus	water plant	green	multiple stems, linear leaves

Table 4.8: Overview of the targets from the outdoor environment

4.4.1 Wooden measuring pole with varying water level

A wooden measuring pole has been used throughout the basic experiments. The wooden pole has been selected by segmentation from the scans with varying water level with water consisting of a mixture of 75% tap water and 25% Schiewater. The four water levels were 40, 20, 10 and 5 centimetre above the bottom of the pool. The measuring pole was partly under water, and the effect of the refraction is clearly visible in the uncorrected scans. Figure 4.32 displays the wooden measuring pole before and after the correction for refraction for a water depth of 10 centimetre.

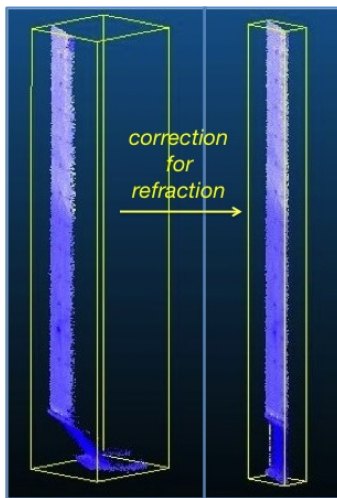


Figure 4.32: Pole before/after correction

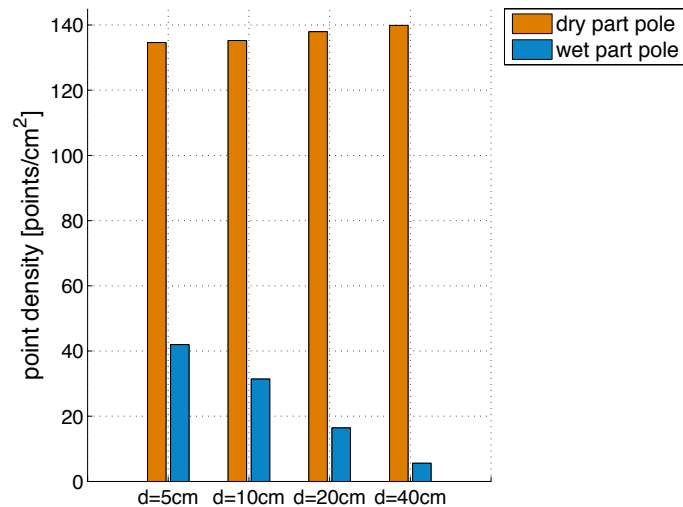


Figure 4.33: Bar plot of point densities wooden pole

The width and length of the wooden pole has been measured, resulting in an area that can be used to determine the absolute point density. The point density is computed for the dry part of the pole and for the wet part that lies under water. The point densities are plotted in figure 4.33. The four dry point densities are roughly the same. The four wet point densities follow a trend that was expected: the point density will decrease when increasing the water level. The point densities of the under water part are 42, 31, 16 and 6 *points/cm²* respectively. If the point density is plotted versus the water depth, the fitted least squares line of these four values will give a trend of -0.9914. The point density of a vertical wooden pole is thus reduced with approximately 1 *point/cm²* for an increase of water depth of 1 centimetre. This least squares trend value applies to this experiment, so for a wooden measurement pole in water with depths ranging from 5 to 40 centimetre and a turbidity of 1.3 *NTU*. In order to validate this obtained trend value, more research on vertical targets in water is required.

The recorded intensity values of the wooden measuring pole are expected to be different for the wet and dry part of the pole. The mean intensity of the wet pole is smaller due to the lower reflectivity when the pole is wet. This is because in wet state, the pole absorbed water and is less reflective. Figures 4.34 and 4.35 display the intensity values for both the wet and dry part of the wooden pole. The water depth was 40 centimetre so above this level the pole was dry. The number of return points for the wet part was much smaller than the dry part which can also be read from figure 4.33. The mean intensity of the wet pole is about half of that of the dry pole. What stands out is that the standard deviations of the intensity do not differ that much for the smooth wooden pole. Other research has shown the same result: for materials with a low reflectivity the standard deviation of the dry versus the wet intensity is negligible small [23]. The wooden measuring pole, that can be identified as bark in figure 2.4, indeed has a low reflectance, either dry or wet.

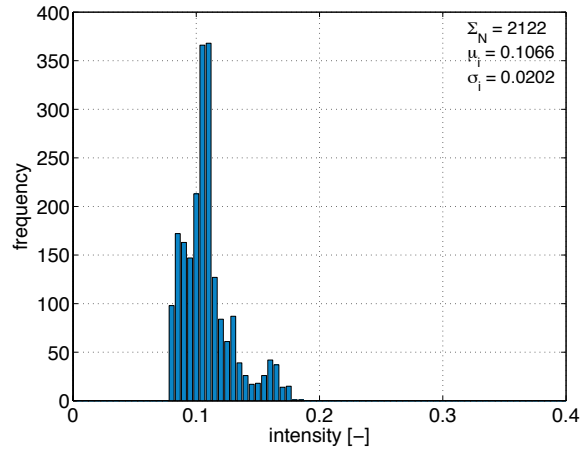
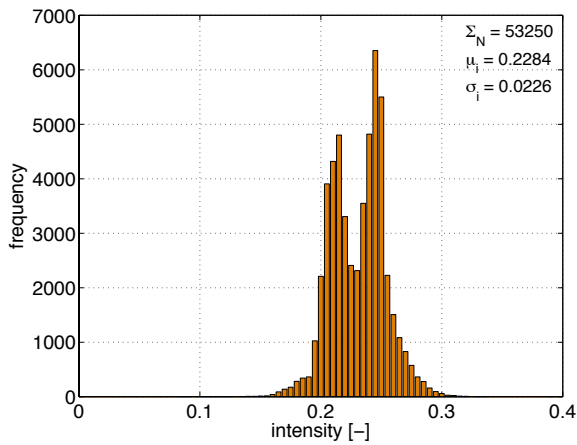


Figure 4.34: Bar plot of intensity values - dry pole Figure 4.35: Bar plot of intensity values - wet pole

The returns of the pole under water expressed as a percentage of the total number of returns are plotted in figure 4.36 for the four water depths. The zero at the y-axis indicates the water level. As can be seen, just below the water surface there is a peak, while at the middle part of the pole the number of returns is very small and close to the bottom of the pool there is another peak. An exception is the pole in water with a depth of 40 centimetre where there are only returns at the upper part of the pole.

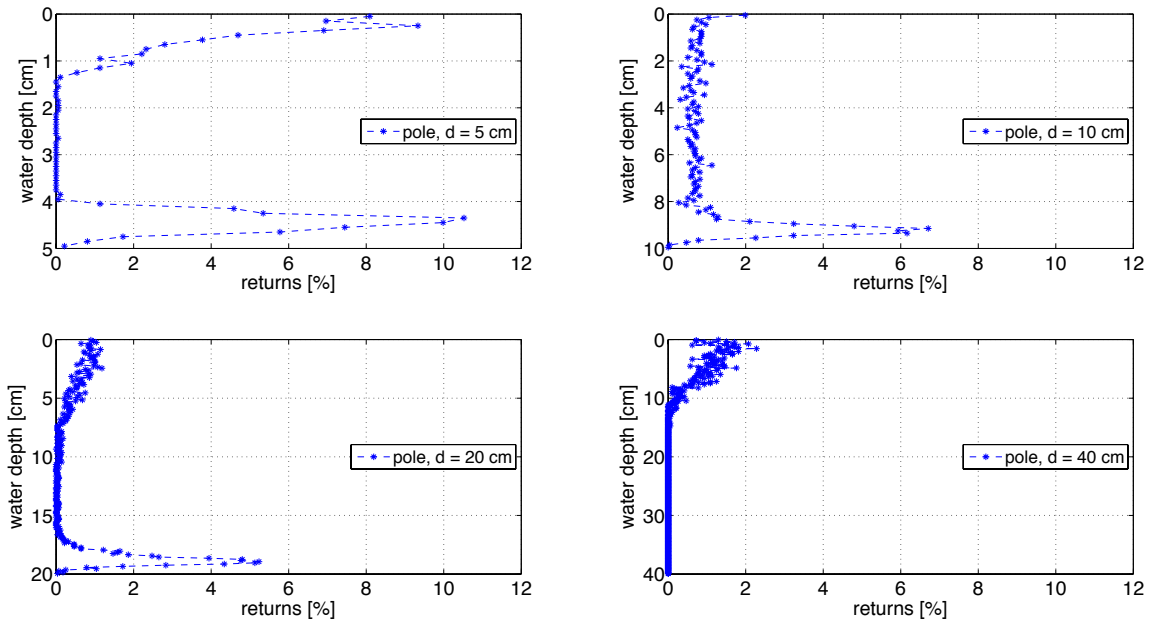


Figure 4.36: Returns of the wet part of the pole for different water depths

The most points are lost at the middle part of the pole for each situation. The pole in the deepest water, that is 40 centimetre, has no return points after a water depth of 12 centimetre, while the pole in 20 centimetre water has return points up to the bottom. The peak at the bottom is likely to be caused by the reflective bottom of the pool itself, which was almost illuminating, causing light to be reflected onto the wooden pole. The peak close to the bottom of the pool is not present for the pole in the largest water depth, as there are no points at the bottom in this situation.

The large number of returns close to the water surface, that is at the zero at the y-axis, is due to the effect of refraction. At the air water boundary the ray of light is refracted. However this is not as straightforward as depicted in for example figure 2.3. When considering the refraction of light at a small scale, there is in fact a transition zone exactly at the boundary. The transition zone can also be detected in the point cloud in figure 4.32, where the air water boundary is clearly recognised by the distortion at this boundary. The distortion is mainly caused by diffuse scattering at the boundary so the ray of light is scattered in multiple directions.

4.4.2 Wooden measuring pole with varying water turbidity

The second experiment concerning the wooden measuring pole is the experiment where the water depth was constant at 40 centimetre and the turbidity varied. Four different water turbidities, as given in table 4.1, have been applied by using tap water and/or water from the Schie. The pole has been selected out of the point clouds, is then corrected for refraction and finally segmented in order to obtain only the pole itself. The intensity values for the four water turbidities are given in figure 4.37.

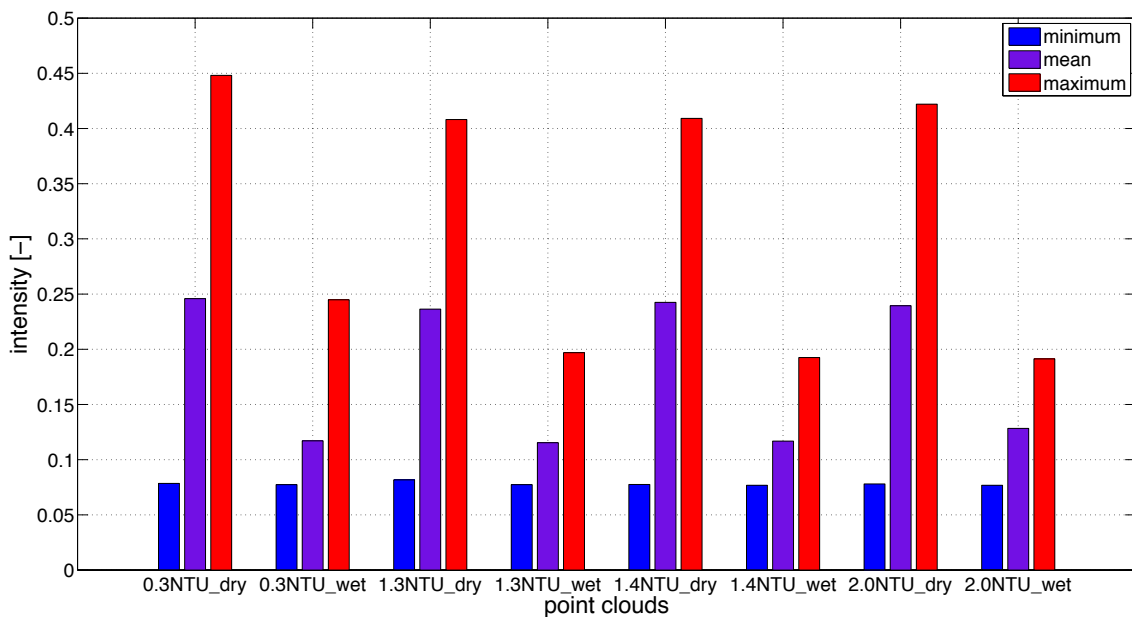


Figure 4.37: Bar plot of the intensity values of the wooden pole for different turbidity values

What stands out in figure 4.37 is that the mean intensity values for the wet pole are somehow constant at 0.12, even though the turbidity increases. So the turbidity of the water has almost no influence on intensity, which is the power of the return signal, in the case of scanning the vertical wooden measuring pole. The intensity values thus did not decrease when using more turbid water in the range of 0.3 to 2.0 NTU. The point densities of the wet part of the pole however did decrease when using more turbid water: from a point density of 52.90 *points/cm*² for a turbidity of 0.3 NTU to 4.35 *points/cm*² for 2.0 NTU. The values between, for a turbidity of 1.3 respectively 1.4 NTU were 10.23 respectively 6.71 *points/cm*². The largest decrease in point density is thus the part between the tap water and the mixed water with a turbidity of 1.3 NTU. Between the water with turbidities of 1.3 to 2.0 NTU this decrease was less significant. The turbidity of the water is thus of importance for the number of return points but is of less importance for the returned intensity values for a wooden measuring pole with water depth 40 centimetre and in the turbidity range of 0.3 to 2.0 NTU. The intensity is actually a measure of received signal power that is scaled from 0 to 1 by the Leica C10.

The intensity values are plotted versus the height of the pole in figure 4.38. As the water level is also plotted in figure 4.38, it becomes clear that in case of a higher turbidity, there are less return points deeper into the water. For the three datasets with turbidities larger than 0.3 *NTU*, there are only return points at the upper part of the submerged pole. Only the dataset with the cleanest water with a turbidity of 0.3 *NTU* has returns at the bottom of the water body, that is at a height of zero in figure 4.38. So the maximum water depth that provides results is 0.1 metre for a turbidity of 2.0 *NTU*. For the dry part of the pole, the dataset with a turbidity of 1.3 *NTU* has no values above 0.8 metre height. This can be explained by the scan settings: this particular dataset has been segmented from a point cloud that did not include the top of the pole in its field of view scan settings.

An interesting feature of the scatter plot as displayed in figure 4.38 are the intensity outliers that are located above the water level at every 5 centimetre. These are in fact the markings on the pole that indicate the water level. The markings have been written by hand with a black marker, and thus have a lower intensity than the unmarked parts of the pole. The markings on the pole are also visible in the point cloud of the pole next to the plot in figure 4.38. These markings are also present under water, however here they can not be distinguished from the return signal.

In figure 4.38, the minimum recorded intensity is also given. There are no intensity values recorded that have intensities lower than 0.075. In other words, the minimum return power of the signal is 0.075. This can thus be seen as the threshold value: only points with intensities larger than 0.075 will be recorded. It is very likely that there are points present that have an intensity smaller than 0.075. As can be seen from figure 4.38, the points that lie below the water level suddenly break off close to this threshold value: the recorded points show a vertical line that is not present anywhere else in the plot. This threshold value for the return power is a feature of the Leica C10 laser scanner so for other laser scanning devices there may be other threshold values.

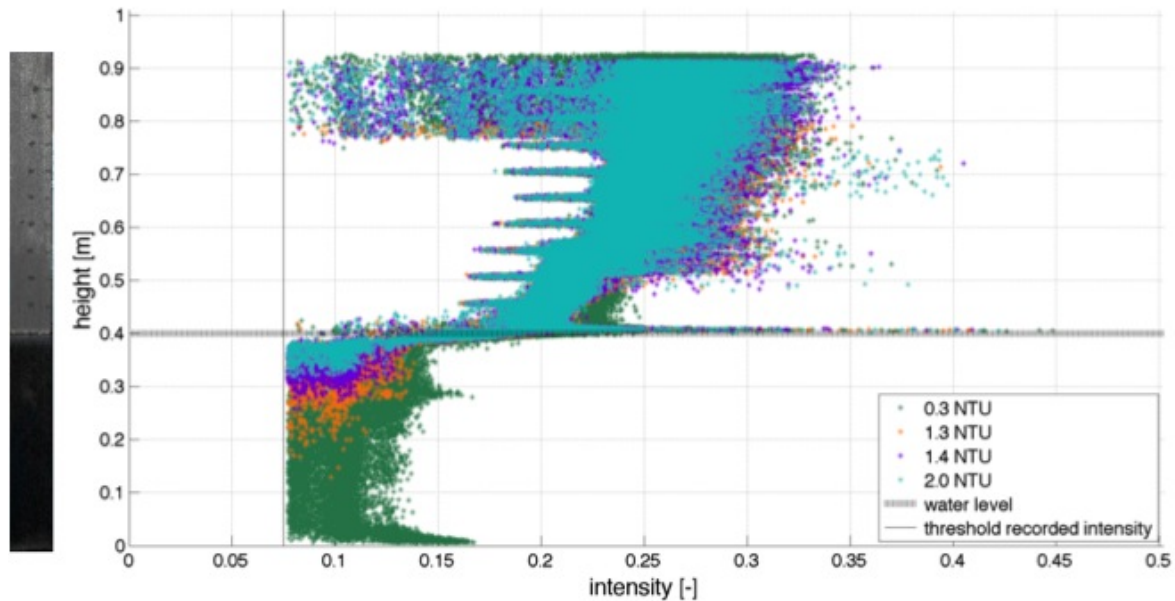


Figure 4.38: Scatter plot of the intensity values versus the height and point cloud of the wooden pole

The ray of light travels through both the air and water before reaching the underwater target. The part travelled through air does not have an influence like the part travelled through the water does have on the return signal. Therefore, the influence of the travelled range through water is examined further. The range of the light through the water has been computed for each point on the pole that is below the water surface. This range has been plotted versus the corresponding intensity values for each point. The resulting plot is presented in figure 4.39.

Obviously, the scans with the less turbid water had more measurement points, N . For a water turbidity of 2.0 NTU , there were no return points of the pole from 10 centimetre from the water surface or deeper. This can also be seen from figure 4.38. The maximum range through water for a water turbidity of 2.0 NTU was 24.8 centimetre. For water turbidities of 1.4 and 1.3 NTU the maximum range through the water that did give results are 32.9 respectively 58.6 centimetre. The maximum range through water for the tap water is 80.8 centimetre. The largest difference is thus between the water sample consisting of clean drinking water with a turbidity of 0.3 NTU and the other three water sample. Between the other three more turbid samples the turbidity is less influential.

When plotting the turbidity values versus the corresponding maximum range through water, a trend of -0.3375 can be computed from the fitted least squares line. So the range through water decreases with $0.3375 \text{ metre}/NTU$. This trend value needs to be validated, which again can be investigated in further research. However what can be stated based on this experiment is that before scanning vertical objects that are partly submerged in water, the water turbidity should be considered: only clear waters will provide sufficient returns when scanning with the Leica C10.

All four datasets have the same pattern in figure 4.39: a quick decrease in intensity at the first 0.05 metre range through the water, to become steady around a mean intensity of approximately 0.1 after the first 0.05 metre. So the intensity values of the upper part of the submerged pole are distinctively larger than the intensity values that are obtained from a ray of light that travelled more than 5 centimetre through the water.

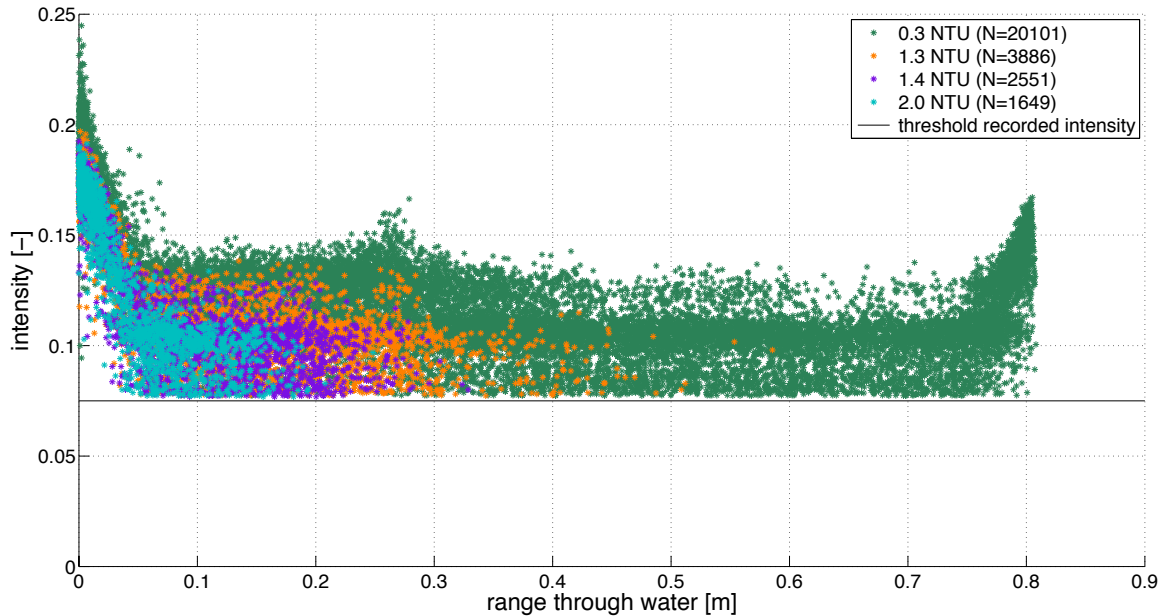


Figure 4.39: Scatter plot of the intensity values versus the range through the water

The scattered points of the four water samples as displayed in figure 4.39 have been averaged into bins of 0.5 centimetre to obtain a better view of the graph. Figure 4.40 shows the four resulting graphs. All of the four graphs indeed show a steep decline at the first part that the laser beam travels through the water, that is from 0 to 0.055 metre range through the water. When fitting a least squares line through the points for this part of the range, the trend is -1.4 m^{-1} for all four water samples. The only difference appears to be that the cleanest water has higher intensity values. Interestingly, the intensity values of the three more turbid water samples did not differ much.

In figures 4.39 and 4.40 a line at an intensity of 0.075 is also plotted. This is again the lower boundary, or threshold, of the intensity that the Leica C10 will record. This intensity can also be read off from figure 4.38. So all points that have a return signal power of 0.075 or lower will be ignored and these points are therefore not recorded.

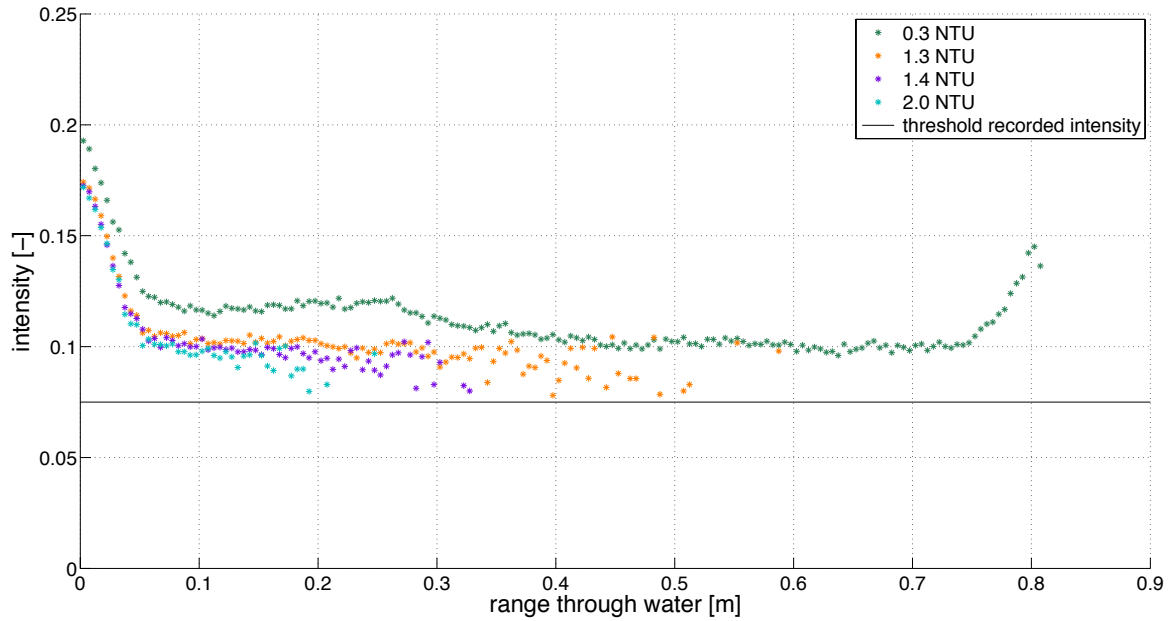


Figure 4.40: Scatter plot of the intensity values versus the range through the water - binned

4.4.3 Metamorphic rocks

Rocks are often present in nature and the built environment. The type of rock used in this experiment are metamorphic rocks of the type slate. Metamorphic rocks are rocks that are formed by change like heating or pressure, as metamorphism means change in form. The 28 rocks that have been scanned are natural raw rocks and all have a different size and shape; overall they are irregular and their shape is somewhat angular.

The dry setting of the rocks are pictured in figure 4.41 and the resulting point cloud showing the intensities are displayed in figure 4.42. The dry scan of the rocks has been repeated three times in order to assess the point precision. The closest distance set is computed where the smallest point cloud was the compared one. After this computation, the RSEV is computed with the formula as given in paragraph 3.4.4. The three RSEV values are between 9.5 and 12.8 millimetre and have a mean of 11.4 millimetre. The RSEV is higher than would be the case when scanning a flat plane. The irregularity of the rocks cause the RSEV to increase compared to a plane: due to this irregularity scanned points may shift a little when repeating the scan. For example in the first scan the point is exactly at the edge of one rock while at the second scan it has moved a few millimetre.



Figure 4.41: Photo of the metamorphic rocks

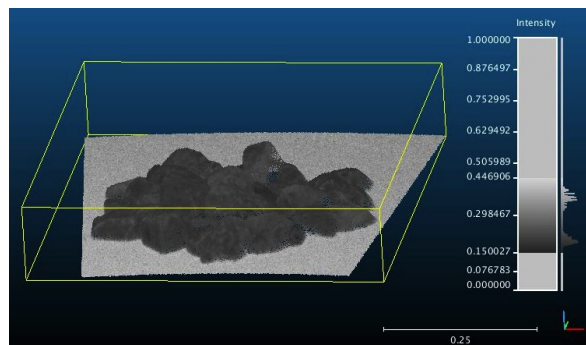


Figure 4.42: Point cloud of metamorphic rocks

The rocks have also been put in the pool and scanned under water that consisted of a water mixture of 75% tap and 25% Schie water. The results however were poor: the dark coloured rocks are not visible through water with a depth of 40 centimetre and a turbidity of 1.3 *NTU*. Figure 4.43 displays the resulting point cloud of the under water scan. As can be seen, the bottom of the pool is visible but where the rocks are located there are almost no points available, where the dry rocks in figure 4.44 are clearly visible. If in both clouds only the rocks are selected without surroundings, the fraction of return points or relative point density, of the wet rocks is only 2% compared to the dry rocks.

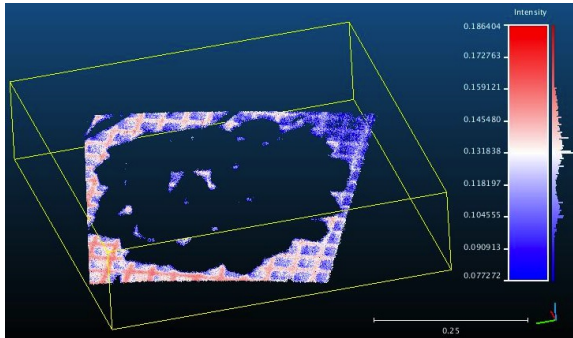


Figure 4.43: Point cloud of the rocks under water

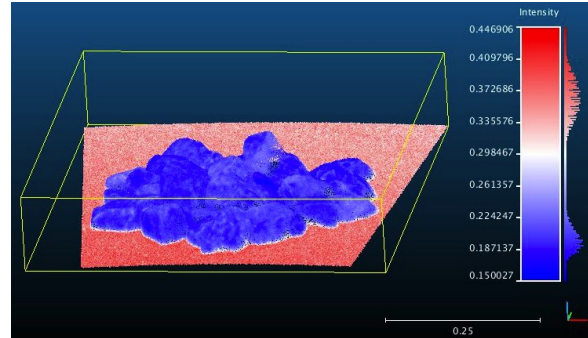


Figure 4.44: Point cloud of the dry rocks

The conclusion that can be drawn from this experiment is that dark grey rocks under 40 centimetre of water with a turbidity of 1.3 *NTU* are not visible in the resulting point cloud when scanning with the Leica C10. The rocks were visible when scanning dry. When the rocks were submerged in the water, the observed colour of the rocks changed: they got darker by eye. The rocks thus absorb water and in this wet state have a lower reflectance than in dry state. This absorption effect in combination with the water conditions caused the wet rocks to give no returns. The absorption effect can be quantified by scanning first the dry and then the wetted rocks through air in further research. A laser scanner that is more powerful, so a laser with higher pulse energy, may be able to see the rocks through these water conditions. The Leica C10 however did not record the rocks when submerged under turbid water with a water depth of 40 centimetre.

Last the surface roughness of the dry metamorphic rocks can be computed given the kernel size, which is in this case the search radius between one object and the other. When using grains of sand, the kernel size is the amount of spreading between the grains. In the case of the irregular rocks, surface roughness plots with kernel size of $k = 0.01$ respectively $k = 0.1$ have been created as shown in figure 4.45 respectively 4.46. The irregular shapes of the rocks are better visible in the case of $k = 0.01$, while the larger kernel size provides a surface roughness that is more smoothed. Due to the differences in rock size and the irregular shapes the kernel size itself varies. Both sizes are acceptable, however the smaller one is preferred as the resulting roughness image also depict the shapes of the rocks.

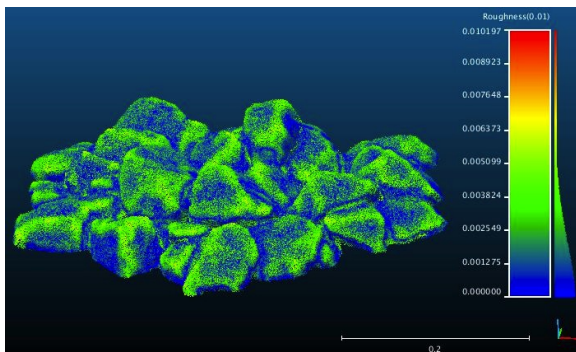


Figure 4.45: Surface roughness rocks $k = 0.01$

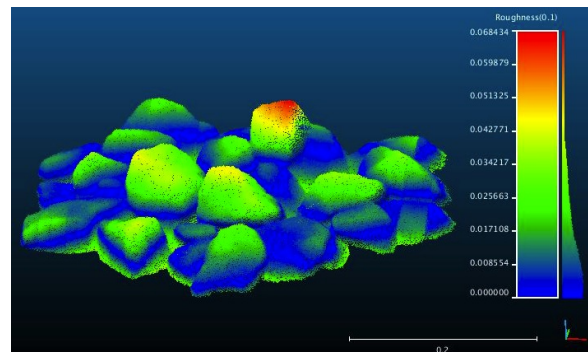


Figure 4.46: Surface roughness rocks $k = 0.1$

4.4.4 Beach sand with varying water level

A bucket filled with beach sand from the Dutch coast is spread over quadrants 1 and 2 in the pool before the pool is filled with water. The water consists of a water mixture of 75% clean water and 25% Schiewater and has a turbidity of 1.3 *NTU*. Scans with a different water level, that is 40 centimetre, 20 centimetre, 10 centimetre and 5 centimetre have been executed, resulting in four point clouds. Figure 4.47 shows the beach sand in the pool with a water depth of 5 centimetre, while figure 4.48 displays the beach sand point cloud that is corrected for refraction under 10 centimetre deep water.

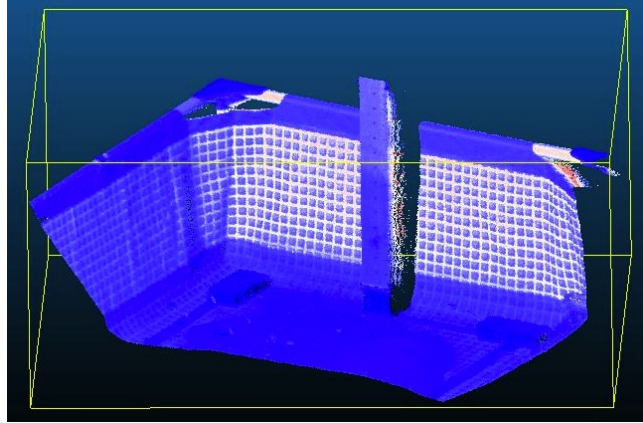


Figure 4.47: Photo of beach sand, depth 5 *cm* Figure 4.48: Point cloud of beach sand, depth 10 *cm*

The correction of refraction is applied to the four point clouds and then the beach sand is segmented from the corrected point cloud. In the segmented points clouds the two red bricks at the corners of the duct tape are also partially included. These red bricks can be seen in figure 4.47. For each water level, a scatter plot of the height from the bottom of the pool, or bathymetry, is made, these are displayed in figure 4.49 up to and including 4.52.

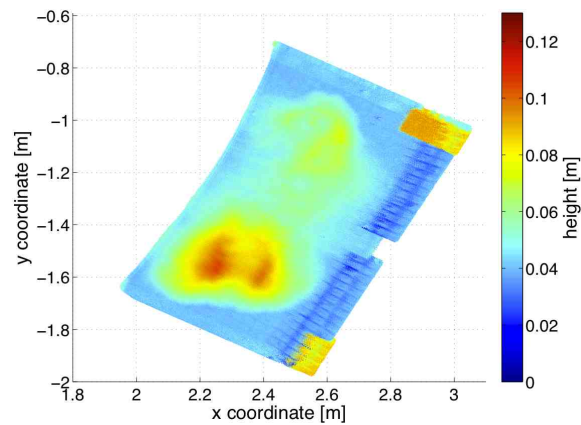
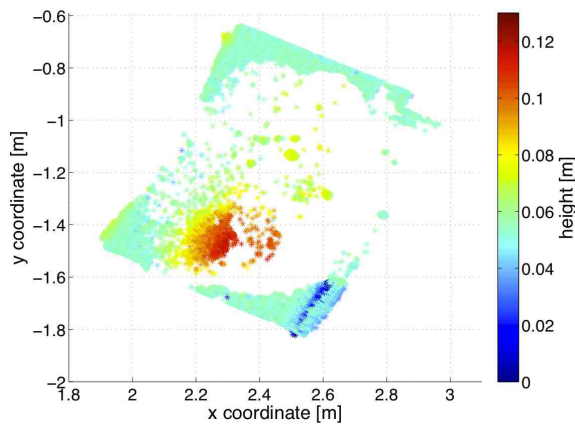


Figure 4.49: Scatter plot beach sand, depth 40 *cm* Figure 4.50: Scatter plot beach sand, depth 20 *cm*

The scatter plot in figure 4.49 for a water depth of 40 centimetre displays a large amounts of holes, where there are no points. None of the red bricks are visible. The turbidity in combination with the water depth and the poor reflectance are the cause for the lack of return points. The reflectance of the targets for a green wavelength of 532 nanometre is the main issue. As can be seen there is a adequate number of return points for the bottom of the pool, which is highly reflecting white with light blue. The reflectance of the bottom of the pool is thus larger than the reflectance of sand. The latter can be read of from figure 2.4 for a wavelength of 532 *nm*. The preordained reflectance of the material that is submerged under water is thus essential for the return signal.

The datasets with a depth of 5, 10 and 20 centimetre water depth do provide return values for the beach sand. As can be seen, the two scatter plots in figures 4.51 and 4.52 look quite similar. Only the dataset with a water depth of 40 centimetre has holes in the data. Concluding the low reflectance of sand combined with the loss of signal due to the water depth and the turbidity cause the lack of return points for sand. The other three scatter plots with a lower water level do not have this problem as the signal in these cases experiences less absorption and scattering due to the depth than is the case with a depth of 40 centimetre. Therefore it is recommended to scan shallow waters and targets that have a higher reflectance than the beach sand used in the lab, for example sand that is whiter.

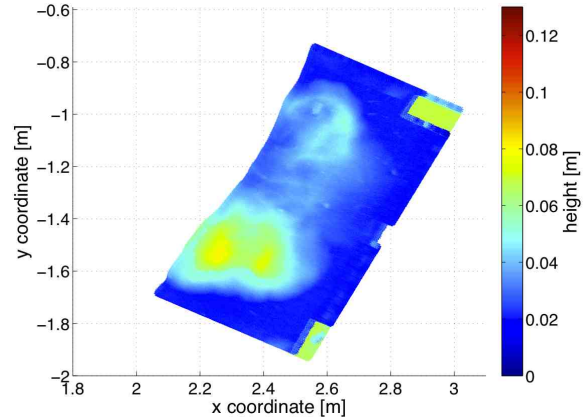
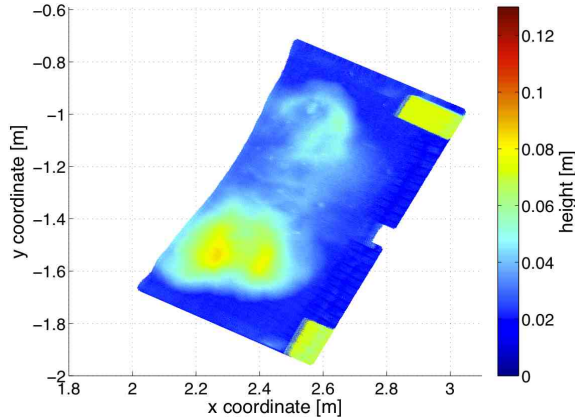


Figure 4.51: Scatter plot beach sand, depth 10 *cm* Figure 4.52: Scatter plot beach sand, depth 5 *cm*

In order to assess the bathymetry differences when scanning through water with varying water depth, the height differences have been computed. First two closest distance point cloud sets have been computed according to the method described in paragraph 4.2.2, to link the corresponding points in the set of clouds. The height differences are computed between clouds with water depths 20 and 5 centimetre as shown in figure 4.53, and between 10 and 5 centimetre as shown in figure 4.54. Overall the differences are small: for the first set of clouds the average bathymetry height differences are 9 millimetre, and for the second set of clouds only 3.6 millimetre. These small differences in the order of millimetre may be caused by the shifting of the sand when pumping the water out of the pool.

The recorded bathymetry is thus quite accurate for water depths up to 20 centimetre under these water conditions in laboratory settings. If the part of the sand that is above the water surface in the dataset with the smallest water depth is set as a base, the differences between this dry part and the same but submerged area can be derived. The difference between the dry part of the sand and the part that is submerged under 20 centimetre of water is only 4 millimetre on average, while the bathymetry differences between the dry and submerged under 20 centimetre of water is even smaller, that is 2 millimetre. The resolution setting was 1 millimetre for the vertical position accuracy so the found results prove that the bathymetry of sand can be scanned with an accuracy in the order of millimetre.

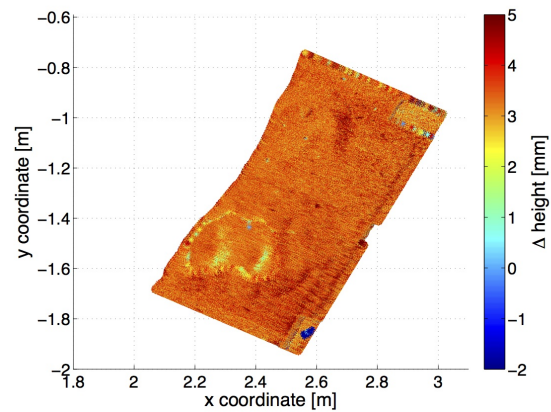
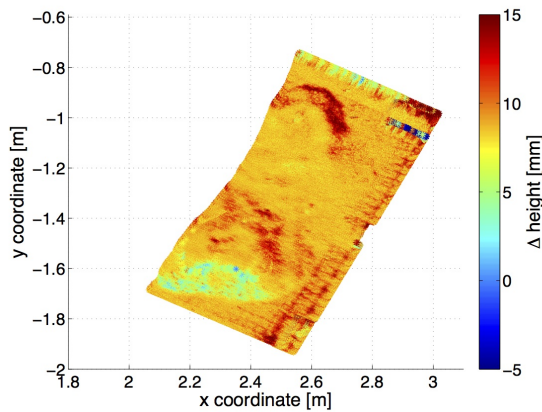


Figure 4.53: Scatter plot beach sand, Δh_{d20-d5}

Figure 4.54: Scatter plot beach sand, Δh_{d10-d5}

In the scan with a water depth of 5 centimetre the largest volume of the sand was submerged, however a part of the sand and the bricks were not. In figure 4.55 a interpolated 3D mesh plot is created which includes the water surface. The scattered values have been interpolated using the nearest neighbour interpolation method. In this plot, the two bricks and the top of the sand are easily detectable and the sand appears to have been spread out rather smooth over the bottom of the pool.

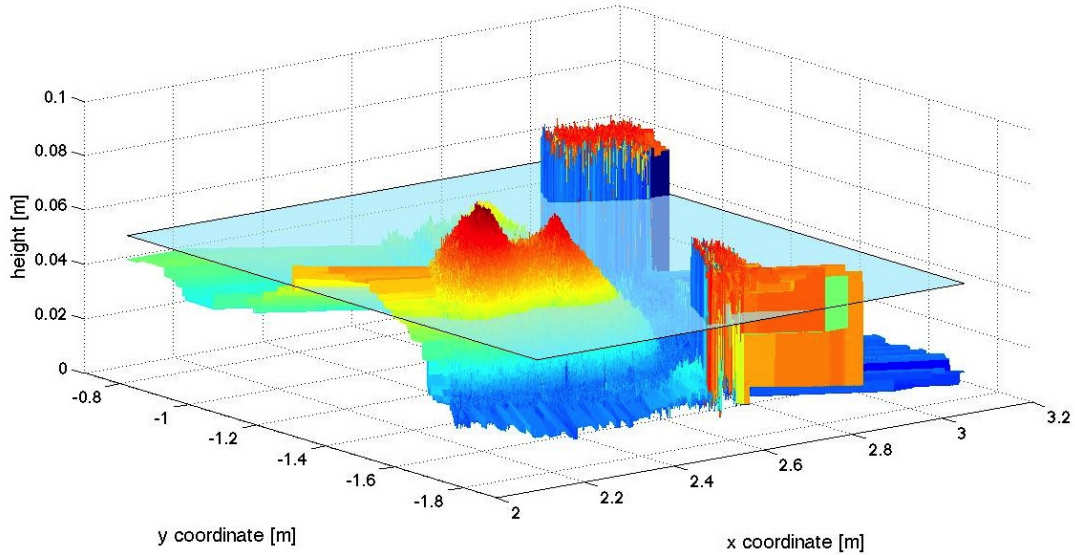


Figure 4.55: Mesh plot of beach sand including water surface, depth 5 *cm*

The range through the water towards the target differed for the four datasets as the water depth varied. The range through the water has been plotted versus the intensity for the four datasets in figure 4.56. Only the beach sand has been selected for these plots, not the red bricks or the bottom of the pool. The averaged intensity values decrease from 0.16 for a depth of 5 centimetre to 0.11 for a depth of 40 centimetre. Indeed, for a larger range through water more of the signal is attenuated leading to smaller return values for the intensity. In figure 4.56 the intensity threshold is also plotted, again this threshold is 0.075, as also found in paragraph 4.4.2. The threshold implies that the complete scatter plot is likely to have intensities lower than 0.075 as in figure 4.56 the scatter plots appear to be cut off at the threshold. The threshold thus influences the results.

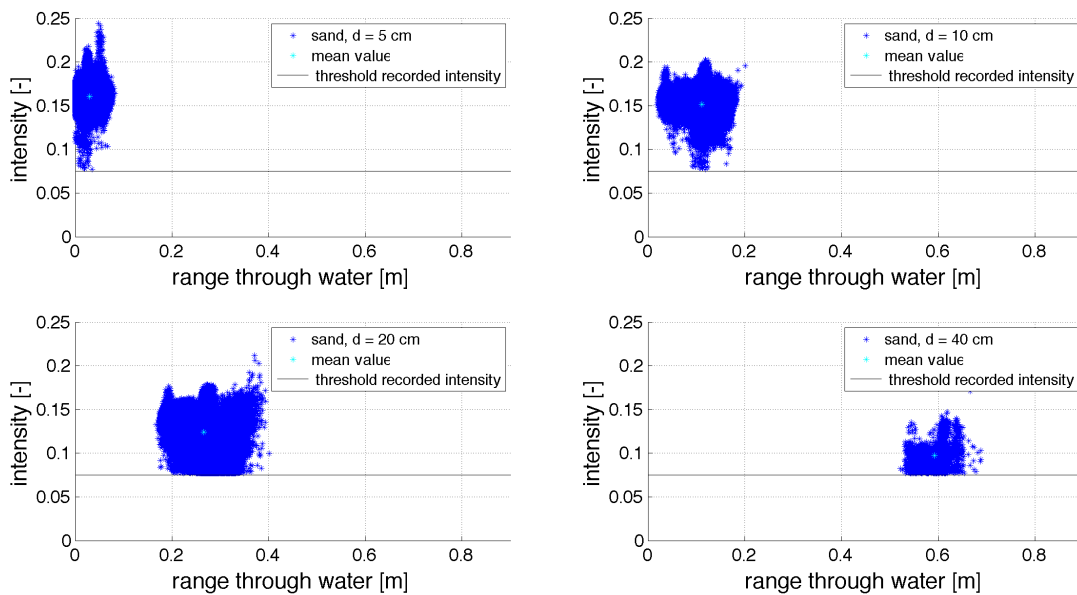


Figure 4.56: Scatter plot of the intensity values versus the range through water for different depths

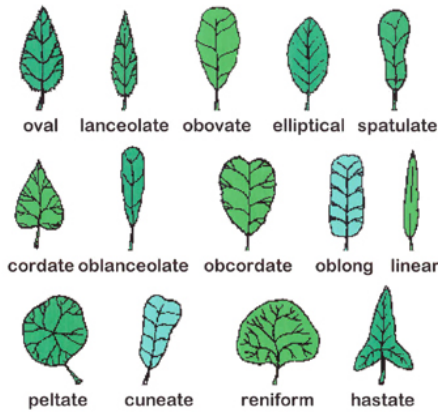
4.4.5 Water plants

Two types of water plants, as displayed in figure 4.57, have been scanned under water. The first type is a water plant of the Anubias family, displayed in figure 4.58. The second water plant is of the Echinodorus family and a detailed picture of this plant is given in figure 4.59. Both of the water plants have their roots in a round plastic cask with a height of 5 centimetre and a diameter of 4 centimetre.



Figure 4.57: The two water plants Figure 4.58: Leaves of Anubias Figure 4.59: Leaves of Echinodorus

There are several different leaf shapes of plants [47]. The fifteen most common leaf shapes are displayed in figure 4.60. The first water plant, the Anubias, has leaves with a cordate shape, while the leaves of the second water plant, the Echinodorus, are of a linear shape. The characteristics of both water plants have been measured and computed, they are given in table 4.9. The leaf width is measured to be the maximum width of a leaf. The leaf area can be computed with the leaf area formula of Montgomery, 1911. The leaf area LA according to Montgomery is: $LA = k L W$, where k is a factor set to 0.75, L is the length of the leaf and W is the greatest leaf width.



	<i>Anubias</i>	<i>Echinodorus</i>
height [cm]	24.3	34.9
number of leaves	11	133
min. leaf length [cm]	2.1	1.0
max. leaf length [cm]	8.6	10.9
mean leaf length [cm]	5.6	4.4
min. leaf width [cm]	1.8	0.2
max. leaf width [cm]	6.8	3.2
mean leaf width [cm]	4.4	1.2
mean length/width ratio	1.24	3.82

Table 4.9: Characteristics of the two water plants

Figure 4.60: Most common leaf shapes [47]

Each water plant has been scanned under water three times for two different water conditions. First both are placed in tap water with a turbidity of 0.3 *NTU* for the first set of scans, then the plants are removed and after changing the water, again placed under water consisting of a mixture of 75% clean water and 25% Schiewater with a turbidity of 1.3 *NTU*. Each plant is scanned with a fitting field of view to obtain only the plant. The resolution settings are custom for a close range so that the horizontal and vertical accuracy is 1 millimetre.

Two of the resulting point clouds of the two water plants in water with a turbidity of 0.3 *NTU* are displayed in figure 4.61. The edge effect as described in paragraph 2.4.4 is visible for both water plants in this figure: the intensity values are evidently smaller at the edge of the leaves. The resolution settings however were sufficient as even the smallest leaves with a width of only 0.2 centimetre were detected.

The leaf area based on dry, manual measurements can be computed for each leaf of the water plants. Comparing these results with the point clouds, it comes clear that even though the leaves can be detected from the point clouds in figure 4.61, the leaf areas can only be derived for the leaves on top or for the leaves that are facing the laser scanner. The three largest leaves of the Anubias water plant, located on top of the plant, have been measured within the point cloud and they coincide well with the corresponding three dry measurement sets. All of the leaves that were in the shadow of other leaves however are only partly visible. Therefore it is not possible to determine the total leaf area directly from the point cloud. Some algorithms exist that are able to compute the total leaf area with the point cloud and type of leaf shape as input [10]. However this is outside the scope of this project and is therefore not included.

What could be measured directly from the point cloud is the ground area. The ground area is the area of the ground that is covered with vegetation. In the point clouds in figure 4.61, the shadow of the water plants is also visible. This shadow can be used to obtain the ground area. The ground area is also used in determining the leaf area index, which is a measure for the area of the leaves of a plant versus the ground area, is $LAI = \frac{LA}{GA}$, where LA is the leaf area and GA is the ground area. A leaf area index of zero implies bare ground while there exist very dense conifer forests with a leaf area index exceeding 10. In theory it is possible to determine the leaf area index for water plants, but the details may be investigated in further research.

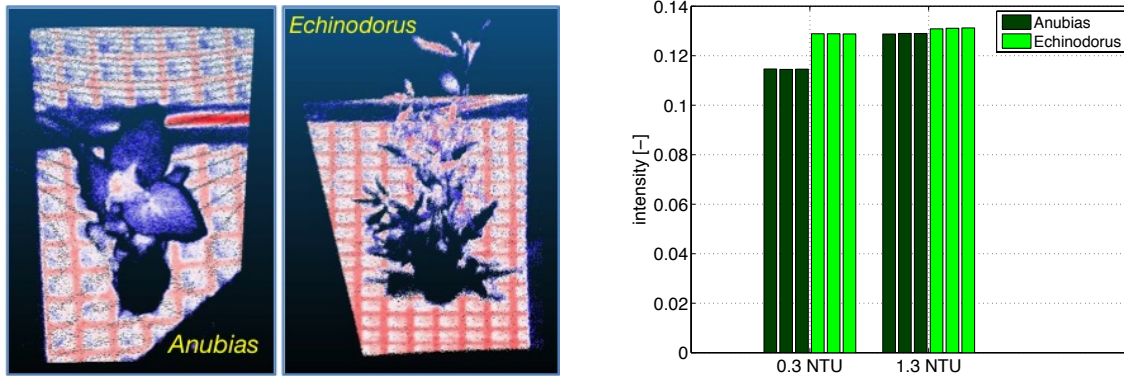


Figure 4.61: Point clouds of the two waterplants Figure 4.62: Bar plot of intensity values water plants

The returned intensity values of the two water plants for the two water conditions are displayed in figure 4.62. The Anubias water plant had a lower reflectance than the Echinodorus water plant as the leaves of the Anubias appeared to be darker green when inspecting the leaves by eye. Both of the water plants can be identified as foliage in figure 2.4. The intensity values of the Echinodorus are almost the same for the two scan conditions. However the Anubias water plant shows an increase in the recorded intensity values for more turbid water. This is unexpected and could be due to a change of the incidence angle when putting the water plant into the water in the second experiment. Though the placing of the water plants has been done carefully, a small human error can cause a major change in incidence angle. A change in incidence angle may cause the laser light to fall on the leaf from another angle, which may cause the intensity increase.

The goal of this particular experiment was to determine whether the water plants are detectable with the laser scanner, and they are. Even though the leaf areas can not be obtained directly from the point cloud, the shapes of the water plants can easily be recognised. The leaf shapes can be classified based on only the point clouds. For small scale ecological studies inquiring the type of water plant this is an advantage. Also, all of the recorded intensity values are lower than the intensity values as obtained in the experiments with the beach sand. So when conducting a scan experiment in nature, the water plants can be detected from the point cloud, not only by vertical location but also by the intensity values in case of a sandy bottom.

4.5 Review of the return signal

The return signal consists of the coordinates and corresponding intensity value for each point. The intensity value is in fact the power of the return signal and it is scaled between zero and one by the Leica C10. Throughout this chapter, the intensity values of several materials have been examined. In this section, the intensity values will be studied in more depth. In the first paragraph, the intensity values of the different materials are put together to see the difference between different materials. In the second paragraph the power of the return signal is computed with use of basic physic laws and compared with the intensity values that are obtained by the laser scanner. If these basic computations hold true then it is possible to predict the return intensity before doing the scanning. This may be an advantage for future underwater scan applications.

4.5.1 Comparison of intensity outcomes

Two different scan cases are assembled: the first case consists of the scans executed with tap water with a turbidity of 0.3 *NTU*, and the second are the scans that were executed with a mixture water with a turbidity of 1.3 *NTU*. The water depth was 40 centimetre for all. The averaged intensity values are displayed in figure 4.63 and figure 4.64 for the tap respectively mixture water. Some of the targets have only been scanned under water. For those that have also been scanned dry, the decrease in intensity that occurred when scanning wet have been computed, these percentages have been given in table 4.10. For the rocks and sand only the dry scan results are given as the wet experiments gave almost no results.

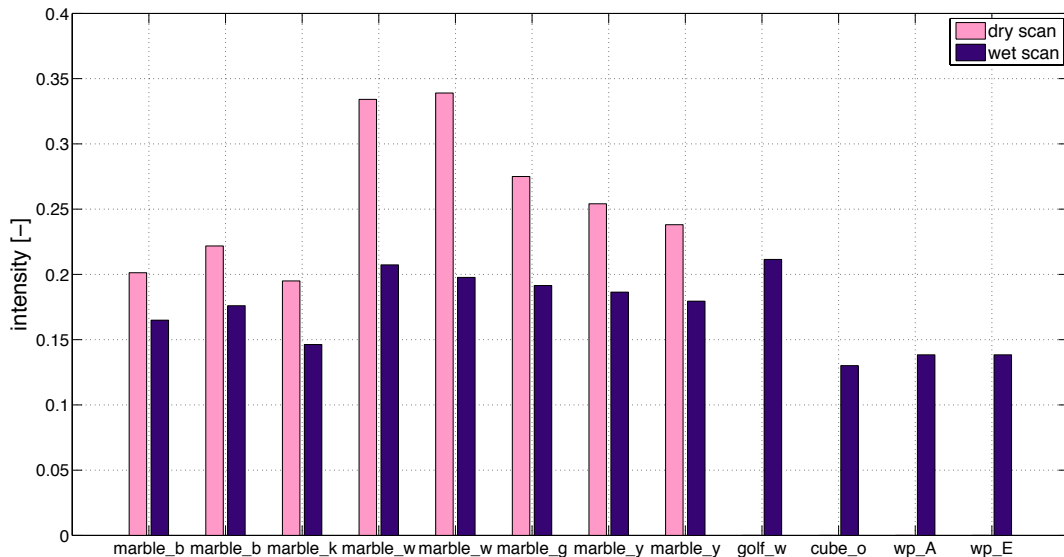


Figure 4.63: Bar plot of the intensity values for all of the experiments with tap water

The mean intensity values in figures 4.63 and 4.64 are the arithmetic means of the returned intensity points. As described in paragraphs 4.4.2 and 4.4.4, there was a threshold for the return intensity in the Leica C10 laser scanner. This threshold, which was 0.075, caused all return values that were lower than this value to not be recorded. As this threshold is a feature of the Leica C10 laser scanner, scanning the same target with another laser scanner may give different results as the threshold may be different or non-existent. The effect of the threshold is that the mean intensity values are slightly larger than would be the case when there was no threshold. The threshold values of various laser scanner devices are not widely known and therefore a study involving this is recommended.

Figure 4.63 shows that the white golf balls had a higher intensity than the white marbles when looking at the wet situation. This was expected: when examining a white marble and a golf ball by eye the golf ball appeared to be brighter and more reflective. The dimples did lower the average intensity values of the golf balls, however it is not known with how much the intensity reduced as there were no golf balls with the same white colour and without dimples available.

A concrete object is less reflective than a glass object of the same observed colour and this resulted in lower intensity values. Indeed, when scanning through the water for ecology purposes it is wise to use a green laser scanner instead of a blue one. A green laser scanner will be able to detect the overall green vegetation better based on the reflectance spectra in figure 2.4.

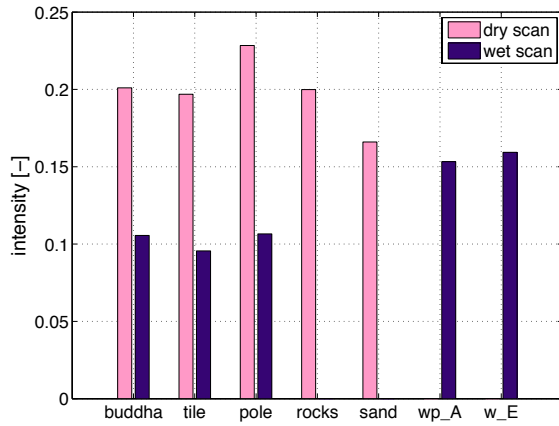


Figure 4.64: Bar plot of the intensity values for all of the experiments with mixture water

turbidity	target	decrease in intensity [%]
0.3 NTU	blue marble	18.1
	blue marble	20.6
	black marble	25.0
	white marble	38.0
	white marble	41.7
	green marble	30.4
	yellow marble	26.6
	yellow marble	24.6
1.3 NTU	concrete buddha	47.5
	green rubber tile	51.4
	wooden pole	53.3

Table 4.10: Decrease intensity values - wet to dry

It should be noted that overall the recorded intensity values for the targets in the mixture water were lower than the recorded intensity values for the targets in the tap water. This is completely due to the turbidity of the water as the water depth and atmospheric conditions were the same for all. The turbidity difference between the two cases is 1.0 NTU.

In figure 4.64 there were some unexpected results based on the averaged intensity values. First of all, the buddha has a higher average intensity than the green rubber tile. This was not expected. The reason for the higher intensity of the buddha is its white markings: the sculpture had some white chalk markings which cause the mean intensity to be higher. The buddha and its markings are displayed in figure 4.25. The explanation for the intensity values from the tile being lower than expected is that the tile absorbed water leading it to be less reflecting.

Moreover the intensity values of the rocks and beach sand have only been plotted for the dry scan. The intensity of the sand was lower than the rocks and buddha, so the rocks and buddha had a higher reflectance than the beach sand. Even though this may feel like it is the other way around, according to figure 2.4 the reflectance of concrete, which is the identified material of both the buddha and the rocks, is indeed larger than the reflectance of sand for a wavelength of 532 nanometre.

As described in paragraph 4.4.5, the intensity values of the water plants did not vary much when comparing the water plants in tap with water plants in mixture water. Because of this, the intensity values as shown in figure 4.64 are higher than the intensity values of the other three wet targets. This is beneficial for further ecological research where the underwater vegetation will be mapped. The rather high intensity values for the water plants is because the water plants are observed as a shade of green by eye, where green is also the colour of the laser light. It is thus beneficial to scan objects that can be observed as green by eye with a laser that has light in the green wavelength spectrum. The rubber tile was also observed as green however it has a very coarse, non shining surface where a part of the signal was lost. The water plants on the other hand have smooth shiny leaves and were better visible when scanning under water. The effect of the roughness of objects has been researched before [33], with the outcome that the surface roughness does cause a decrease in intensity. The results obtained in this project confirm this.

The decrease in intensity when scanning through the water compared to the dry situation is given in table 4.10. The marbles that have been scanned under water with a turbidity of 0.3 *NTU* had a decrease in intensity ranging from 18 to almost 42 percent. It can be found that the higher the expected reflectance of the marble as given in figure 2.5 for a wavelength of 532 *nm*, the larger the decrease in intensity value when scanning through the water. The other materials that were scanned under 40 centimetre of water with a turbidity of 1.3 *NTU* had a decrease in intensity of around 50%. So when scanning very shiny materials like glass marbles, there are more variations when comparing the dry and wet situation. In previous research reflective targets with a calibrated reflectivity have been scanned [45]. In this experiment the reflectivity of the targets was not calibrated. However, the results obtained here concur with the experiments with calibrated reflectivity: the intensity varies more for highly reflective materials.

For all other materials that do not have a shiny, highly reflective surface and that reflect light diffusely, the decrease in intensity can be expected to be approximately 50% when scanning under water with a depth of 40 centimetre. Other research has shown the reduce in intensity values comparing dry and wet objects to be smaller, that is around 20% [23]. However, the experiments performed in that experiments did not include scanning through the water. It did include the difference between dry and wet materials, where in the case of the wet scans the materials were moistened. Several objects showed a decrease in intensity values because the material absorbed water and became less reflecting. The finding of those tests [23] confirms the behaviour of the materials when submerged in the water. The materials that absorbed water when submerged in this experiment were the rubber tile, the metamorphic rocks and the wooden measuring pole. The behaviour of materials when comparing dry with wet scans should therefore be taken into account.

4.5.2 Power of the return signal

The returned intensity values are in fact the power of the return signal scaled from zero to one. It is possible to compare the recorded intensity values with the return power based on computations. It should be noted that even though basic physic laws [13] will be used, the computation as done here does make use of some assumptions and is therefore not directly applicable to other cases. First it should be noted that the recorded intensity as discussed in this section and thesis in fact is the scaled return power of the signal itself.

The expected return signal power is computed based on rather simple spectrophotometric equations. This is necessary as there are no measures done of the several fluxes of radiation. Radiation can be described as the process in which energy is emitted by one body, transmitted through an medium, and absorbed by another body. The radiation fluxes can be measured and with this the signal strength of the laser light can be computed based on the radiometry field. Many more parameters are needed such as atmospheric parameters and specific target related parameters. It is however not possible for the experiments in this project to incorporate these radiometric calculations, besides it is outside the scope. Hence the return power is computed according to spectrophotometric laws. If the estimation of the power of the return signal holds, this is beneficial for further research: the return intensity values can then be predicted before doing the scanning. Also, if the prediction of the power of the signal turns out to be below the threshold of 0.075 for the Leica C10, the user will know that scanning will not be genuine.

As the recorded intensity values are scaled between zero and one by the laser scanner, this scale will be used furthermore in the computations in this paragraph. All of the computed powers will also be scaled between zero and one and can be seen as a percentage of the output signal. The signal that leaves the laser scanning device thus has a power of 100%, or scaled between zero and one, is one. The power transmitted by the laser scanner is in formula:

$$P_{out} = 1 \tag{4.1}$$

The signal is assumed to not lose any power when travelling through the air. This assumption can be justified because the scan conditions were the same for each experiment: the atmospheric conditions were controlled. Beside, on such short range, that is up to 4 metre for the laboratory experiments, the loss of the signal in air is expected to be negligible.

When arriving at the boundary of the two media, a part of the ray is reflected from the water surface and another part of the ray will pass through the boundary into the water. The reflectance at the surface can be computed with the indices of refraction of air and water as given in paragraph 2.1.2, which are:

$$n_{air} = 1.0002782 \quad n_{water} = 1.335 \quad (4.2)$$

The part of the signal that is reflected at the water surface is:

$$P_{reflected} = \left(\frac{n_{water} - n_{air}}{n_{water} + n_{air}} \right)^2 \quad (4.3)$$

Filling in the indices of refraction gives a reflected power of 0.0205, so approximately 2%. The part of the power of the signal that passes through the air water boundary into the water is:

$$P_{transboundary} = P_{out} - P_{reflected} \quad (4.4)$$

The power that is reflected or in other words lost at the boundary of the two media is rather small, approximately 2% of the power transmitted by the laser scanner, which leaves approximately 98% of the transmitted power to pass through the air water boundary into the water. The reflected part power is the same amount, that is 2%, for all of the experiments as the indices of refraction are the same. The remaining 98% of the signal, that is $P_{transboundary}$, then arrives in the water and here a part of it is transmitted through the water, while another part is absorbed by the water. The transmittance, so the part that travels through the water to the target is:

$$T_{water} = e^{(-\mu L)} \quad (4.5)$$

where μ is the wavelength dependent, attenuation coefficient [m^{-1}] of the media, which is water, and L is the path length [m]. The attenuation coefficient μ consists of the absorption and scattering coefficient and it is a measure of how quickly a signal, so radiance, at wavelength λ is attenuated when passing through a medium. So if the attenuation coefficient is large, the signal is quickly weakened as it passes through the medium. The attenuation coefficient for water depends on the wavelength of light and the turbidity of water. Experiments in rather clear creek water [18] lead to an empirical formula for the attenuation coefficient of water, dependent on the turbidity expressed in NTU and specified for a wavelength of 532 nanometre. The attenuation coefficient of water can be computed with this formula:

$$\mu = 0.0881NTU + 0.448 \quad (4.6)$$

where NTU is the turbidity of the water. The turbidity for the experiments was 0.3 NTU for tap water, and 1.3 NTU for the mixture of water from tap and Schie. The path length is the length that the light travelled through the water towards the target. The path length can be computed for each point in a dataset with some basic trigonometry.

The transmission of the light through the water is also a percentage so scaled between zero and one. The power of the signal that reaches the target is then:

$$P_{attarget} = P_{transboundary} T_{water} \quad (4.7)$$

At the target the signal is partly absorbed by the target, partly scattered in other directions and partly reflected back. In order to obtain the signal from the target, these two occurrences are simplified. The spectral signatures of the materials from nature or the build environment over the visible light spectrum are given in figure 2.4. The materials that are considered in this section are the beach sand, the wooden measuring pole, the buddha and the water plants. These four materials can be identified as respectively sand, bark, concrete and foliage in figure 2.4. The reflectance values of the four materials have been read off for a wavelength of 532 nanometre from figure 2.4:

$$r_{sand} = 0.19 \quad r_{bark} = 0.11 \quad r_{concrete} = 0.21 \quad r_{foliage} = 0.18 \quad (4.8)$$

So the power back from the target with reflectivity r_{target} will thus be:

$$P_{backfromtarget} = r_{target} P_{attarget} \quad (4.9)$$

The signal then travels back through the water so the transmittance needs to be applied again on the power, and at the water air boundary the reflectance needs to be taken into account. The signal that returns at the laser scanner is then:

$$P_{in} = (P_{backfromtarget}T_{water}) - P_{reflected} \quad (4.10)$$

The resulting power P_{in} is thus a fraction of the outgoing power P_{out} . It is expected that the return power will coincide with the recorded intensity values, so P_{in} will be no more than 0.25 for a highly reflective target.

4.5.3 Working example: recorded versus computed signal

The recorded power intensity versus the computed return signal is plotted for the three water depths of sand that had sufficient returns, that is depth of 5, 10 and 20 centimetre, in figure 4.65. The intensity values decrease with an increase in water depth. The computed return signal power did as well, however for the dataset with the largest water depth there is significant more spread in the data than for the two other datasets. In the dataset with a water depth of 20 centimetre, the intensity threshold of 0.075 on the x-axis clearly influences the returns as the data is cut off at a horizontal value of 0.075. The other two datasets seem not to be influenced by this threshold as the intensity values are overall larger than 0.075 and not close to the threshold value of 0.075. So the threshold does play a role when scanning through deeper water. This can be explained by the signal loss in the water: the larger the range through water the larger the absorption and scattering losses in water and thus the smaller the return signal. The range through water is thus crucial. If the value of a return signal comes under the threshold value of 0.075, this specific value will not be recorded.

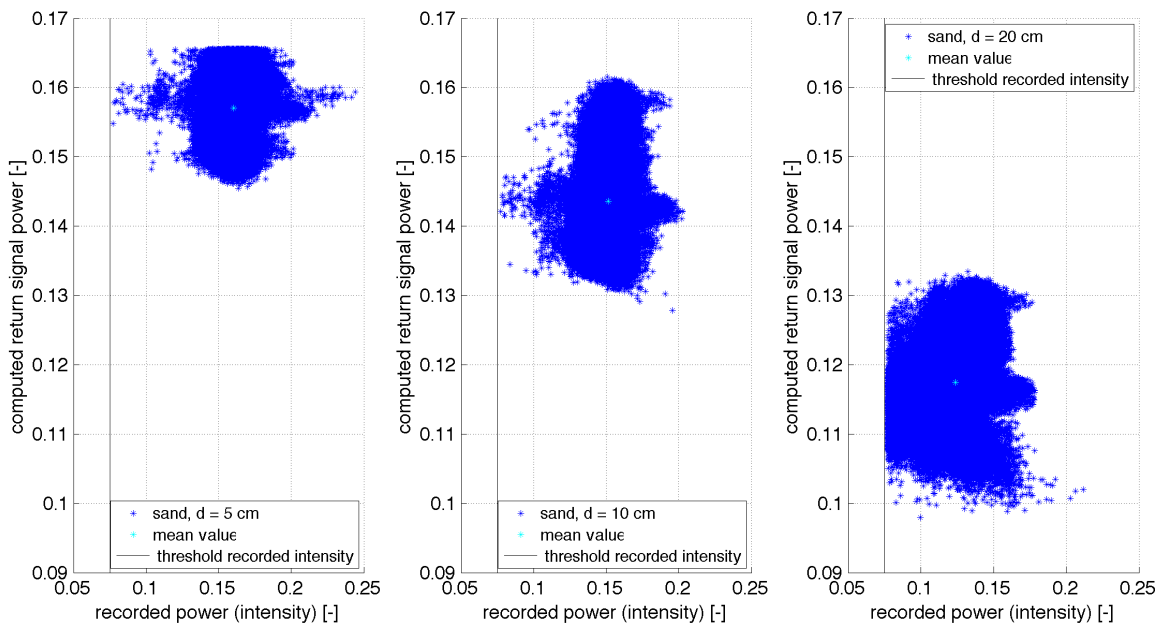


Figure 4.65: Scatter plot of beach sand return intensity versus computed return signal power

The residuals as described in paragraph 3.4.1, which are in this case the difference between the recorded intensity and the return signal power, are given in figure 4.66 for the beach sand. The three data sets follow a distribution that appears to be a normal distribution. All possible, valid parametric probability distributions have been fitted to the three data sets with a function from the Matlab support website. This function, named *allfistdist*, fits multiple probability distributions to a given data set and gives the distribution that provides the best fit. A description of this function is given in Appendix C. After applying this function to the three separate data sets consisting of the residuals, the distribution that provides the best fit turns out to be the same for the three data sets, that is the t-location-scale distribution, also known as student's t distribution or simply t distribution. The t distribution is defined by the location, scale and shape parameter. The t distribution resembles a normal distribution when the data set is large.

In figure 4.66, the data set with the largest water depth shows two peaks. This is due to the influence of the threshold value: because of this, some points are not present in the recorded intensity values. The root mean squared error as given in paragraph 3.4.1 is computed for the three datasets and gives the values 0.0085, 0.0115 and 0.0146 for the datasets with respectively 5, 10 and 20 centimetre. So the larger the depth the larger the difference between the computed and recorded intensity.

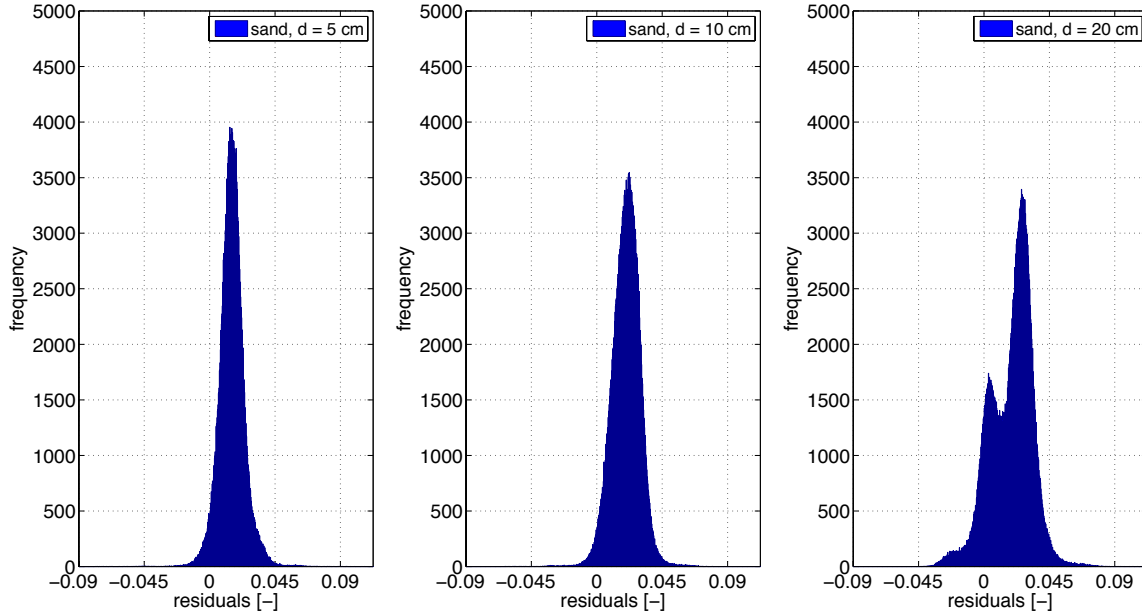


Figure 4.66: Bar plot of residuals return signal of beach sand

The differences between the computed and recorded intensities of the buddha and the pole have also been examined, the resulting scatter plots are displayed in figure 4.67 respectively 4.68. In both cases the water depth was 40 centimetre, the turbidity was 0.3 *NTU* and only the submerged part of the pole that stood vertical in the water has been selected. The differences between the recorded and computed values were comparable with the beach sand for the buddha, with a root mean squared error of 0.0181. The root mean squared error of the pole was much larger than all other, that is 0.0361. So the computations of the return power shows larger deviations from the return intensity for an vertical object that is submerged in the water than objects on the bottom of the water body. The return intensity values of the beach sand, which was a target that was spread over the bottom of the pool, shows the best estimation results.

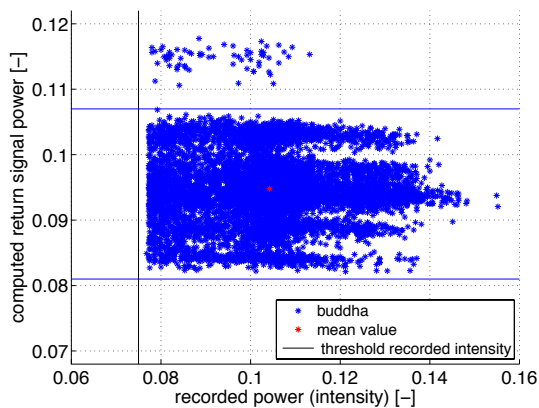


Figure 4.67: Scatter plot of buddha return intensity versus computed return signal power

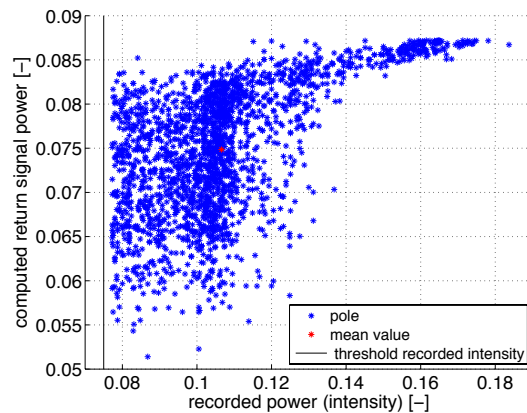


Figure 4.68: Scatter plot of pole return intensity versus computed return signal power

The intensity values of the four water plants are the last target to be considered. The scatter plots of the two water plants for two different situations concerning the water turbidity are displayed in figure 4.69. The root mean squared error values did not differ much between the two plants for the same water turbidity. For a turbidity of 0.3 *NTU*, the Anubias had a root mean squared error of 0.0228 and the Echinodorus 0.0249. For a turbidity of 1.3 *NTU* the Anubias had a root mean squared error of 0.0433 and Echinodorus 0.0354. Even though the turbidity of the water was accounted for in the computation of the return signal power, an increase in turbidity thus causes the computed values to deviate more from the recorded intensities than is the case for a lower turbidity. In other words, the computation is sensitive to the turbidity.

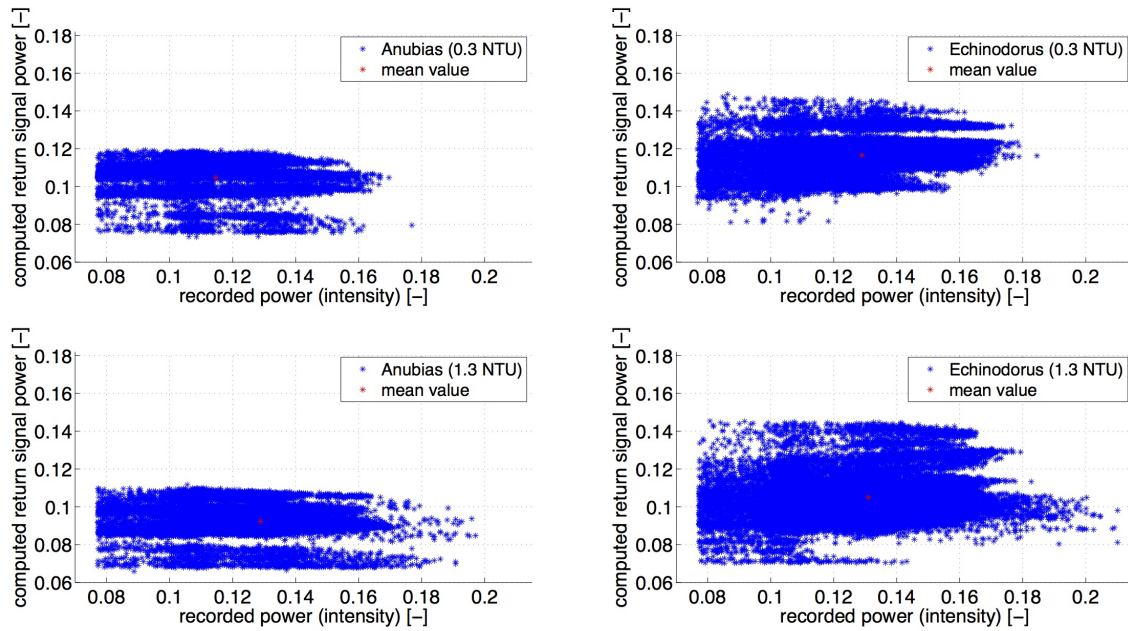


Figure 4.69: Scatter plot of water plants return intensity versus computed return signal power

The power of the signal can thus be computed before conducting scan experiments based on simple equations. If the target is known, the expected reflectance of a scan target can be derived from the reflectivity curves for wavelengths in the visible light spectrum as given in paragraph 2.1.4. An important factor is the natural variability of an object, which results in different reflectivity values on this object. This is for example the case for beach sand, which comprises of sand grains, shells and other small particles. Even the buddha, which has been produced, shows this variability as its white markings have a higher reflectivity than the rest of the buddha. This natural variability exists for all targets from nature, and also for most rough surfaced building materials like the red bricks. The natural variability is inevitable and will always cause some difference between computed and recorded intensity values. Therefore one must bear in mind that the reflectance of a material, like given in figure 2.4, does not take into account the natural variability and the resulting computed return power is thus not more than an estimation.

Further the turbidity of the water may not always be known when scanning outdoors. For rather clear waters it is reasonable to estimate the turbidity and compute the attenuation coefficient for a range of turbidity values, for example 2 to 5 *NTU* for rather clear outdoor waters. However the really muddy waters prove impossible to scan with the Leica C10. The path length through water can also be computed for different values of the water depth. Finally the return signal power can be computed, which will also be a range of values as there are multiple inputs. The obtained signal power will then be able to give an expectation of the range of return intensity values. Improvements to this simplified method to determine the signal power are required. However even with the simplified equations the RMSE values were not too large so the applied method to obtain an impression of the return power holds.

4.6 Initial conclusions and further scan recommendations

The main conclusion after conducting the basic experiments is that scanning through the water with the green-wavelength terrestrial laser scanner Leica C10 is not only possible but the laser scanning device is also suitable for this purpose. In spite of the before described limits of the Leica C10, the results are overall promising for a wide range of through water scan applications.

4.6.1 Findings from the basic experiments

Experiments with the Leica C10 with water depths of up to 40 centimetre for clear water with a low turbidity below 1 *NTU* can be performed with satisfying returns, as well as experiments with depths of up to 20 centimetre for more turbid water with a turbidity between 1 and 2 *NTU*. The maximum water depth of 50 centimetre from literature seems to be appropriate for a terrestrial laser scanner, given that the water turbidity is lower than 1 *NTU*. As most of the coastal (sea)waters in the Netherlands are rather turbid due to a high concentration of suspended solids, the maximum applicable depth is expected to be less than 40 centimetre. In this case, the hypothesis is that the maximum applicable depth is 20 centimetre for targets that have a preordained reflectance of 17% or higher, based on the experiments with beach sand with variable water level as done in paragraph 4.4.4.

A range of different objects have been scanned in this research project. Of all experiments, only materials that have a low reflectance of less than 5% are not suited as an underwater scan target when scanning through water for a range of water depths and water turbidities, and taking into account the intensity threshold of the Leica C10. Also, when placing materials in the water, some materials may become darker by eye when being saturated with water. The absorption of water caused the materials to become less reflective, sometimes leading to no returns. One should bear this in mind before setting up an experiment.

The water plants as assessed in paragraph 4.4.5 were included to determine whether the scanner is able to distinguish the plants from the bottom or bathymetry. The laser scanner indeed distinguished the water plants including their detailed leaf rather well. This is promising for the field experiments where beach pools with underwater vegetation will be scanned.

The resolution setting to be used for all short to medium range experiments should be the custom set one. This means that the maximum range should be measured or estimated and put into the custom resolution; the horizontal and vertical accuracy will be available automatically after setting the maximum range. These custom settings will contribute to the best scan results for both laboratory and outdoor experiments. Of course first a low resolution scan should be made to lock the target.

The laboratory experiments provided an adequate range of applicable ranges for the outdoors experiments. The most important conclusion for the outdoors experiment is the one that has been drawn multiple times throughout the basic experiments: when scanning through the water take into account the target reflectance, water depth and turbidity, and the behaviour of the target before attempting to scan. Also the practical findings as described in the following paragraph should be taken into account.

4.6.2 Practical findings

There were some practical findings concerning the workability that will be taken into consideration for the field experiments. The height of the laser scanning device caused a problem for a not so tall user. The problem of not seeing the air bubble can easily be overcome by using a tribrach for levelling purposes. The second problem, which is not being able to see the screen of the device when the device has been mounted too high on the tripod, can only be solved by making sure there is a step present. In the field this can be for example a wood log, or the tripod can be set near a little hill. Because in the field there will be no wall of a pool present, the workability concerning the height can be overcome.

Another practical finding is that even though one person is well able to gather the instruments needed and set up the laser scanning the device, in the field one person alone may not be enough. The field experiments will therefore be conducted with two persons so that the needed equipment can be divided between them. The largest, most heavy and least maneuverable equipment are the tripod and the trunk holding the laser scanning device. The other equipment can be packed in a backpack.

After locking the target in the laser scanner, the scan with the custom resolution will be performed. This custom resolution scan may take a long while to finish for a larger field of view needed for larger targets and therefore there needs to be enough time to do all these high resolution scans.

In addition, the raw data needs to be preprocessed using the Cyclone software as described in Appendix C. The preprocessing takes a long time, about two hours, for multiple scans with a wide field of view. After the preprocessing is done and the data is collected, loading the large data sets into open source software like CloudCompare may also cause a problem when the working memory of the laptop or desktop is not sufficient. Other modification to the data in for example Matlab also proved impossible with an insufficient working memory. A working memory of 4 gigabytes proved to not be able to process the data sets. A working memory of 8 gigabytes or preferably even more is mandatory. The memory of the USB stick also needs to be large enough to avoid transferring problems. The USB stick used in these experiments could hold a maximum of 16 gigabytes of data and this was enough. Obviously the laptop or desktop itself also needs to have enough memory to be able to store the numerous data sets. A large external hard drive can also function as a memory.

Chapter 5

Case Study I: Wood Samples in Lab

Wood structures in marine environments usually experience heavy dynamic loading during their life cycle. Beside the permanent load of the construction there are dynamic loads present like loads caused by mooring boats and loads due to waves and tides. Like any other construction, marine constructions are inspected regularly to examine the structure. Wood is one of the most used materials in marine constructions. The wooden piles in marine structures are generally inspected manually by experienced commercial divers. Laser scanning techniques may be useful for these inspections in the future.

The goal of the experiments in this chapter is to find out whether the scanner is able to detect damages on the wood samples. If so, the scanner could be used by authorities to improve inspection of wood structures in a marine environment, like mooring poles in a harbour. Various wood samples have been scanned in laboratory settings. Two of the wood samples are mooring poles from the harbour of Rotterdam respectively Vlissingen, one sample is a foundation pile from Rotterdam and the last sample is a pile from a marine construction in South Africa.

5.1 Experimental set up and description of wood samples

The experimental arrangements of the wood in laboratory were the same as the arrangements and set up of the basic laboratory experiments of chapter 4 and in figures 4.3 and 4.4. The experiments were performed in the Water Laboratory as described in paragraph 4.1.1 with the equipment as given on the equipment list in paragraph 4.1.2. The scan targets of this chapter are the four wood samples, which were available from the section of Structural and Building Engineering. Moreover, four water samples have been used in this chapter. The turbidity of these water samples expressed in *NTU* are given in table 4.1. The wood samples were placed in the four quadrants of the pool that have been marked on the bottom of the pool. The samples have been placed so that each sample can be scanned individually without part of it being placed behind another sample. In figure 5.1 the quadrants containing the different samples are presented.

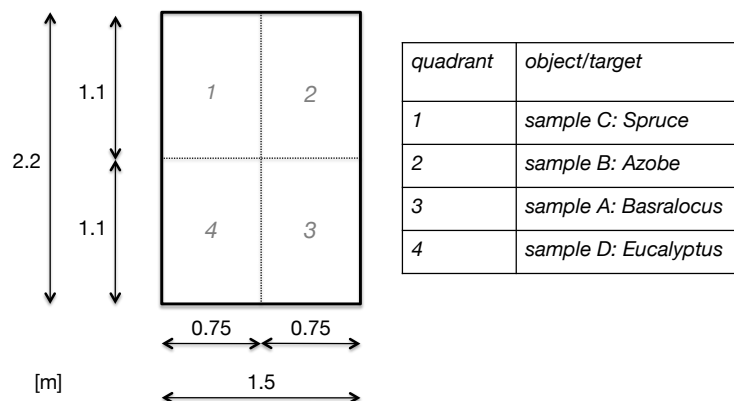


Figure 5.1: Placement of the wood samples in the quadrants

Figures 5.2 and 5.3 display pictures of the dry respectively wet samples set up in the pool. The picture in figure 5.3 is a picture of the experiment with tap water with a water depth of 40 centimetre. The bricks and buckets with sand that are stacked on top of three of the wood samples are there to avoid floatation.



Figure 5.2: Experimental set up wood - dry

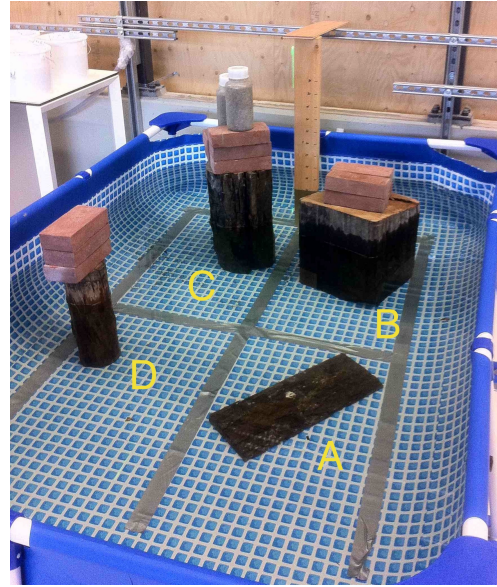


Figure 5.3: Experimental set up wood - wet

5.1.1 Features of the wood samples

The characteristics of the wood samples are given in table 5.1. Four different kinds of wood from different constructions have been used, however all four samples have one thing in common: they all have been used under conditions in which water was present. Two samples were part of a mooring poles, one was a part of a foundation pile and the last sample was used in a marine construction.

As can be seen from figure 5.2 and read off from table 5.1, two of the samples have a cylindric form, one sample is a cuboid and the last sample is plate-like. The plate-like wood sample however used to be a cuboid so the wood sample used to stand vertical in the water instead of horizontal submerged in the water. The plate-like wood sample, sample A, is placed in quadrant 3 and is also the only sample that is fully submerged during the underwater scans. The other three samples were partly submerged in the 40 centimetre deep water, as can be seen from figure 5.3.

sample	A	B	C	D
common name	Basralocus Angelique	Azobe	Spruce Norway Spruce	Eucalyptus Gympie messmate
latin name	<i>Dicorynia guianensis</i>	<i>Lophira alata</i>	<i>Picea abies</i>	<i>Eucalyptus cloeziana</i>
origin	Suriname	Congo	Northeastern Europe	Queensland, Australia
usage	mooring pole	mooring pole	foundation pile	marine construction
location	harbour of Vlissingen	harbour of Rotterdam	Rotterdam	South Africa
shape	plate	cuboid	cilinder	cilinder
dimensions [cm]	l=48, w=18, h=4	l=31, w=32, h=62	d=22, h=62	d=13, h=51

Table 5.1: Characteristics of the four wood samples

Samples A and B used to be mooring pole in a harbour. The two wood species are Basralocus and Azobe, which are also two of the three most common wood species used in marine structures in sea- and brackish water environments [11]. These wood species are often used because of their high natural durability [4] when applied to constructions in marine environments. The origins of the four kinds of wood are indicated in figure 5.4.

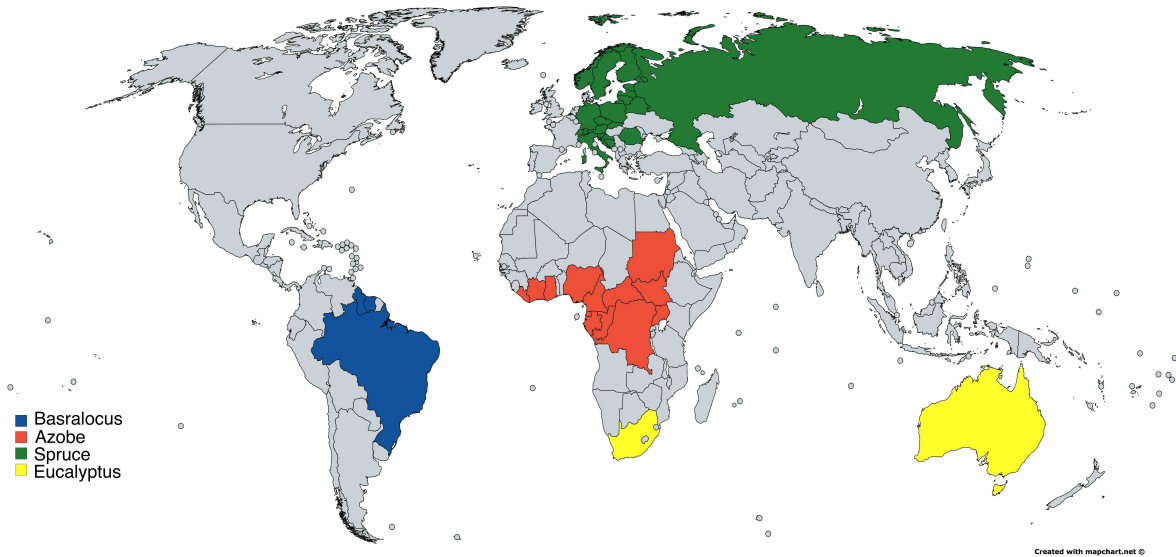


Figure 5.4: Origins of the four kinds of wood

5.1.2 Common damage to wood in a marine environment

In marine environments, there are several probable causes of the deterioration of wood. Degradation of wood due to mechanical damage is more severe in seaports than inner harbours because of the tides. A wooden pile in an environment that includes tides is most affected by wear, abrasion and splashing. These effects can be counteracted by adding an extra layer of timber. In the tidal zone, which is between low and high water, alternate wetting and drying of the wood concurs. This alternate wetting and drying does not only damage the wood mechanically but is this zone is also the desirable habitat of organisms that degrade the wood.

Figure 5.5 displays the damage profile of wood in a marine environment. The most damaged part of the wood is that part that is exposed to the tides, which is the tidal zone between high and low tide in figure 5.5. The part of the pole that is drilled into the soil does not experience much damage. The other zones of a wooden pole in a marine environment are the submerged zone, which is the part of the pole that is always under water; the splash zone, which is the part of the pole that is above high tide water level but wetted by splashes caused by waves and passing boats; and the atmospheric zone which is the upper part of the pole that is in principle not affected by the tides and water.

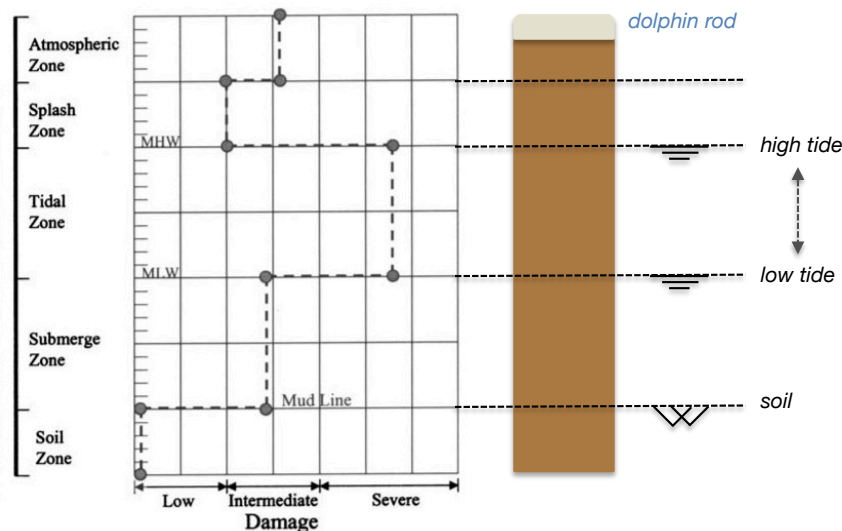


Figure 5.5: Damage profile of wood in marine environment, modified from Lopez-Anido et al [24]

The organisms that degrade wood can be principally divided into four categories: fungi, insects, bacteria and marine borers [7]. Fungi may cause molds, stains and decay. Molds and stains do not have a large effect on the strength of the wood, but the absorbency of the wood increases significantly and this increase in absorbance and porosity can lead to colonisation of wood-decay fungi [7]. The fungi that cause decay of the wood rely on the temperature and the moisture content of the wood. However, if the wood is completely soaked with water, this decay will not occur. The foundation pile, which is sample C, that has been used in the experiments has thus not been affected by these fungi.

The damage to wood by insects can be prevented by proper handling. It is thus assumed that none of the samples has been exposed to insects. Bacteria however may be present in wood samples that have been wet for a considerable length of time [7]. The bacteria mainly cause a bad smell and an increase in the absorptivity of the wood which can lead to a manifestation of decay fungi.

The largest problem of seaports and ports where seawater and brackish water is present is the presence of marine borers. These organisms are not able to survive in fresh water so inner harbours will not be exposed to these creatures. The most attacked location of marine borers on a wooden structure is in the tidal zone [30]. As the mechanical damage also occurs mostly at the tidal zone, this zone is always the most severely damaged zone compared to the other zones in figure 5.5.

The most destructive of the marine borers is the shipworm [7]. In its early stage, the shipworm is a free-swimming organism, in figure 5.6 phase *B* and *C*, looking for a lodgment on the wood. After finding such a place, as indicated with *D* in figure 5.6, the shipworm buries themselves in the wood. The boring shells on the head of the shipworm then develops and the shipworm will start boring in the wood, indicated with *E* and *F*. The tail does not grow thus stays the same size, which causes the shipworm to be trapped in the wood while boring. A shipworm can reach the size of 0.3 to 1.2 metre, depending on how many other shipworms are present in the wood [7].

One of the wood samples that was a mooring pole, sample A, was inhabited by shipworm. Figure 5.7 shows the plate-like wood sample that once stood vertical in the water. Two details are circled in this picture. The sample has many holes with a size between 0.2 to 1 centimetre that have been bored in the wood by the shipworm. The surface of the wood sample appears to be only slightly perforated, however after close inspection the interior of the wood is almost completely ruined.

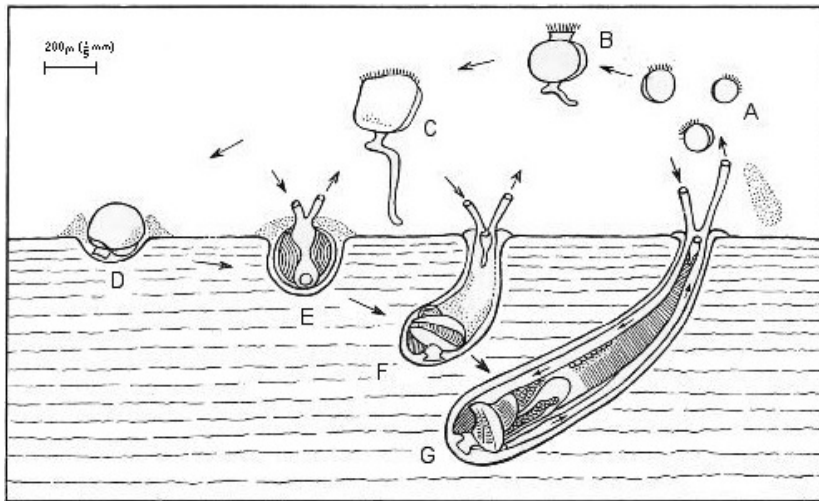


Figure 5.6: Shipworm manifestation in wood [31]



Figure 5.7: Wood sample A

The damage to the wood caused by both mechanical causes and organisms like the shipworm are clearly visible by eye. The damage that is caused by marine borers have a size in the order of millimetre, where the largest holes bored by the shipworm are up to a centimetre. Other wood samples, like sample B, does not seem to be inhabited by shipworm, however the wear is clearly visible as the wood is splintered here and there. Besides a part of sample B shows some decay, which may be caused by fungi. It is assumed that this part of the wood was above the water table. Sample C and D mainly seem to have large cracks. The laser scanning device should be able to detect all of these damages based on the resolution settings, which are custom resolution with a horizontal and vertical spacing of 1 millimetre and a maximum range of 4 metre.

5.2 Detailed scans of the individual wood samples

The four wood samples have been scanned individually to see whether the laser scanner is able to detect the damages. All of the wood samples were dry and have been put on the white flooring in the Water Laboratory to create a contrast in intensity which made it easier to distinguish the floor from the wood sample in CloudCompare.

5.2.1 Wood sample A: Basralocus

The Basralocus wood sample has been used as a mooring pole in the harbour of Vlissingen and is approximately 60 years old. Figure 5.7 indicates that the sample has been inhabited by shipworm as it has many holes. Also a white slimy substance is visible on the wood, which is circled in detail I. Detail II gives some of the larger holes on the wood sample. The sample was part of a mooring pole and it was located at the tidal zone as displayed in figure 5.5. The sample is severely damaged. In figure 5.8 the point cloud of the sample is presented. In this figure, the sample has been segmented from the floor with use of the segmentation tool in the CloudCompare software. The two details as circled in figure 5.7 are again indicated in figure 5.8.

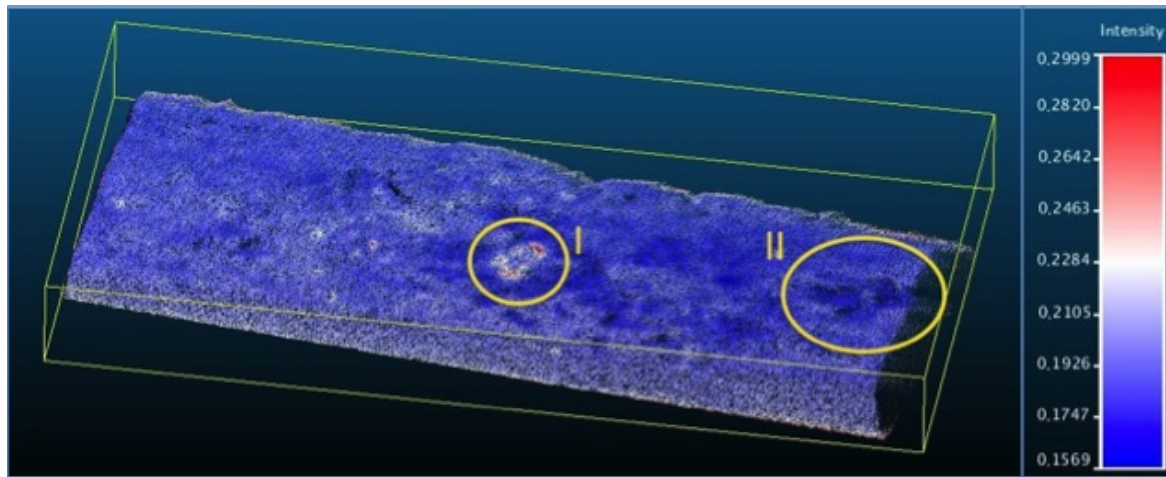


Figure 5.8: Point cloud of intensity values wood sample A: Basralocus

The holes caused by the shipworm can be distinguished from figure 5.8. It should be noted that the part of the hole that is visible by both eye and laser scanner is located on the surface of the wood. This opening is smaller than the hole in the inner part of the wood because of the manifestation and growth of the shipworm as indicated in figure 5.6.

The point spacing of 1 millimetre was significantly smaller than the holes so the laser scanning device was able to detect the different-sized irregularities on the wood. There were some locations on the wood where there were less points due to the shadow effect: these parts lay in the shadow as seen from the origin of the laser scanner. Also exactly at the location of the hole there were no return points: instead small black openings are visible in the point cloud in figure 5.8 where the hole are located.

5.2.2 Wood sample B: Azobe

The Azobe mooring pole from the harbour of Rotterdam was by far the largest and heaviest wood sample. The four sides of the cuboid have each been scanned. The results were less promising than the results obtained with the Basralocus wood sample. This was due to the colour of the wood: the Azobe sample was much darker leading to less return points than would be the case for a lighter sample. The cracks could be distinguished from the point cloud, however the cracks themselves, especially the larger ones, were even darker than the wood because of the shadow effect. So the irregularities themselves can only be partly distinguished but it was not possible to detect the depths of the cracks.

Figures 5.9 and 5.10 show a photo of the Azobe wood sample respectively a part of the point cloud capturing a relief on the wood. The wood sample had a lot of cracks and damages but no visible holes caused by marine borers. It was possible to map the reliefs on the wood up to a scale of 5 millimetre.



Figure 5.9: Wood sample B: Azobe

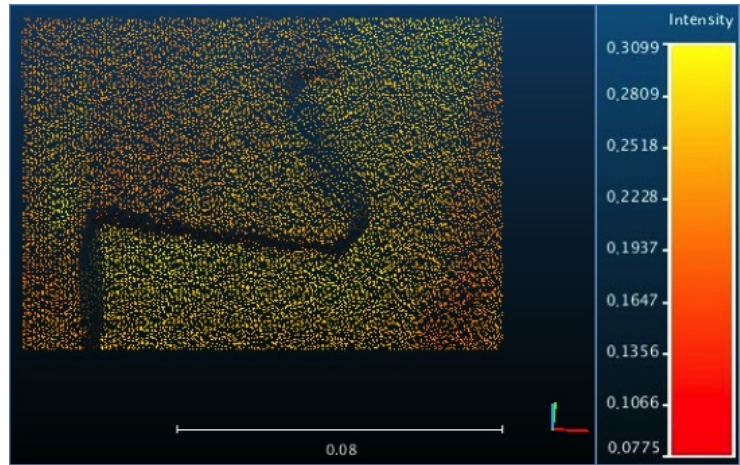


Figure 5.10: Point cloud of relief on wood sample B

5.2.3 Wood sample C: Spruce

The Spruce foundation pile from Rotterdam is from the year 1902 and its surface has many cracks and splinters. Figure 5.11 shows the sample together with an indication of the largest crack which is 2.5 centimetres wide and runs from top to bottom. The same crack is indicated in one of the resulting point clouds that is displayed in figure 5.12. The yellow coloured line in figure 5.12 is a measuring rod used for recognition and orientation of the sample. The Spruce wood has a much brighter wooden colour than the Azobe. Therefore more points were present leading to a larger point density when comparing sample C to B. All of the regularities up to a size of 5 millimetre could be detected. Again, when scanning in deep cracks points were lost because of the shadow that lies in these cracks.



Figure 5.11: Wood sample C: Spruce

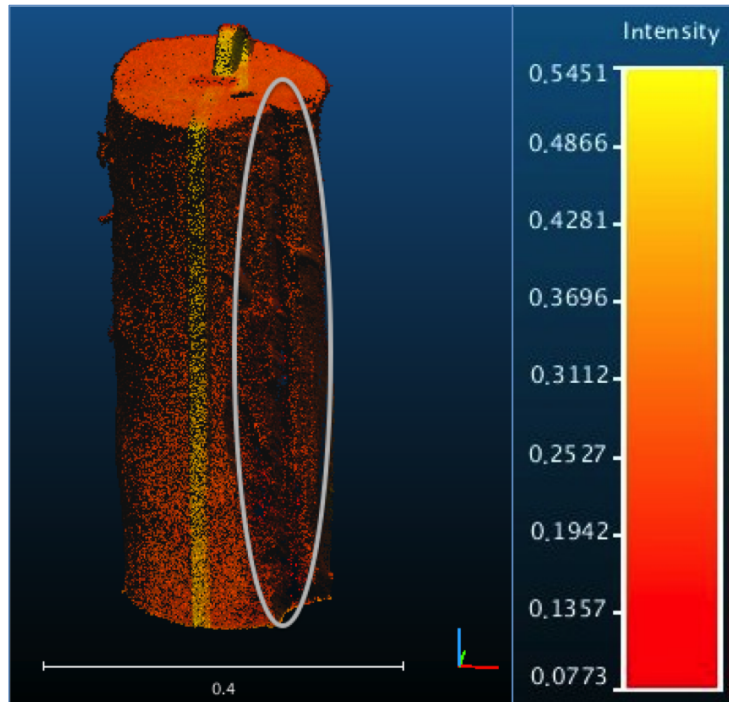


Figure 5.12: Point cloud of wood sample C

5.2.4 Wood sample D: Eucalyptus

The Eucalyptus wood sample from a marine construction in South Africa is the smallest pile. It has mainly damage that is possibly caused by wear as the sample has multiple cracks and splinters. The sample appeared to be a bit reddish so it was expected that this would influence the results based on the reflectance curve for colours in figure 2.5. According to this curve, green-wavelength laser light is less sensitive to red materials. Surprisingly the expected effect of the red colouring of the Eucalyptus sample could not be detected in the results. In fact, the point density and intensity range is quite similar to that of sample C, the Spruce wood. A picture of the wood piece is given in figure 5.13. The largest crack is indicated in this picture and can also be distinguished from the point cloud in figure 5.14. The yellow coloured line in figure 5.14 is again a measuring rod used for recognition and orientation of the sample.



Figure 5.13: Wood sample D: Eucalyptus

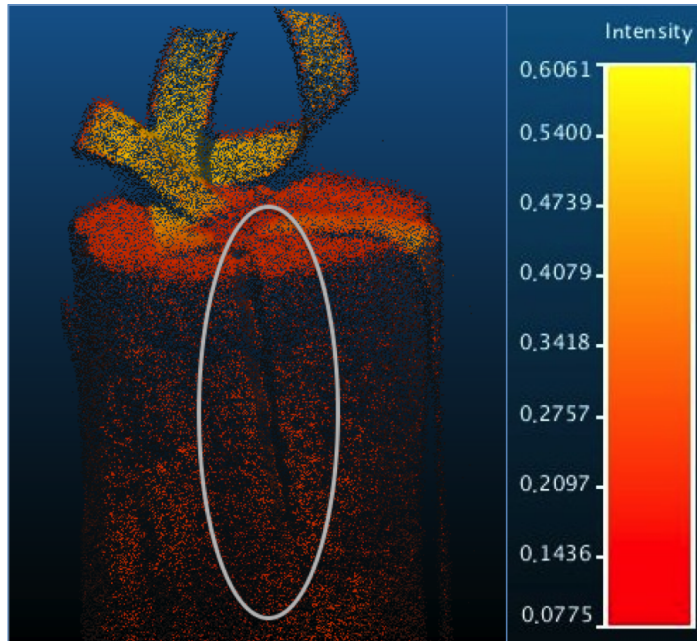


Figure 5.14: Point cloud of wood sample D

As expected, the laser scanning device was possible to detect the cracks without problems. Though the wood is quite dark it did not pose problems when scanning the samples dry. Only the sample that had a significant darker colour wood, which was sample B, the Azobe wood, gave some problems at dark spots on the wood where the number of returns was low. It is therefore expected that when scanning through the water, sample B is expected to have no or insufficient returns.

5.3 Wood experiments under water

Four different underwater experiments have been performed. The water differed in type of water, that is water from the tap, water from the river the Schie or a mixture of both. The four water samples had turbidities of 0.3 *NTU* for the tap water up to 2.0 *NTU* for the Schiewater. Table 4.1 provides an overview of the turbidity measures of the four water samples. The Schiewater is a representative of the water that is used in a Dutch harbour. All of the underwater scans were performed with a water depth of 40 centimetre. Of the four samples, only sample A was completely submerged in the water while samples B, C and D all had a part above the water surface. Figure 5.3 is a picture of the wet experiment with tap water. All of the samples were dry when put in the pool and three of them started to float while filling the pool with tap water. To avoid floatation some bricks and buckets with sand were put on these samples. Figure 5.2 displays the wood samples in dry state.

5.3.1 Prospect of the underwater wood scans

The wood samples absorbed water leading them to become less reflective. In figure 5.3 this effect is noticeable as the samples appeared to be darker. When dry the Eucalyptus wood appeared to have a reddish colour, however when submerged in the water the wood appeared to become more brownish. The other three samples also absorbed water and became less reflective.

Some of the materials that were used in chapter 4 also absorbed water and became less reflective. This effect, together with the signal loss when scanning through the water caused some targets to give no returns. The scans in which the samples were completely dry did give results, but the combination of scanning through the water and the absorption of water caused there to be no returns when scanning through water. This effect can be separated when scanning wetted targets through air. The water turbidity also played a role as the larger the turbidity the more of the signal is lost in the water. Some materials were simply not visible through the water with the laser scanner, while others were only visible under certain water turbidity and depth conditions. It is expected that the same problems will arise with the scanning of the wood samples.

5.3.2 Results of the underwater wood experiments

The results of the underwater experiments with the wood samples were not promising. The results are expressed in relative point density as outlined in paragraph 3.4.5. The dry scans of section 5.2 were used as a ground truth for the relative point density, so the number of returns from the dry scans were set to 100%. For each situation and wood sample the relative point density expressed as a percentage was then determined. The results are gathered in table 5.2.

<i>relative point density</i>	A: Basralocus	B: Azobe	C: Spruce	D: Eucalyptus
dry scan ~ ground truth	100%	100%	100%	100%
tap water - 100/0 - 0.3 <i>NTU</i>	60%	≪1%	6%	2%
mixture - 75/25 - 1.3 <i>NTU</i>	5%	no data	2%	≪1%
mixture - 50/50 - 1.4 <i>NTU</i>	≪1%	no data	≪1%	no data
Schie water - 0/100 - 2 <i>NTU</i>	no data	no data	no data	no data

Table 5.2: Relative point densities of underwater scans wood samples

Of all four wood samples, only sample A gave a sufficient number of returns for generating a surface profile when scanning under 40 centimetre of water with a turbidity of 0.3 *NTU*. For more turbid water, also sample A did not provide the results necessary to detect the surface profile of the wood. The scans of the other samples did not result in sufficient data for any of the underwater scans. The Spruce sample had only 6% of returns when scanning under water. These points were scattered at locations where the wood was lightest, and only within the uppermost 10 centimetre of water. With this amount of returns it was not possible to generate a surface profile. Only when enough points are present a surface profile can be generated in which the damage on the wood can be distinguished.

The scan angle on the object is most likely of influence on the results besides the water turbidity. There is a difference of this scan angle when scanning a horizontal object compared to a vertical object. However the influence of the scan angle on through water scans has not been investigated here.

The Basralocus wood sample is the only wood sample that had sufficient returns, that is a relative point density of 60%, for the through water scan with the tap water. After applying the correction for refraction, the surface profile of the wood was examined. The results are displayed in figure 5.15. Again the white slimy substance, detail I in figure 5.8, is easily detectable because of its deviating intensity. The laser scanner is more sensitive to white colours than brown bark as the first has a larger reflectivity. Because there is quite a difference in green reflectance between the bark and the white substance on the surface of the bark, the intensity difference is large. The intensity difference is approximately 0.07, where the intensity boundaries are between 0.07 and 0.20 for the Basralocus wood sample.

The various irregularities can be detected from the point cloud in figure 5.15. The experiment comprises one scan but when scanning over a period of time the difference in surface profile can also be mapped. When scanning through the water with the Leica C10 it thus is possible to detect damage to the wood but only under rather clear water conditions.

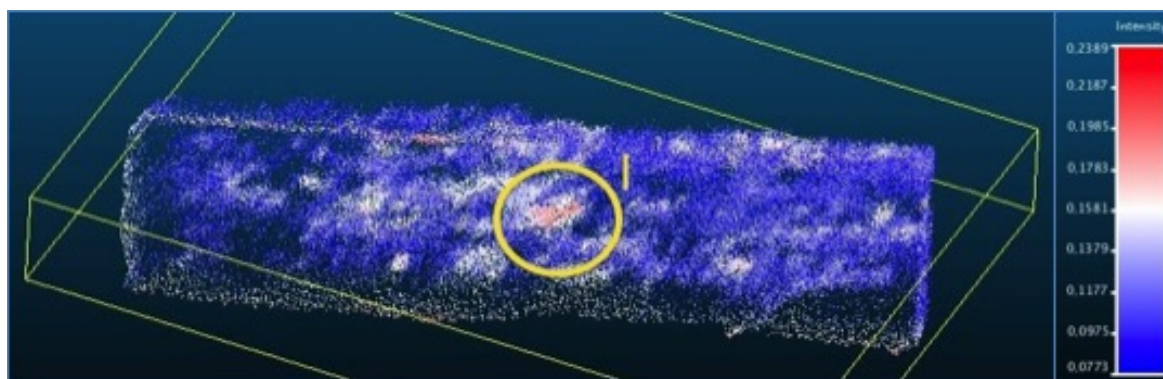


Figure 5.15: Point cloud of intensity values wood sample A: Basralocus - underwater result

5.4 Scan recommendations for marine wood inspection

The implementation of laser scanning techniques for inspection purposes of wooden marine structures is not only desirable but also realisable in the near future. Laser scanning is mainly promising for inspections where the wood will be scanned repeatedly over a period of time. The resulting detected change in surface profile of the wood can then be used for assessment of the extent of damage and estimation of service life of the wooden structure.

The Leica C10 ScanStation is a terrestrial laser scanner designed for scan purposes that principally do not include scanning through the water. Even though it is possible to use the Leica C10 in through water scan applications, the laser scanner proves to only be able to scan a wooden target under certain favourable water conditions. In practice, these water conditions are uncommon. The Schie water represents water that also flows through a typical Dutch harbour, however this experiment did not result in data for any of the wood samples. This particular laser scanning device is thus not suited for inspection of wood structures in marine environment. A laser scanner that is specifically designed for scanning targets through the water is expected to be capable of scanning submerged piles under more common outdoors water conditions. It is thus strongly recommended to check whether the laser scanning device is suitable for through water scanning.

One of the effects that occurred was the change in colour of the wood sample because the sample absorbed water and became less reflective. It is useful to create another case study in which the difference is mapped. In such a study a sample can be scanned both dry and wet to determine the difference. Unlike this case study, the wet sample is then scanned only through the media air, not water. In this case study it was not possible to divide the effect of absorbance from the influence of the travel distance of the signal through water. The proposed case study does not include scanning through water so the absorbance effect itself can then be determined.

Another disadvantage of the Leica C10 is the minimum vertical downward scan angle. The Leica C10 is not able to scan downward under an angle that is smaller than 45° . In figure 5.16, the laser scanner is displayed in a plausible scan setting for inspection of mooring poles in a harbour. In the situation on the left the scanner is only able to scan the head of the mooring pole because of this scan angle limitation. In the situation on the right, the mooring pole is located far enough from the pier so that the scanner can also see the most damaged zone of the wooden pile, which is the tidal zone.

The two identified problems when scanning wood samples in marine environment with the Leica C10 are the vertical downward scan angle and the ability to scan through more turbid waters. These two problems can be solved by choosing an other laser scanner. There exist laser scanners that are specifically designed for these kind of marine inspection purposes. Laser scanners that are designed specifically for marine purposes will not experience the lack of returns when scanning through more turbid waters. These scanners are overall more powerful and depending on the application the wavelength of the laser light differs. It is also possible to put a terrestrial laser scanner on a vessel equipped with an IMU, which stands for Inertial Measurement Unit. In this situation it is possible to scan the wood structure close by and any limitation in vertical scan angle can be avoided.

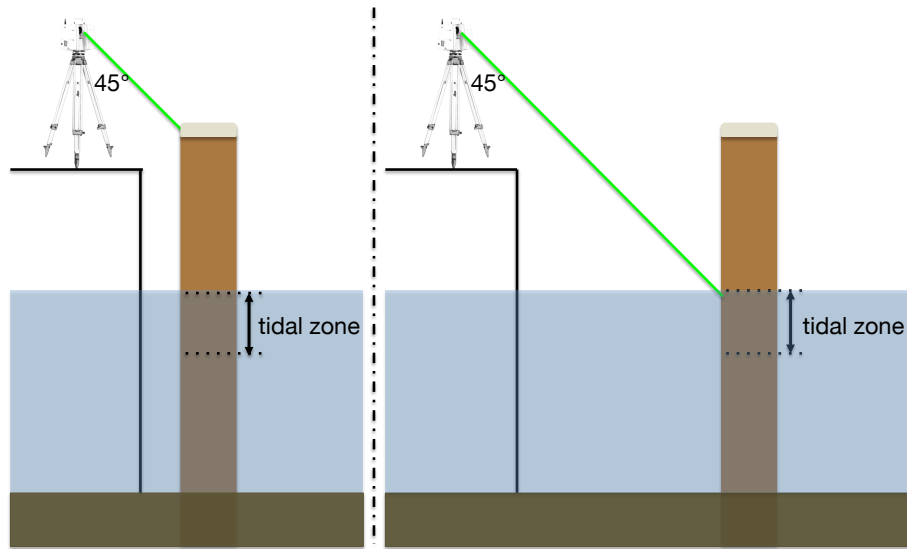


Figure 5.16: Schematic view of Leica C10 on harbour site

One more practical recommendation is the time period for scanning in the field. It is recommended to scan under low tide so that the most damaged part of the pile, which is the tidal zone of the wood structure is above the water. Even with a laser scanner designed for through water scanning this is recommended as the best results are always obtained without the extra medium that is the water. Without the water present the attenuation of the signal in the water is not present. Without this extra medium there will be more return points and thus a more detailed surface profile of the wood compared to a scan that did include the medium water.

Further it is recommended to use the custom resolution scan settings in the laser scanner after locking the scan target in a quick scan with low resolution setting. Depending on the maximum range, for short range the smallest possible point spacing of the Leica C10 is 1 millimetre. This resolution provides a point cloud from which a highly detailed surface profile can be derived. With this point spacing the mean of the nearest neighbour values of the dry scan of the *Basralocus* wood sample is 1.3 millimetre. For the wet scan the mean of the nearest neighbour is 3.2 millimetre. The points that were lost were located at the darker spots. These dark spots were mostly holes caused by the shipworm. Concluding the scanning of wood structures is possible with the proper laser scanning device and scan set up and the correct resolution scan settings.

Chapter 6

Case Study II: Coastal Dune Pools

The accurate mapping of the underwater environment is essential for many study areas. Various bathymetry studies have been performed in order to generate an underwater profile of for example a river bed. The generated underwater profile of a river bed provides information about for example morphological flow and distribution patterns. Ecological studies of underwater environments also demand an accurate map of the present vegetation. A terrestrial laser scanner is often used for these kind of applications as it is portable and provides a high resolution.

The field work included in this research comprises the scanning of two different coastal dune pools with the Leica C10 ScanStation. The goal of this case study is to discover whether the terrestrial Leica C10 laser scanner is able to detect the underwater bathymetry and vegetation. Both of the scanned pools have been explored thoroughly before their scan date and both are located near the Dutch coast in the province South Holland, the Netherlands.

All of the laser scanning equipment as assembled on the equipment list of paragraph 4.1.2 was used for the field work with the exception of the scan targets. The two separate scan targets are dune pool I and II. The field work equipment also included an home-made measuring pole and a smartphone equipped with an application for positioning. The height of both scan locations obtained from this mobile positioning application have been verified with data from the Height Model of The Netherlands, also known as AHN-2. The AHN-2 data is represented according to the Amersfoort/RD new geographic coordinate system. The AHN-2 is a free accessible digital terrain model of the Netherlands that has a resolution of 50 centimetre [2].

As it is impossible for one person to carry all of the necessary equipment, help was arranged for the two field experiment days. Two persons are able to carry all of the equipment, though especially for rough terrain carrying all equipment proved to be quite heavy. For further field work projects it is thus wise to arrange more (wo)manpower.

6.1 Dune pool I

The first dune pool is selected for its white sand on the bottom of the pool and the various types and green colours of underwater vegetation.

6.1.1 Location, surroundings and outdoor environment

Dune pool I is located in the municipality of Wassenaar. The dune area is called Berkheide and exists of parabolic shaped dunes, little valleys and open grasslands with low trees and vegetation. The geolocation of the chosen pool is $52^{\circ}10'40''\text{N}$, $4^{\circ}22'37''\text{E}$ and height 6.99 metre. The location is projected in the WGS 84 Web Mercator geographic coordinate system. The dune area is one of the typical Dutch dunes located near the coast. Figure 6.1 displays an aerial photograph.

The dune environment is assigned as nature reserve so there are no buildings present in the dune area. The area is accessible only by foot or bike over shell-paths and gravelled paths. The hike to the pool through the dune area was quite lengthy and tough because of the carried equipment in combination with the weather conditions. The dune pool was scanned on August 24, 2016, which was a hot, cloudless summer day. The pool is located off the path down a small sand slope where no walkers will normally go. The maximum water depth of the pool is almost 40 centimetre.



Figure 6.1: Aerial photographs of dune pool I

6.1.2 Experimental field set up

The laser scanner has been set up so that it was able to see the part of the pool that was closest by and the vegetation at the bank of the pool. The pool has been chosen especially for its many different types of underwater vegetation. Some of the vegetation is partly submerged in the water so these specific plants have been mapped both above and beneath the water surface. The maximum water depth was approximately 50 centimetre.

Figure 6.2 shows a picture of the pool. The laser scanner has been set up underneath a tree as can be seen from figure 6.3. The scanner itself was thus in the shadow but the pool itself was for the most part in direct sunlight. The ground was soft so the laser scanner has been placed carefully. After levelling the device caution was necessary to not tilt the device by standing or walking close by.

Previous experience learned to not scan right towards the sun. As the scan day was very sunny this has been taken into account when setting up the laser scanning device. The operating temperatures of the Leica C10 are between 0 and 40°C as can be read off from table 3.1. The temperature during the scan day was 37°C at its maximum so within this operating temperature range but to avoid any overheating the device was placed underneath a tree.



Figure 6.2: Picture of dune pool I



Figure 6.3: Scan set up of dune pool I

6.1.3 Scan results of dune pool I

The scan results of dune pool I showed some peculiarities. The black holes in the return point cloud as displayed in figure 6.4 indicate that no data is present. Some black parts are caused by other vegetation on the bank that block a part of the pool from view.

Not all black parts are caused by this blockage though. The other locations in the point cloud where no data is present are due to the shadow of overhanging trees. The laser scanning device is located under a tree as can be seen in figure 6.2. This tree, together with an other tree on the right side of the scanner, shade a part of the pool and exactly at this shaded part of the pool no data has returned.



Figure 6.4: Point cloud intensity values of dune pool I

The manufacturer of the laser scanner, Leica, promises that the Leica C10 is fully operational from bright sunlight to complete darkness as also recounted in paragraph 3.1.1. So according to Leica and consistent with the basic theory of laser scanning technique, it should not matter whether an object is illuminated by the Sun or an artificial light source or not illuminated at all. In theory the illumination of the object by the laser light itself is enough enlightening to be able to detect the object. The bottom of the pool consists for the most part of tan, light-brown sand together with light green vegetation. The laser scanner was able to see the bottom at locations where the Sun illuminated the bottom of the pool. However at locations of shade the bottom of the pool the scanner did not detect the bottom leading to no return data presented as black holes. So for this particular field case study the lighting did matter.

The intensity range of the resulting scan was between 0.07 and 0.28. The intensity value of 0.07 is again the intensity threshold that has also been found in various experiments described in chapter 4. If this intensity threshold would not exist more data points will return however it is questionable if these points can be considered as legitimate data or noise. The lower intensity values were the muddy, sandy bottom of the pool while the upper values belonged to the vegetation present in the pool.

The paragraph concerning the experiments with the water plants in laboratory settings, paragraph 4.4.5, gave some insights into scanning underwater plants. From this laboratory experiment became clear that the intensity values of the water plants did not differ much when comparing the dry scans with the underwater scans. This finding also holds true for the field experiment. The field of view scan settings were intentionally set rather broad so that some of the vegetation that was present at both bank and in the pool could be mapped both dry and under water. The intensity differences between submerged and dry plants within the same type of vegetation proved to be rather small for all kinds of vegetation. The average intensity differences were 0.02. In addition, the intensity differences between different types of vegetation proved to be small as well. Where by eye the different green colours of the different types of vegetation could be distinguished rather easily, this was much harder in the returned point cloud. This was especially the case for all of the underwater vegetation.

Last there was an unexpected and unsolved problem with the return data. The data was correct on both the screen of the Leica C10 laser scanning device and in the Leica software Cyclone [22]. A description of the processing with Cyclone is given in appendix C. The data could be preprocessed without problems and then converged to another file format. After retrieving the new file and loading it in CloudCompare, the data was faulty. This happened for all types of files and all different preprocessing options. A solution has not been found to this problem due to time constraints. Instead the data has been examined with the Cyclone software.

6.2 Dune pool II

The second dune pool is selected for the canes that are partly submerged in the water and partly above the water surface and the mossy bottom of the pool

6.2.1 Location, surroundings and outdoor environment

Dune pool II is located in the Oostduinpark in The Hague. Its geolocation is $52^{\circ}07'03''\text{N}$, $4^{\circ}18'18''\text{E}$ and height 3.55 metre and this location is projected in the WGS 84 Web Mercator geographic coordinate system. Figure 6.5 shows an aerial picture of the pool. The second dune pool in the Oostduinpark dune area is more accessible than the first scanned pool in dune area Berkheide. It is possible to park nearby the pool and walk over paved roads and shell-paths to the pool.

The pool has been scanned on the 27th of August, 2016. During the scan it was hot and sunny and the couple of clouds present did not cover the Sun. Because of the hot weather, a lot of day trippers past by to go to the beach. Luckily the pool was rather small so the scans did not take that long so the hinder to passersby was minimal.



Figure 6.5: Aerial photographs of dune pool II

6.2.2 Experimental field set up

The second dune pool was small and shallow and partly covered with canes. The canes were partly submerged in the water but for the most part above the water surface as can be seen from figure 6.6. A part of the water in the pool had evaporated on the scan day compared to the exploration day. This was due to the heat wave that occurred the week before the scan day. The water depth had thus reduced from approximately 20 to 10 centimetre at its maximum.

The tripod holding the laser scanner had been set up rather wide so that the device was close to the ground. The minimal downward scan angle was taken into account so that the scanner could see also the part of the pool close by. Figure 6.7 displays the set up for the second dune pool.

Both pool and laser scanner were exposed to direct sunlight. Because it was a hot day with temperatures above 30°C , the device experienced some overheating and the van on the device was working overtime. To avoid this in further field experiments it is advised to take an umbrella or parasol. However be careful not to shade the scan target with this sun screen. When shading the scan target it is possible that the same black holes will appear in the return data as occurred in the experiments with the first dune pool as described in paragraph 6.1.3. Fortunately the pool was small, even more so because part of it had evaporated in the days before, so the scans did not take a long time. The laser scanning device performed well.

Notable is that the dune pool selected as dune pool II was not the first choice pool in the Oostduinpark. On the exploration day another pool was selected. Due to the heat wave however eutrophication took place in this pool. The eutrophication can be defined as the over-enrichment of water by nutrients. Because of this phenomena the first choice pool appeared murky and thus unsuitable for scanning.



Figure 6.6: Picture of dune pool II



Figure 6.7: Scan set up of dune pool II

6.2.3 Scan results of dune pool II

Figures 6.8 and 6.9 display the point cloud containing the intensity values respectively the RGB image of the second dune pool. The RGB image is captured by the laser scanner. The mossy bottom of the pool is visible in figure 6.9. The mossy bottom is bright red in figure 6.8. The bottom was thus detected by the laser scanner. However the black spots that are present in both figure 6.8 and 6.9 are not due to blockage or shade. A probable cause of the black holes is the incidence angle of the laser beam on the water surface and the scan angle on the target. Nearby the scanner the incidence angle is much smaller than further away. The effect of the incidence and scan angle has not been investigated in this project. However for further scan experiments it is worth examining more closely.

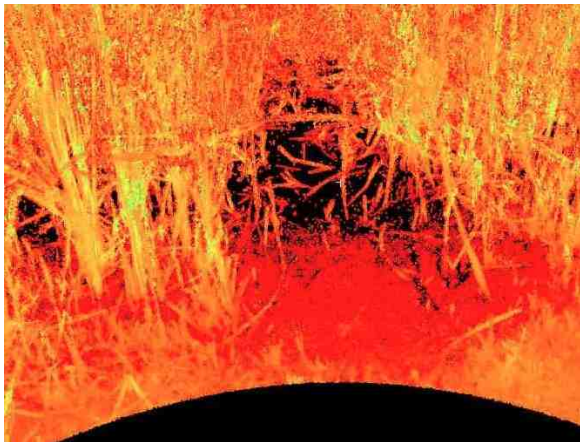


Figure 6.8: Intensity point cloud of dune pool II



Figure 6.9: RGB image of dune pool II

The intensity range of the second dune pool was the same as for dune pool I, that is between 0.07 and 0.28. The lowest value is again the intensity threshold of the Leica C10 laser scanner. In figure 6.8 the lightest colours correspond to the largest intensity values while the dark red colour represents the smallest intensity values. At the bottom of the pictures displayed in figures 6.8 and 6.9 a black curved area is visible. This is caused by the field of view of the Leica C10 laser scanner. The Leica C10 is not able to scan downwards under an angle smaller than 45° as displayed in figure 3.4. The horizontal field of view is 360° . Both pictures are viewed from the laser scanner and it can not see anything below an angle of 45° downwards.

The scan data of the second dune pool experienced the same technical problem as dune pool I. The data of both pools has been collected on separate days and preprocessed with Cyclone. In Cyclone the scan data was visible and adjustable however after the conversion the data was faulty. Again no solution has been found due to time constraints. The images displayed are thus from Cyclone.

6.3 Findings and recommendations

The differences between different types of vegetation becomes smaller when the vegetation is submerged in the water compared to vegetation above the water surface. While different vegetation could be distinguished easily when located above the water surface, this division proved to be much harder for submerged vegetation. For ecology studies in which the different vegetation types need to be mapped this particular laser scanner is thus not suited. However for ecology studies that only want to map if there is any vegetation present in the underwater environment, so for example studies that aim to distinguish the sandy bottom from the vegetation, the Leica C10 can be used.

The main practical finding concerned the movability of the Leica C10 laser scanner. The laser scanner is packed in a red trunk with wheels as displayed in figure 3.2. The scanner in its trunk can be pulled behind like a regular suitcase. For paved roads it is no problem to pull the Leica trunk. However in the case of shell-paths and gravelled paths it becomes much harder and after a while one gets weary. And moving on sand paths is impossible. As the case study in this chapter comprised of two experiments in the dunes, all of the above mentioned paths were travelled. A wagon would solve a bit of the problem however such a car adds weight so pulling the wagon with the trunk in it will be even heavier. Taking the other equipments was not that difficult even though the tripod was pretty unwieldy. If a wagon can be used all of the equipments can be assembled in the car. It is still wise to undertake the field work with at least two persons so one can take turns pulling the wagon.

The main problem experienced was the processing issue with the data. The data was correct in the Leica software, Cyclone, but faulty after transforming it into another file and viewing it in for example CloudCompare. The reason for this problem is unknown as this problem did not occur with any of the other experiments in chapter 4 and 5. There has been no solution to this problem, instead the data was viewed and examined within Cyclone.

A suggestion for further field work experiments is an ecological survey consisting of mapping various types of water plants. Due to time constraints it was not possible to explore the underwater scan results comprising of the underwater vegetation further. It is worth investigating this though as laser scanning for ecological studies is highly desired for many applications.

Conclusions and Recommendations

In this graduation research project multiple objects have been scanned through the water with a 532 nanometre green-wavelength terrestrial laser scanner. First the research questions from paragraph 1.2.3 will be answered for the basic experiments and then for the two case studies. Further the limitations of the laser scanner device that has been used in this project will be given, to finish with the possibilities when observing through the water with a terrestrial laser scanner.

Answer to research questions basic laboratory experiments

The research questions from paragraph 1.2.3 concerning the basic experiments, which are research question i. up to and including vii., can be answered with the findings from the basic laboratory experiments as described in chapter 4.

- i. *Regarding the measurement geometry and including the travel distance of the laser light from origin to target, what height and scan angle of the Leica C10 laser scanner device are required?*

The laboratory scans have all been performed within a short range, that is within 4 metre from the origin of the laser scanner. This range was also set in the resolution setting for the range. The laser scanning device was set at 1.75 metre height. This height was mostly for workability purposes: if the laser scanning device would be set higher it would be impossible to see the air bubble for levelling the device. Besides, the screen of the device would also be too high to operate on for the user.

The laser beam was directed downwards at the pool and targets within it. The vertical scan angle of the Leica C10 was thus between 0° and 45° , while a horizontal field of view of 70° was needed to scan the whole pool from left to right. The vertical field of view of the Leica C10 was the limiting factor when scanning downwards as the minimum scan angle is 45° and the device itself can not be rotated. For studies that include scanning through the water, an other laser scanning device that is able to scan downwards, so at a angle of 90° , is highly recommended.

The scan angle of the Leica C10 determines the angle of the beam of light on the water surface and thus the angle of incidence on the air water boundary. The angle on the target itself depends on the shape of the target. The effect of the different scan angles was negligible when scanning a target on the bottom, like the bathymetry of the sand. However for vertical objects like the wooden measuring pole the scan angle did matter. The effects of the scan angle on the target have not been investigated in this studies. The effects of the scan angle when scanning a target that is submerged in water is worth investigation in future studies.

- ii. *What resolution scan settings, leading to a certain point density, of the Leica C10 laser scanner, are preferred?*

The resolution settings can be set by the user specifically for the range. If the maximum range is known or can be measured or estimated, the custom resolution settings provide the highest resolution that is possible for this specific range. The maximum range was 4 metre which leads to a horizontal and vertical resolution of 1 millimetre. In comparison, the highest standard resolution has a range of 100 metre and a horizontal and vertical resolution of 1 centimetre. Custom settings have proven to give smaller point spacing and are thus preferred. It should be noted that before setting the resolution settings to custom, a low resolution scan always needs to be performed to lock the target. This is necessary because a scan with custom resolution settings may take a long while when the target is not yet locked. So for short to medium range scanning purposes, custom scan settings are preferred after the target is locked.

iii. *What is the influence of the travel distance, both through air and water, on the return signal?*

Even at short range, the travel distance influences the return signal. Two components concerning the return signal have been investigated thoroughly, that is the return signal power, which is the recorded intensity value, and the number of return points, often expressed in point density. Experiments have been performed scanning a target both dry and wet under different water conditions. The atmospheric conditions, lightning and surroundings were set to be the same for the laboratory experiments.

The travel distance through the air did not influence the return signal because of the short range. Besides, the atmospheric conditions, lightning and surroundings are constant so these cancel out for the laboratory scans. When scanning outdoors this may change as the range is usually larger and the weather conditions are variable.

The range through water is determined by the water depth, the incidence angle of the ray of light on the water surface and the refractive indices of the two media. The range through water ranged between 0.5 and 0.7 metre for a depth of 40 centimetre. The intensity decreases for an increase in water depth, but the pattern of the returns is the same for each depth. What stood out most is the intensity threshold of 0.075 that causes the signal to be incomplete. It is assumed that there will be points with a smaller intensity than 0.075 but these are not recorded. Apart from this, the largest change is the number of return points. With a water depth of 40 centimetre there were almost no return points for a target on the bottom on the pool like the beach sand. However, the other three depths, that is 5, 10 and 20 centimetre did provide data.

If the range through water becomes too large, the water is too turbid and the reflectivity of the target is too low at the wavelength of the laser, the signal will not return to the laser scanner. And if the signal has enough power to return but is below the intensity threshold of 0.075, the point will not be recorded. In this research only the reflectance at 532 nanometre of various targets has been investigated.

iv. *How does the return signal change in relation to an increase in water depth?*

The influence of the increasing depth on the return signal has also been discussed at subquestion iv. When increasing the depth, the range through water will increase as well. The increase in range through water causes a part of the signal to be lost. The intensity threshold value of 0.075 is very important in this matter because it cuts off part of the data. An increase in water depth is thus an important part of the range through water.

The Leica C10 proves to be able to scan various targets through little turbid water up to a water depth of 40 centimetre. The strength or power of the signal, expressed in Joules, is important for this limiting water depth and turbidity. A scanner with a larger power will be able to measure the bathymetry of deeper and more turbid waters. The maximum applicable water depth for the Leica C10 was set to 1 metre according to literature. For completely clear, still waters and with highly reflective targets, for example white rocks or white sand, this water depth is achievable. However, for more turbid situations, 40 centimetre has found to be the applicable water depth.

v. *What influence have the characteristics of the medium water, like salt content, turbidity, contamination, on the scan results?*

The water turbidity is one of the three main influencing factors on the return signal in this study. The signal losses in the water are due to absorption and scattering. For more turbid waters these losses are larger.

The salt content has not been tested in the laboratory, however literature has shown that the refractive index of water varies with less than 1%, for a wide range of temperatures and salinity. Therefore the influence of the salt content is expected to be negligible. The scans with mixture water showed some other visible contamination like floating particles of wood and sponges. If these particles were larger than the point spacing, they would show up in the resulting point cloud at the air water boundary. They had no influence on the targets located under water though.

The flow is another characteristic of the water that influences the results. Water flow causes distortion in the form of diffuse scattering when the signal travels through the moving water. Scanning through flowing water is possible for shallow, clear waters as shown in a study scanning the bedding of a clear, shallow and fast flowing mountain channel [26] [27]. The effects of the water flow have not been included in this study but should be taken into account for the field experiments.

- vi. *What influence have the characteristics of the object, like material, shape, colour, smoothness, on the results?*

The characteristics of the object are the third main influence on the return signal. Between the influences of the water depth and the water turbidity, the reflectance of the object at the wavelength of the laser light is found to be the most influencing factor of all on the return signal. The main property of the object is thus the reflectivity, which is defined by mainly the material and the colour of the object. Examples of reflectance spectra have been presented and based on the reflectance at 532 nanometre an estimation of the return power can be made. There is always some natural variability which should be taken into account. The Leica C10 is especially suited for vegetation as these reflect well at a wavelength of 532 nanometre.

The influence of the material and colour on the reflectivity can be separated by scanning two objects with exactly the same standard colour but different material, for example a concrete cube and a glass marble. In these experiments it was not possible to obtain such materials and therefore the influence of material and colour can not be distinguished here.

An rather unexpected but important factor was that some materials absorbed water and reflected less in wet state. This effect lead to almost no return points when scanning under water. This was due to both the absorption which could be seen as the darker colour and the signal losses due to the turbid water. The two causes can be separated with the following experiment: first scan an object dry, then soak the object with water and scan it while it is wet but not under water. The difference between the wet object that is scanned dry and the wet object that is scanned while submerged under water is then caused by the signal losses solely. The absorptive behaviour of a target needs to be taken into account.

Last the shape and smoothness of the objects have been examined. The roughness or smoothness does not influence the returned intensity values for either dry or wet scans. Even though no experiment has been set to prove the following statement, literature research has confirmed the hypothesis that when the colour and scan conditions are equal, the point density reduces for rough surfaces. The roughness or smoothness of an object is thus especially important for the number of return points.

- vii. *How does the raw data need to be processed and corrected for refraction?*

The processing steps are all described in section 3.3 and Appendix C. In short, the raw data is first processed with Cyclone, then viewed and selected in CloudCompare. The correction for refraction is applied to the data in Matlab and, in case needed, the data is again viewed in and divided with CloudCompare. For visualisation purposes both CloudCompare and Matlab have been used. The correction for refraction has been done according to Smith [37] and making use of coordinate system transformations.

Answer to research questions case study I: wood samples in lab

The research questions concerning case study I have been given in paragraph 1.2.3. Four wood samples have been scanned in the laboratory under both dry and underwater conditions.

- viii. *What resolution is needed to detect the damages present on the wood samples?*

A surface profile of the wood can be generated if a sufficient amount of return points is available. The damage to the wood can be detected if the size of the damage is larger than the point spacing. The wood samples have been scanned with a point spacing of 1 millimetre and this was sufficient to detect the damages. The holes and cracks in wood can be distinguished by their dark spots. Within the spots no return data is available but the contour of the holes and cracks can be identified. Most of the holes had a diameter of 5 millimetre or larger and these could be easily detected.

In the Leica C10, the resolutions settings were set to custom which allows the user to set the maximum range. For short range the maximum possible horizontal and vertical resolution is 1 millimetre. In this experiment the range was up to 4 metre and the horizontal and vertical resolution were 1 millimetre. This resolution was sufficient to be able to see the damage on the surface profile of the wood.

ix. *Is there a difference between the wood samples in the through water scan results?*

Only the sample that was completely submerged in the water and located horizontally on the bottom of the pool was visible in the underwater scan with clear water conditions. This was the Basralocus sample which was part of a mooring pole. The point density was 60% compared to the dry scan of the sample. Remarkable is that these results were obtained under 40 centimetre of water while the vertical pine wood sample only had 6% returns and these were only in the upper 10 centimetre of the water. The poor results are mainly due to the absorption of water of the three targets leading to a lower reflectance. By eye a change in colour could be detected when the wood samples were soaked with water. Other issues are the signal losses due to the water turbidity and also it is expected that the scan angle on the target is of influence. The effect of the incidence angle on the scan target however has not been investigated so the effect of the scan angle solely can not be quantified.

x. *What influence has the turbidity of the water on the resulting wood scans?*

When examining the results obtained with the Basralocus wood sample the turbidity plays a large role. In the underwater scans the water depth was constant, as was the placing of the wood sample, the set up of the laser scanner and the atmospheric conditions. The only parameter that was varied was the turbidity. When scanning the sample through tap water with a turbidity of 0.3 *NTU*, the returns were 60% compared to the dry scan for the Basralocus sample. Water with a turbidity of 1.3 *NTU* had only 5% returns which was insufficient to generate a surface profile. The water that represents water in Dutch harbours had a *NTU* of 2.0 and for this situation no data returned. The other three samples did not give sufficient returns when scanning through water.

xi. *Simulating the water of a harbour, is the laser scanner able to see whether the mooring pole is damaged?*

The water that is similar to water in a harbour is the Schie water. This water, with a turbidity of 2.0 *NTU*, was drained directly from the Schie river in Delft. The Schie river flows through multiple small harbours in Delfland, then splits and runs multiple Dutch harbours. However the experiment with the Schie water did not provide any data when scanning with the Leica C10. For through water scan applications in marine environment it is therefore recommended to use an other laser scanner that is especially designed for through water scans.

Answer to research questions case study II: coastal dune pools

The subquestions from paragraph 1.2.3 concerning case study II can be answered after the field work.

xii. *Which environmental conditions should be taken into account beforehand?*

It is recommended to visit the site beforehand to explore the surroundings, accessibility and scan target. The water conditions also need to be examined on this exploration day. A rule of thumb is that if the bottom of a pool is visible by eye and the maximum water depth is estimated or measured to be less than 25 centimetre, scanning is possible. After the exploration day a scan day can be planned. On this scan day the weather conditions need to be taken into account. Specifically whether it is sunny or cloudy, if there is a chance of precipitation and what the wind conditions are. If the water surface is not flat but disturbed by precipitation and surface winds scanning underwater targets is not possible.

xiii. *Can the laser scanner detect the bathymetry of a pool?*

The Leica C10 can detect the bathymetry of the pool up to a scale of 5 millimetre under rather clear water of 20 centimeter at its maximum depth. However when the bottom of the pool was overshadowed by a tree there were no returns for this part. For underwater scan applications the lightning is thus crucial.

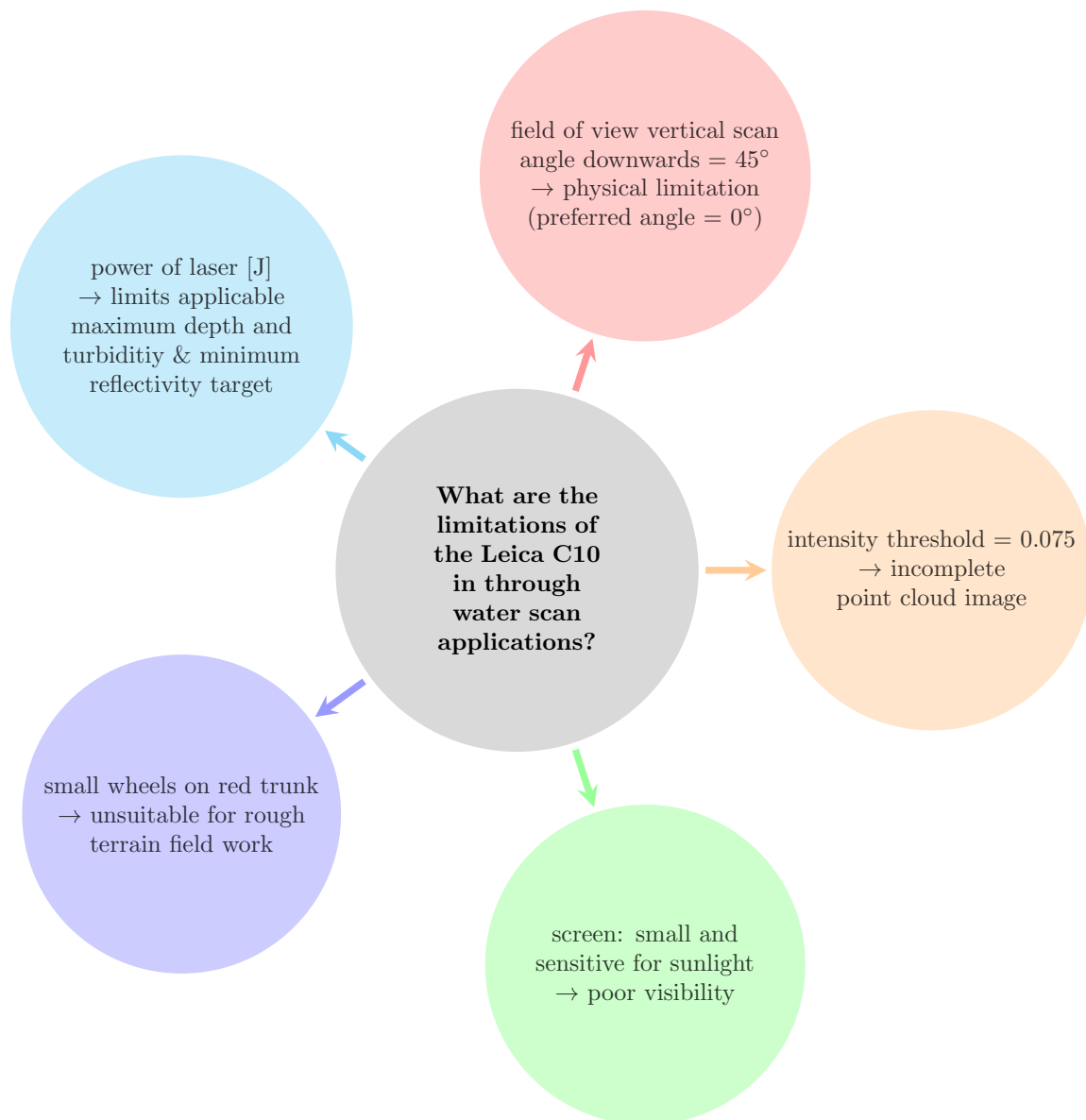
xiv. *Can the laser scanner distinguish the various types of vegetation present in the dune pools?*

The differences between different types of vegetation are too small to be detected in the resulting point cloud based on intensity values. It different types of vegetation have a different shape they can be distinguished for each other. It is thus not recommended to use this laser scanner for a study where the different types of underwater vegetation need to be differentiated. For ecology studies where the amount of underwater vegetation as a whole needs to be mapped the Leica C10 is suited.

Limitations of the Leica C10 ScanStation

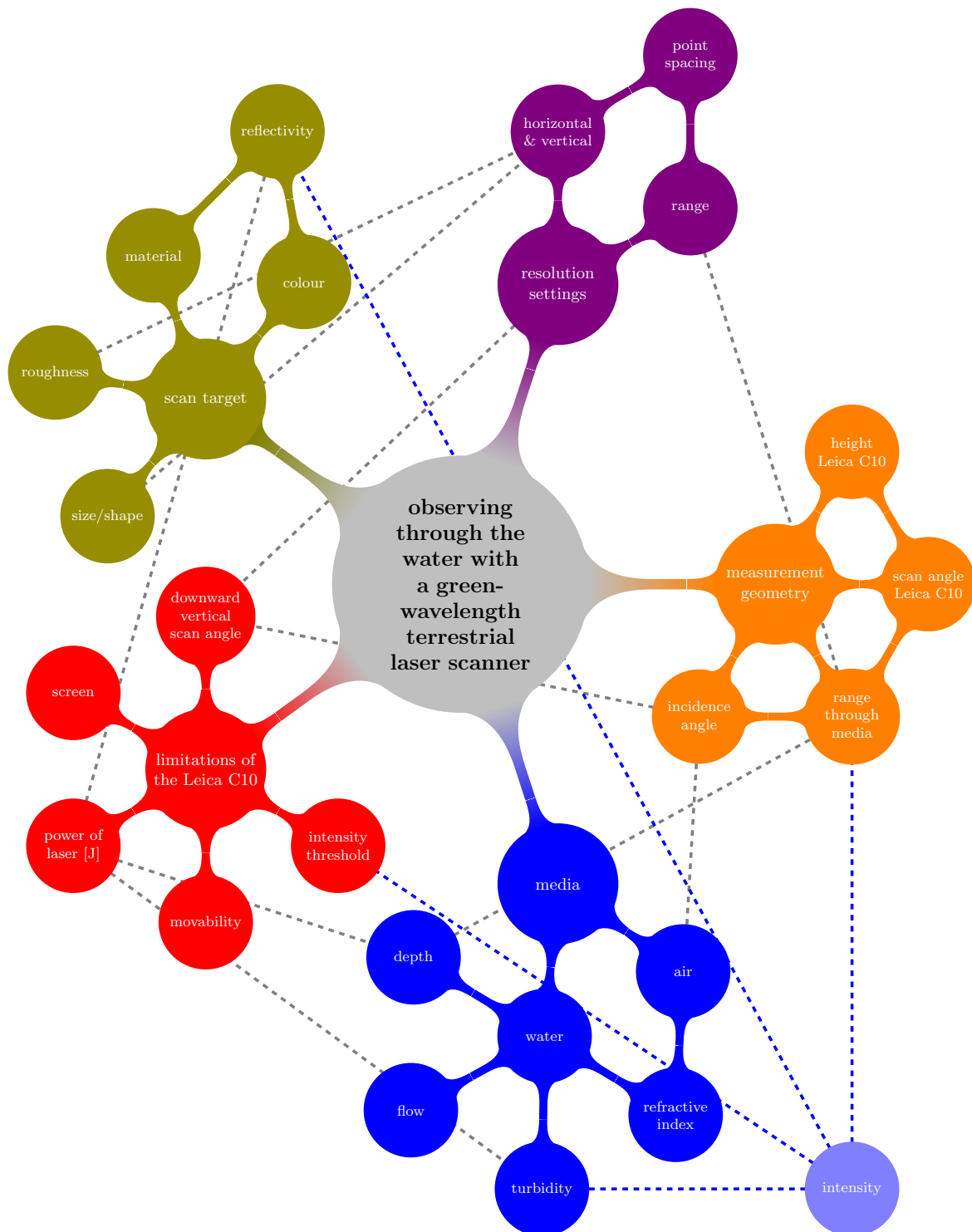
The manufacturer of the laser scanning device that has been used here promises a certain operating range. This operating range has been discussed and there have been some findings specific for the underwater scan application that were not known beforehand. As the Leica C10 ScanStation is not designed specifically for through water scan applications, the limitations were unknown. The uncovered limitations of the Leica C10 for this application have been gathered in a diagram. Some of these findings are not only for underwater scans but may also be important for other scan applications, like the movability of the scan equipment.

Concluding, the Leica C10 is a proper and portable laser scanner that can be used for certain underwater scans that have a water depth of maximum 20 centimetre and a scan target that has a high reflectance at 532 nanometre. Before planning a scan project the environment, media and targets need to be examined closely. Based on this review a well considered choice can be made for the type of laser scanner that is most suited for the project.



Observing through the water with a terrestrial laser scanner

A mind map is created to summarise the findings and results obtained in this research project. In this mind map the subjects that are related or that influence each other are linked by dotted lines. The intensity is added as well as the intensity is one of the determining output parameters of a scan. The overall conclusion of this research project is that observing through the water with a green-wavelength terrestrial laser scanner is achievable and it is a favourable mapping technique when the scope of the project and the operating range of the laser scanning device are well-explored. In addition, enough (wo)manpower should be arranged for the field work.



Bibliography

- [1] 3Deling, 3D laser scanning services, *Project Examples*, <http://www.3deling.com/>
- [2] Actueel Hoogtebestand Nederland (Height Model of The Netherlands), www.ahn.nl and online AHN viewer <http://ahn.arcgisonline.nl/ahnviewer/>, AHN-2 data obtained in 2016
- [3] Bailly, J.-S., Le Coarer, Y., Languille, P., Stigermark, C.-J., Allous, T. (2009) *Geostatistical estimations of bathymetric LiDAR errors on rivers*, *Earth Surface Processes and Landforms* 35, 2010
- [4] Blass, H.J., Aune, P., Choo, B.S., Görlacher, R., Griffiths, D.R., Hilson, B.O., Racher, P., Steck, G. (1995) *Timber Engineering STEP 1: Basis of design, material properties, structural components and joints*, published by Centrum Hout, The Netherlands, ISBN 90-5645-001-8, 1995
- [5] Charlton, M.E., Large, A.R.G., Fuller, I.C. (2002) *Application of Airborne Lidar in River Environments: the River Coquet, Northumberland, UK*, *Earth Surface Processes and Landforms*, 2003
- [6] Ciddor, P.E. (1996) *Refractive index of air: new equations for the visible and near infrared*, *Applied Optics*, Vol. 35, No. 9, 20 March 1996
- [7] Clausen, C.A. (2010) *Wood Handbook, Wood as an Engineering Material, Chapter 14: Biodeterioration of Wood*, General Technical Report FPL-GTR-190, U.S. Department of Agriculture, Forest Service, Forest Products, 2010
- [8] CloudCompare- 3D point cloud and mesh processing software - Open Source Project (2015) *Cloud-Compare Version 2.6.1 User manual*, February 2015, <http://www.danielgm.net/cc/>
- [9] Daimon, M., Masumura, A. (2007) *Measurement of the refractive index of distilled water from the near-infrared region to the ultraviolet region*, *Applied Optics*, Vol. 46, No. 18, 20 June 2007
- [10] Eitel, J.U.H., Vierling, L.A., Long, D.S. (2010) *Simultaneous measurements of plant structure and chlorophyll content in broadleaf saplings with a terrestrial laser scanner*, *Remote Sensing of Environment* 114, 2010
- [11] Gard, W., Montaruli, N., van de Kuilen, J.-W. (2012) *End-of-Life Wood Quality of Mooring Poles*, World Conference on Timber Engineering, Timber Engineering Challenges and Solutions, Auckland, New Zealand, 15 - 19 July 2012
- [12] Gem City Images (2011) *Wind Creating Ripples On A Puddle of Water*, 2010, <http://www.gemcityimages.com/2011/03/wind-creating-ripples-on-puddle-of.html>
- [13] Giancoli, D.C. (2009) *Physics for Scientists & Engineers with Modern Physics*, fourth edition, published by Pearson Education, Inc., United States of America, ISBN 978-0-13-157849-4, 2009
- [14] Heritage, G.L., Milan, D.J. (2009) *Terrestrial Laser Scanning of grain roughness in a gravel-bed river*, *Geomorphology* 113, 2009
- [15] Hodge, R., Brasington, J., Richards, K. (2008) *In situ characterization of grain-scale fluvial morphology using Terrestrial Laser Scanning*, *Earth Surface Processes and Landforms* 34, 2009
- [16] Jerlov, N.G. (1976) *Marine Optics*, published by Elsevier Science, Amsterdam, the Netherlands, eBook ISBN 9780080870502, 1976

- [17] Kinzel, P.J., Wayne Wright, C., Nelson, J.M., Burman, A.R. (2007) *Evaluation of an Experimental LiDAR for Surveying a Shallow, Braided, Sand-Bedded River*, Journal of Hydraulic Engineering 133, July 2007
- [18] Kristensen, E., Suraswadi, P. (2002) *Carbon, nitrogen and phosphorus dynamics in creek water of a southeast Asian mangrove forest*, Hydrobiologia 474, April 2002
- [19] Laser-Scan Limited (1969) *Laser-Scan - The SWEEPNIK Film Measuring system*, Laser-Scan Limited brochure, Cambridge Science Park, England, 1969, http://www.pghardy.net/lsl/brochures/lsl_76_sweepnik_film_measuring.pdf
http://www-outreach.phy.cam.ac.uk/camphy/sweepnik/sweepnik_index.htm
- [20] Lake Access - an impact metro project (1999) *Turbidity in Lakes*, Natural Resources Research Institute, University of Minnesota, Duluth, 1999, <http://www.lakeaccess.org/russ/turbidity.htm>
- [21] Lee, Z., Shang, S., Hu, C., Du, K., Weidemann, A., Hou, W., Lin, J., Lin, G (2015) *Secchi disk depth: A new theory and mechanistic model for underwater visibility*, Remote Sensing of Environment 169, 2015
- [22] Leica Geosystems (2012) *Leica ScanStation C10/C5 User Manual*, version 5.0, 2012, <http://hds.leica-geosystems.com/en/Leica-ScanStation-C10.79411.htm>
- [23] Lichti, D.D., Harvey, B.R. (2002) *The effects of reflecting surface properties on time-of-flight laser scanner measurements*, ISPRS, Symposium on Geospatial Theory, Processing and Applications, Ottawa, 2002
- [24] Lopez-Anido, R., Michael, A.P., Goodell, B., Sandford, T.C. (2004) *Assessment of Wood Pile Deterioration due to Marine Organisms*, Journal of Waterway, Port, Coastal and Ocean Engineering, Vol. 130, No. 2, March 1, 2004
- [25] McKean, J. Nagel, D., Tonina, D., Bailey, P., Wayne Wright, C., Bohn, C., Nayegandhi, A. (2009) *Remote Sensing of Channels and Riparian Zones with a Narrow-Beam Aquatic-Terrestrial LIDAR*, Remote Sensing 9, 2009
- [26] Miura, N., Asano, Y. (2013) *Green-Wavelength Terrestrial Laser Scanning of Mountain Channel*, ISPRS Annals of the Photogrammetry, Remote Sensing and Spatial Information Sciences, Vol. II-5, 2013
- [27] Miura, N., Asano, Y. (2014) *Acquisition of underwater topography in a mountain channel using Terrestrial Laser Scanning*, Remote Sensing for Agriculture, Ecosystems, and Hydrology XVI, 2014
- [28] de Moel, P.J., Verberk, J.Q.J.C., van Dijk, J.C. (2005) *Drinkwater - principes en praktijk*, tweede herziene druk, TU Delft/SDU, Den Haag, the Netherlands, ISBN 90-12-10946-9, 2005
- [29] Munson B.R., Young D.F, Okiishi T.H, Huebsch, W.W. (2005) *Fundamentals of Fluid Mechanics*, John Wiley & Sons, Inc., New York, sixth edition, ISBN 978-1118399712, 2005
- [30] Nguyen, M.N., Leiceste, R.H., Cookson, L.J. Foliente, G.C. (2006) *An Engineering Model of Marine Borer Attack on Timber Piles*, World Conference on Timber Engineering, Portland, USA, 2006
- [31] Oliver, A.C. (1974) *Timber for Marine and Freshwater Construction*, Timber Research and Development Association; Rev. and metricated edition, 1974
- [32] Parkins, C. (2013) *The Colour of Light*, image retrieved from <https://chrsparkins.wordpress.com/2013/09/01/the-colour-of-light/>
- [33] Pesci, A., Teza, G. (2008) *Effects of surface irregularities on intensity data from laser scanning: an experimental approach*, Annals of Geophysics, Vol. 51, October/December 2008
- [34] Public Lab (2014) *NIR and water*, October 6, 2014, <https://publiclab.org/notes/cfastie/10-06-2014/nir-and-water>

- [35] van Ree, J.M. (2006) *Determination of the precision and reliability parameters of terrestrial laser scanners - by creating a practical experiment set-up*, MSc thesis report Geomatics, Delft University of Technology, 2006
- [36] Sadar, M. (2009) *The Basics of Turbidity Measurement Technologies - Prepared for the Methods and Data Comparability Board QA/QC Sensors Group*, Aquatic Sensor Workgroup, July 16, 2009
- [37] Smith, M.W., Vericat, D., Gibbins, C. (2012) *Through-water terrestrial laser scanning of gravel beds at the patch scale*, Earth Surface Processes and Landforms 37, 2012
- [38] Smith, M.W., Vericat, D. (2014) *Evaluating shallow-water bathymetry from through-water terrestrial laser scanning under a range of hydraulic and physical water quality conditions*, River Research and Applications 30, 2014
- [39] Soudarissanane, S., Lindenbergh, R.C, Menenti, M., Teunissen, P. (2011) *Scanning geometry: Influencing factor on the quality of terrestrial laser scanning points*, ISPRS Journal of Photogrammetry and Remote Sensing 66, 2011
- [40] Stewart, J. (2008) *Calculus - Early Transcendentals*, published by Brooks/Cole, Cengage Learning, United States of America, ISBN 978-0-495-38273-7, 2008
- [41] Streicher, M., Hofland, B., Lindenbergh, R.C (2013) *Laser Ranging for Monitoring Water Waves in the new Deltares Delta Flume*, ISPRS Annals of the Photogrammetry, Remote Sensing and Spatial Information Sciences, 2013
- [42] Teaching Great Lakes Science, *Water Clarity*, Michigan Sea Grant, University of Michigan and Michigan State University, the Great Lakes Observing System, Eastern Michigan University, the National Oceanic and Atmospheric Administration (NOAA), the Center for Ocean Sciences Education Excellence-Great Lakes, NOAA Great Lakes Environmental Research Laboratory, <http://www.miseagrant.umich.edu/lessons/lessons/by-broad-concept/earth-science/water-quality/water-clarity/>
- [43] United States Geological Survey, *Lidar for Science and Resource Management - Experimental Advanced Airborne Research Lidar (EAARL)*, United States Geological Survey, St. Petersburg Coastal and Marine Science Center, April 17 2014, <http://coastal.er.usgs.gov/lstrm/tech/tech1-earl.html>
- [44] Verschuur, G.L. (1997) *Transparency Measurements in Garner Lake, Tennessee: The Relationship between Secchi Depth and Solar Altitude and a Suggestion for Normalization of Secchi Depth Data*, Lake and Reservoir Management 13:2, 1997
- [45] Voegtle, T., Wakaluk, S. (2009) *Effects on the measurements of the terrestrial laser scanner HDS 6000 (Leica) caused by different object materials*, IAPRS, Vol. XXXVIII, France, September 2009
- [46] Vosselman, G., Maas H.-G. (2010) *Airborne and Terrestrial Laser Scanning*, published by Whittles Publishing, Scotland, UK, ISBN 978-1904445-87-6, 2010
- [47] Whiting, D., Roll, M., Vickerman, L., Johnson, S. (2015) *Plant Structures: Leaves - CMG Garden-Notes #134*, copyright 2003-2014, Colorado Master Gardener Program, Colorado State University, U.S. Department of Agriculture, <http://www.ext.colostate.edu/mg/Gardennotes/134.html>, September 2015
- [48] X-Rite Pantone, Huda, M. (2015) *Color Measurement 101: What is a Spectrophotometer?* August 17, 2015, <http://blog.xrite.com/what-is-a-spectrophotometer/>

Appendices

Appendix A Manual 'how to scan with the Leica C10'

One of the deliverables of this thesis is the manual 'how to scan with the Leica C10'. In this manual the basis steps for scanning with the Leica C10 are described. These steps may not include all of the steps one would need, for instance the use of different stations and the use of targets is not included. Anyhow, this manual will provide newbies with some basic knowledge enough to make their first scans.

A.1 The five Ws and one H

Before scanning, consider the five Ws and one H as often used in (science) journalism and research:

- Who
- What
- When
- Where
- Why
- How

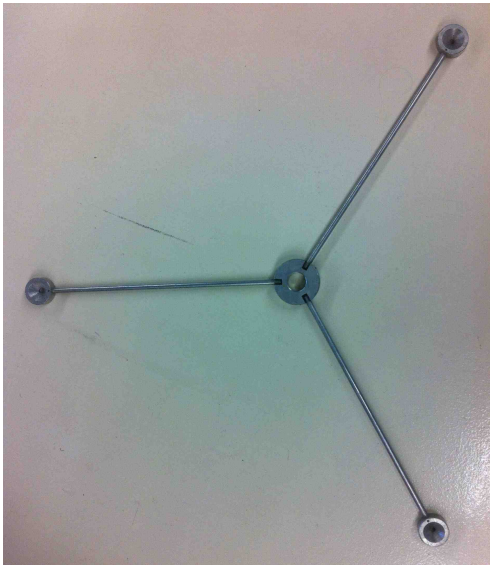
It is advised to make questions of the five Ws and one H and to answer these questions before scanning. For example, determine what the scan target is, how you are going to scan this target, why this is important and who is going to scan and who is there to help. Lastly, consider the workability of the scan project as it is a great influence on both the experimental set up as the time required to do the scanning.

A.2 Packing list

- (Leica) tripod
- tripod star in case of a smooth floor
- tribrach (which is a levelling head with an optical plummet)
- Leica C10 ScanStation in its red trunk, together with Leica measuring rod
- 4 batteries for the Leica C10 (2 in use, 2 reserve) from the battery charger
- USB stick, size 16 GB or larger
- laptop with Cyclone software (at Delft University of Technology: laptop TUD251188)
- safety shoes with steel toes (as required in some labs)
- notebook and pen
- depending on the scan target, some basic tools like a measuring pole and/or measuring rod, (duck) tape, markers, towels etc



Leica tripod



Tripod star



Tribrach



Red trunk with Leica C10 scanner



Leica C10 batteries on charger

A.3 Scanning with the Leica C10

The following steps describe the basics of scanning with the Leica C10 ScanStation. These are only the basics, more advanced scan options are not described here. For more advanced steps, see the user manual of Leica [22].

step 0 check out the location

- indoors vs. outdoors
- ground cover: build vs. natural
- light: artificial vs. natural
- amount of space around the experiment
- safety: lab rules vs. outdoors common sense



step 1 collect all the equipment needed

- see packing list (A.2)



step 2 set up tripod

- use tripod star in case of smooth flooring
- set up tripod at desired height
- attach tribrach to top tripod



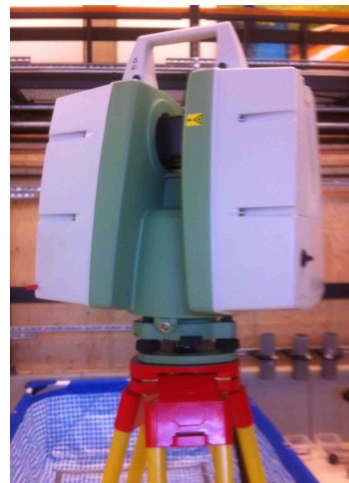
step 3 level tripod with tribrach

- look at optical plummet on tribrach
- make sure water bubble is in the middle



step 4 set up laser scanner

- remove tribrach
- attach laser scanner to top tripod
- measure height origin laser light with Leica measuring rod - write this down



step 5 fine tune levelling laser scanner

- level laser scanner with plummet on device
- put in 2 batteries (one on each side)
- press "on" (hold for 2 seconds)
- select "level and laser plummet" on top of screen
- level in device itself



step 6 check out main menu

- basic icons in main menu:
 - Scan
 - Manage
 - Tools



step 7 create new project and start

- select "Manage" in main menu
- select "Projects" in manage menu
- press "New" on bottom screen
- give name and creator of the project
- select project and press "Cont" to start



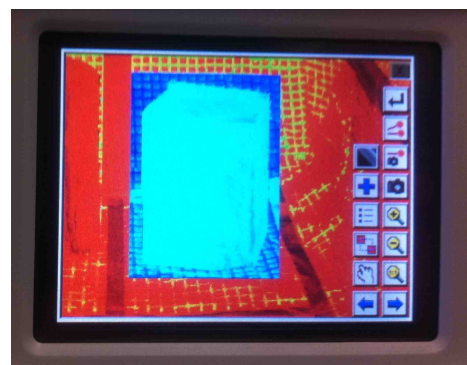
step 8 set up for first 'explore' scan

- select "Scan" in main menu
- set up first station (standard setup is ok)
- select "Fld of View" in scan parameter
- choose "Custom View"; give degrees as guess
- select "Resolution" in scan parameter
- choose "Lowest resolution"
- press "Scan" on bottom screen



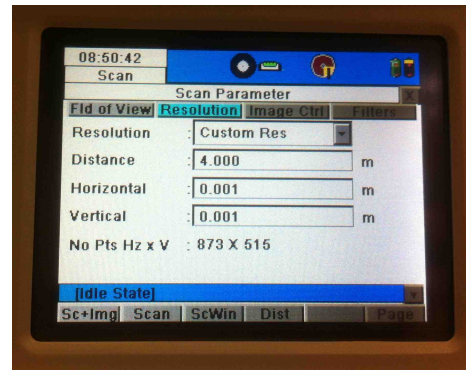
step 9 check out first 'explore' scan

- use hand icon to move around
- use magnifying glass icon to zoom in/out
- use icon with red squares to select area (degrees) for next scan
- press enter icon to go to scan parameters



step 10 set up for 'target' scan

- update "Fld of View": select area or manual
- choose resolution
 - choose "Highest resolution"
 - choose "Custom resolution" to set own range, accuracy
- press "Scan" or "Sc+Img" on bottom screen



step 11 retrieve data from laser scanner

- put USB stick (size 16GB or larger) in device
- select "Tools" in main menu
- select "Transfer" in tools menu
- select "Projects" in transfer menu
- press "Cont" on bottom screen



step 12 take down equipment

- press "on" (hold for 2 seconds) to shut down
- wait until the van stops
- take the 2 batteries out
- dismantle laser scanner
- dismantle tripod, tripod star
- put back all batteries on charger



A.4 Postprocessing steps with Cyclone

The raw scan data, which is in the format '.bin', needs to be converted to another format, for example '.ptx' or '.xyz'. Both of these formats can be opened by the often used open source software for point clouds, CloudCompare. CloudCompare is also able to convert '.ptx' to '.xyz'. The latter, '.xyz', can be opened by Matlab. Other software may be able to open these formats, depending on the software itself. The steps that need to be taken to convert the data with Cyclone, which is the software of Leica, are described below. The steps described are for the laptop of the Delft University of Technology (TUD251188) which has the Cyclone license for version 9.0 of Cyclone. Noticeably these steps do also apply for other laptops/computers with the software.

postprocessing steps convert raw data with Cyclone

- put USB stick with raw data in laptop
- open Cyclone (on desktop TUD251188)
- choose "Servers" → "TUD251188" (either shared or unshared)
- right mouse click: "Create new database" → give name, for example "X"
- right mouse click on "X" → "Import ScanStation C5/C10 data" → select USB → select folder "Scanner-Projects" → select desired project → import
- default settings for importing ok, continue
- open project → right mouse click on "SW.005" → "open Truspace"
- in Truspace: "file" → "Open local Modelspace view"
- right mouse click on "Open local Modelspace view" → "Open temporary Modelspace view"
- in local Modelspace view: "selection" → "select all"
- check bottom screen how many point clouds have been selected before proceeding
- "file" → "export" → choose format: '.ptx' or '.xyz' (advice: '.ptx')
- wait until converting is done; warning: can take a while for large point clouds

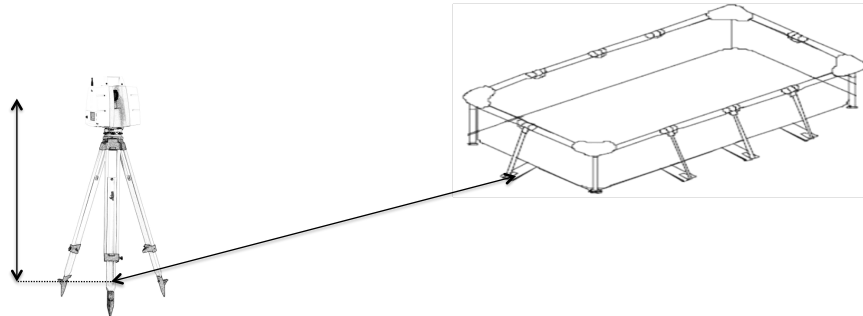


Appendix B Overview of the laboratory experiments

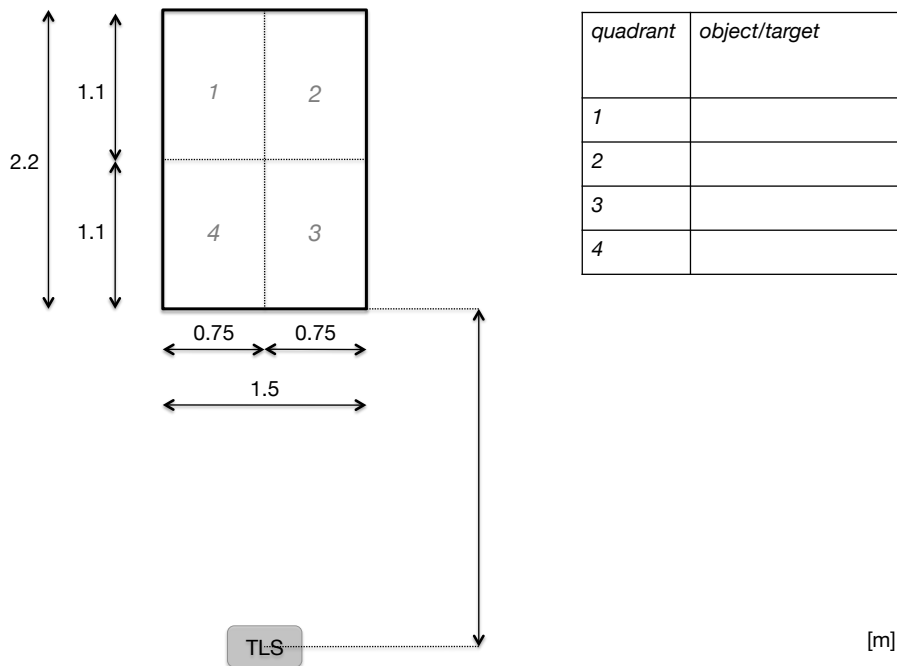
In this appendix an overview is given of the laboratory projects and their characteristics. An empty lab card that has been used in all of the laboratory experiments of chapters 4 and 5 is displayed and an overview of all of the lab experiments are given.

B.1 Example of lab card

date:	name:	experiment:
-------	-------	-------------



[m]



[m]

B.2 Overview of laboratory experiments

lab scan project	target(s)	water type	water depth [cm]	measuring pole visible	number of raw scans	size [MB]
buddha	concrete buddha sculpture	dry	-	no	8	27
		7525	40			
cubes	coloured concrete cubes	tap	40	no	4	27
pool	dry reference scan pool duct tape wooden measuring pole	dry	-	yes	7	634
rocks	metamorphic rocks	dry	-	no	10	117
		7525	40			
rubber	green rubber tile	dry	-	no	11	170
		7525	40			
sand	beach sand wooden measuring pole	7525	40	yes	7	505
		7525	20			
		7525	10			
		7525	5			
spheres	coloured glass marbles	dry	-	no	23	249
		tap	40			
	dimpled titanium golf balls	tap	40	no		
waterplants	water plants	tap	40	no	12	92
waterplants7525	water plants	7525	40	no	10	69
wood	wood samples wooden measuring pole	dry	-	yes	34	3.585
		tap	40			
wood5050	wood samples wooden measuring pole	5050	40	yes	1	412
wood7525	wood samples wooden measuring pole	7525	40	yes	8	465
woodsamples	wood sample A	dry	-	no	35	471
	wood sample B					
	wood sample C					
	wood sample D					
woodschie	wood samples wooden measuring pole	Schie	40	yes	5	417
					175	7.240

resolution	highest	custom
range [m]	100	4
horizontal [m]	0,02	0,001
vertical [m]	0,02	0,001

scanner geometry			
height [m]	horizontal distance [m]	minimal range [m]	maximal range [m]
1,748	1,23	2,47	4

quadrant	width [m]	length [m]	area [m ²]
q1	0,455	0,7	0,3185
q2	0,455	0,7	0,3185
q3	0,455	0,5	0,2275
q4	0,455	0,5	0,2275

Appendix C Software, tools and scripts

The software, software tools and scripts that were used in this graduation work are gathered together in this appendix.

C.1 List of software

The software that has been used in this thesis is listed alphabetically below.

CloudCompare	version 2.5.4 © EDF R&D / TELECOM ParisTech (ENST-TSI)
CloudCompare viewer	version 1.30 © EDF R&D / TELECOM ParisTech (ENST-TSI)
Cyclone	version 9.0, © 2014, Leica Geosystems HDS
iWork	version iWork '09 © 2003–2010 Apple Inc.
MATLAB	version R2012b (8.0.0), © 1984-2012 The MathWorks, Inc
Microsoft Office	version 2008 © 2007 Microsoft Corporation
Paintbrush	version 2.1.2 © 2007-2015 Soggy Waffles
TeXworks	version 0.4.4, © 2007-2012, Jonathan Kew, Stefan Löffler, Charlie Sharpsteen

C.2 List of CloudCompare tools

All of the tools and windows that were used in CloudCompare during the processing are listed in the table below. There exist many more tools, which descriptions can be found in the CloudCompare user manual [8].

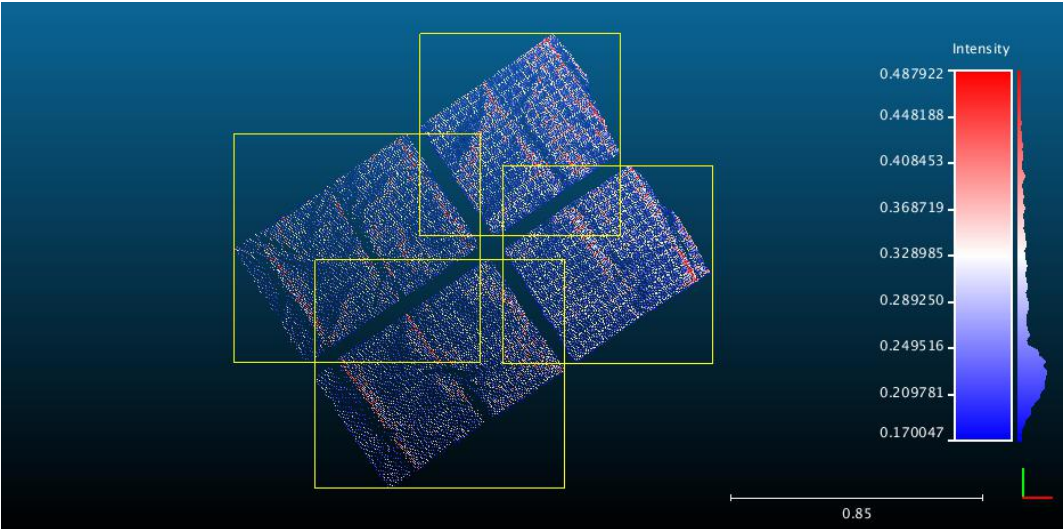
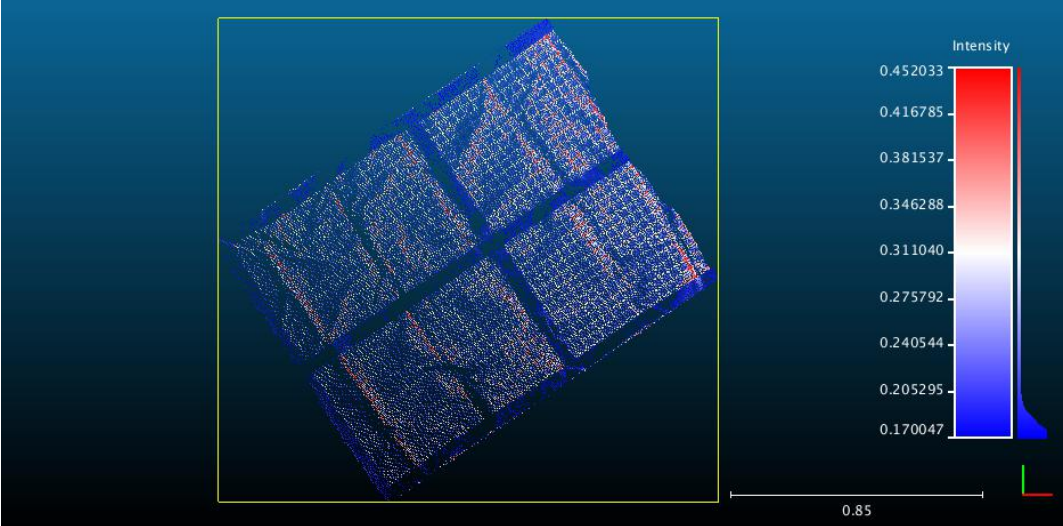
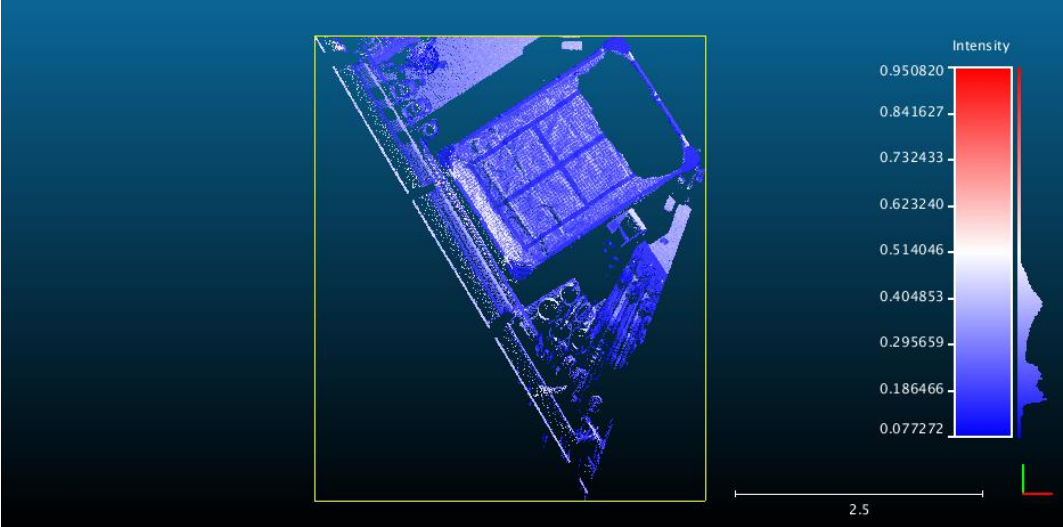
location (in menu bar)	description
File → Open	opens file: .ptx .bin .txt and many other formats
File → Save	save selected cloud/viewport; choice of format
Edit → Clone	clones selected cloud
Edit → Segment	segmentation cloud: polygonal selection, segment in/out, confirm
Edit → Scalar fields → Show histogram	shows histogram of selected cloud
Edit → Scalar fields → Filter by Value	filters range (min to max) of (intensity) values from scale
Tools → Density → Accurate	density: at a given scale
Tools → Density → Approximate	density: distance to nearest neighbor
Tools → Other → Roughness	computes the surface roughness, given the Kernel size
Tools → Distances → Closest point set	gives the closest points between reference and compared cloud
Display → Render to File	saves the viewed point cloud including scales as image (e.g. .jpeg)
Display → Save viewport as object	saves current 3D view; viewport can be loaded in other sessions
DB tree window	overview of all clouds and viewports
Properties window	properties: object, cloud, scalar field (intensity/RGB), color scale
Console window	shows all modifications (black text), including errors (red text)
3D View window	displays current 3D point cloud view

Overview of used tools and windows in CloudCompare

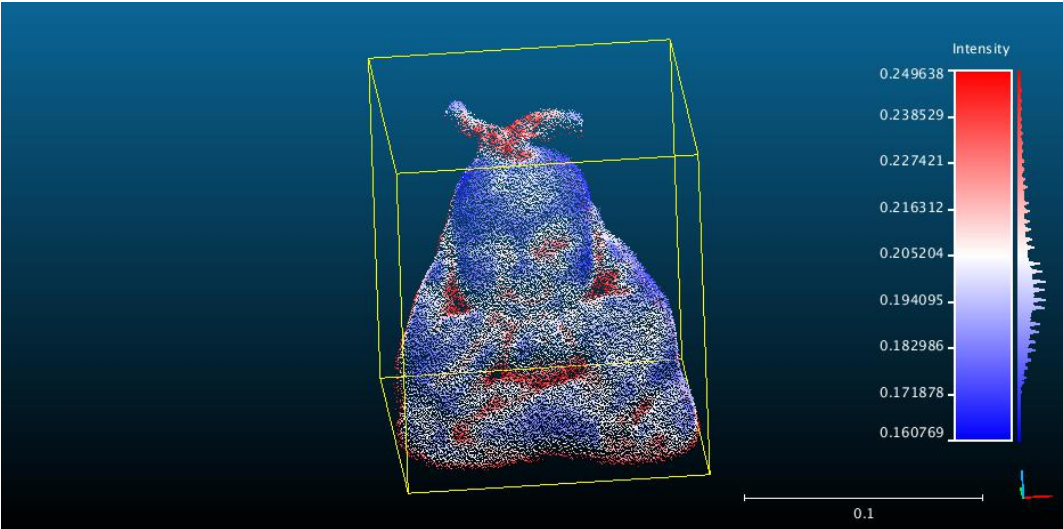
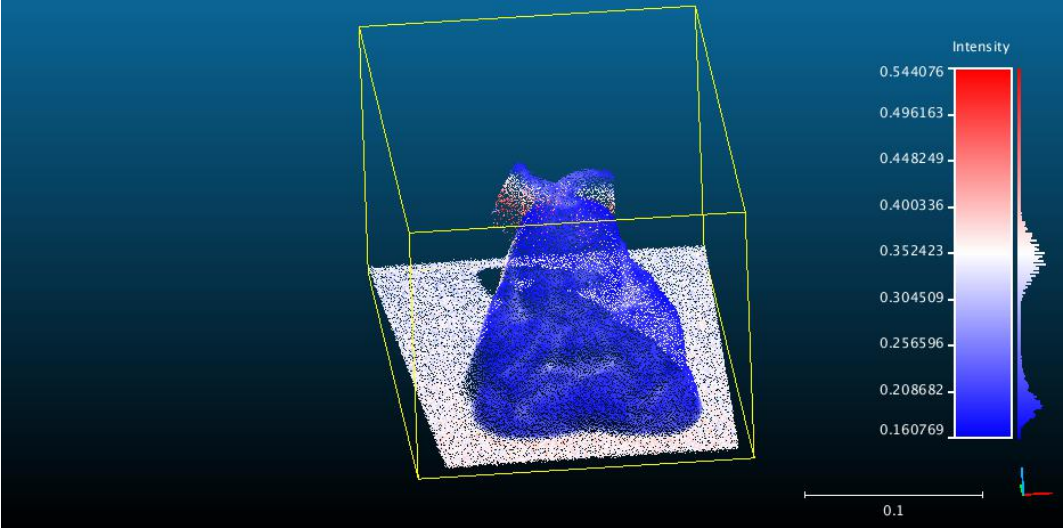
C.3 Process of filtering and segmentation in CloudCompare

Most of the point clouds have been segmented and/or filtered using CloudCompare. The segmentation and filtering are necessary as it reduces the size of the point cloud, leaves out unwanted points and separates the scan target from the surroundings. When filtering by value, the values to be filtered are the intensity or other value that is computed (for example the roughness). Segmentation is done manually: the desired target can be selected within a polygon. In some case, first filtering and then segmentation are applied to obtain the separate scan target.

The steps of the segmentation will be displayed in the figures below. The segmentation is that of the dry scans of the pool, where the four quadrants were selected using segmentation.



An example of filtering by value is given in the two figures below, where the dry scanned point cloud of the buddha sculpture is being filtered. It should be noted that filtering by value is only possible if the scan target has a distinct other colour and thus intensity, than the surroundings. If not, data will be lost in the scan target during filtering, which is undesirable. Note that the colour bar with the intensities will modify its range automatically after filtering.



C.4 Matlab script: correction for refraction

The following script provides the correction for refraction that has been applied to the wet data sets. An example of this correction is given in figure 4.32 for the wooden measuring pole.

```
%% thesis
clear all
close all; clc

%% load clouds [X Y Z R G B Intensity Nx Ny Nz]
% wet clouds
cloud1=load('cloud1.txt');
cloud2=load('cloud2.txt');

%% select data [X Y Z]
c1=cloud1(:,1:3);
c2=cloud2(:,1:3);

%% define waterdepth [m]
d=[0.4; 0.4]; % water depth
minz=[min(c1(:,3)); min(c2(:,3))]; % z location bottom (minimum or set it)
zw=minz+d; % z coordinate water surface

%% cartesian to cylindrical coordinate system
[theta1,rho1,z1]=cart2pol(c1(:,1),c1(:,2),c1(:,3));
[theta2,rho2,z2]=cart2pol(c2(:,1),c2(:,2),c2(:,3));

%% refractive indices
nw=1.335; % refractive index water
na=1.0002782; % refractive index air
n=nw/na;

%% correction for refraction
% angles
alpha1=atan((rho1./z1));
alpha2=atan((rho2./z2));
beta1=asin(sin(alpha1)/n);
beta2=asin(sin(alpha2)/n);

% rho water
rhow1=zw(1)*tan(alpha1);
rhow2=zw(2)*tan(alpha2);

% corrected points: rhor and zr
rhor1=((rho1-rhow1)/(n^2))+rhow1;
rhor2=((rho2-rhow2)/(n^2))+rhow2;
zr1=((cos(beta1).*(rho1-rhow1))./(n*sin(alpha1)))+zw(1);
zr2=((cos(beta2).*(rho2-rhow2))./(n*sin(alpha2)))+zw(2);

%% cylindrical to cartesian coordinate system (under water part only)
[x1,y1]=pol2cart(theta1,rhor1);
[x2,y2]=pol2cart(theta2,rhor2);

%% output corrected clouds [X Y Z i]
cloud1c=[x1 y1 zr1 cloud1(:,7)];
cloud2c=[x2 y2 zr2 cloud2(:,7)];

%% write corrected clouds to .txt file [X Y Z Intensity]
dlmwrite('cloud1c.txt',cloud1c, 'delimiter', '\t', 'precision', '%.4f')
dlmwrite('cloud2c.txt',cloud2c, 'delimiter', '\t', 'precision', '%.4f')
```

C.4 Matlab script: power of the return signal

```
%% thesis
% power of the return signal - spectrophotometry

clear all
close all
clc

%% load clouds sand [X Y Z Intensity], corrected for refraction and segmented only sand
cloud4=load('sand.cloud4cwqs.txt'); % d=20cm
cloud6=load('sand.cloud6cwqs.txt'); % d=10cm
cloud7=load('sand.cloud7cqs.txt'); % d=5cm

%% load cloud pole [X Y Z Intensity], corrected for refraction, wet part onlu
cloudp=load('pole40wet.txt'); % d=40cm

%% load cloud buddha [X Y Z Intensity], corrected for refraction
cloudb=load('buddha.cloud4ci.txt'); % d=40cm

%% load cloud water plants [X Y Z Intensity], corrected for refraction
% tap water NTU=0.3, d=40cm
cloudAt=load('waterplants.Allcs.txt');
cloudEt=load('waterplants.E5cs.txt');
% mixture water NTU=1.3, d=40cm
cloudAm=load('waterplants7525_A9cs.txt');
cloudEm=load('waterplants7525_E6cs.txt');

%% define waterdepth [m]
d=[0.2; 0.1; 0.05; 0.4; 0.4; 0.4]; % water depth [m]
minz=[min(cloud4(:,3)); min(cloud6(:,3));...
      min(cloud7(:,3)); -1.75; min(cloudb(:,3)); -1.75]; % z location bottom
zw=minz+d; % z coordinate water surface

% range in water Rw
[theta4, rho4, z4]=cart2pol(cloud4(:,1), cloud4(:,2), cloud4(:,3));
[theta6, rho6, z6]=cart2pol(cloud6(:,1), cloud6(:,2), cloud6(:,3));
[theta7, rho7, z7]=cart2pol(cloud7(:,1), cloud7(:,2), cloud7(:,3));
[thetap, rhop, zp]=cart2pol(cloudp(:,1), cloudp(:,2), cloudp(:,3));
[thetab, rhob, zb]=cart2pol(cloudb(:,1), cloudb(:,2), cloudb(:,3));
[thetaAt, rhoAt, zAt]=cart2pol(cloudAt(:,1), cloudAt(:,2), cloudAt(:,3));
[thetaEt, rhoEt, zEt]=cart2pol(cloudEt(:,1), cloudEt(:,2), cloudEt(:,3));
[thetaAm, rhoAm, zAm]=cart2pol(cloudAm(:,1), cloudAm(:,2), cloudAm(:,3));
[thetaEm, rhoEm, zEm]=cart2pol(cloudEm(:,1), cloudEm(:,2), cloudEm(:,3));

alpha4=atan((rho4./z4));
alpha6=atan((rho6./z6));
alpha7=atan((rho7./z7));
alphap=atan((rhop./zp));
alphab=atan((rhob./zb));
alphaAt=atan((rhoAt./zAt));
alphaEt=atan((rhoEt./zEt));
alphaAm=atan((rhoAm./zAm));
alphaEm=atan((rhoEm./zEm));

rhow4=zw(1)*tan(alpha4);
rhow6=zw(2)*tan(alpha6);
rhow7=zw(3)*tan(alpha7);
rhowp=zw(4)*tan(alphap);
rhowb=zw(5)*tan(alphab);
rhowAt=zw(6)*tan(alphaAt);
rhowEt=zw(6)*tan(alphaEt);
rhowAm=zw(6)*tan(alphaAm);
rhowEm=zw(6)*tan(alphaEm);

% locations water surface
[x4, y4]=pol2cart(theta4, rhow4);
[x6, y6]=pol2cart(theta6, rhow6);
[x7, y7]=pol2cart(theta7, rhow7);
```

```

[xp, yp]=pol2cart (thetap, rhowp);
[xb, yb]=pol2cart (thetab, rhowb);
[xAt, yAt]=pol2cart (thetaAt, rhowAt);
[xEt, yEt]=pol2cart (thetaEt, rhowEt);
[xAm, yAm]=pol2cart (thetaAm, rhowAm);
[xEm, yEm]=pol2cart (thetaEm, rhowEm);

% range in water
Rw4=sqrt ((cloud4(:,1)-x4).^2+(cloud4(:,2)-y4).^2+(cloud4(:,3)-zw(1)).^2);
Rw6=sqrt ((cloud6(:,1)-x6).^2+(cloud6(:,2)-y6).^2+(cloud6(:,3)-zw(2)).^2);
Rw7=sqrt ((cloud7(:,1)-x7).^2+(cloud7(:,2)-y7).^2+(cloud7(:,3)-zw(3)).^2);
Rwp=sqrt ((cloudp(:,1)-xp).^2+(cloudp(:,2)-yp).^2+(cloudp(:,3)-zw(4)).^2);
Rwb=sqrt ((cloudb(:,1)-xb).^2+(cloudb(:,2)-yb).^2+(cloudb(:,3)-zw(5)).^2);
RwAt=sqrt ((cloudAt(:,1)-xAt).^2+(cloudAt(:,2)-yAt).^2+(cloudAt(:,3)-zw(6)).^2);
RwEt=sqrt ((cloudEt(:,1)-xEt).^2+(cloudEt(:,2)-yEt).^2+(cloudEt(:,3)-zw(6)).^2);
RwAm=sqrt ((cloudAm(:,1)-xAm).^2+(cloudAm(:,2)-yAm).^2+(cloudAm(:,3)-zw(6)).^2);
RwEm=sqrt ((cloudEm(:,1)-xEm).^2+(cloudEm(:,2)-yEm).^2+(cloudEm(:,3)-zw(6)).^2);

%% set parameters
nw=1.335; % refractive index water
na=1.0002782; % refractive index air

NTU=[0.3 1.3 1.4 2.0]; % turbidity [NTU]
uwater=0.0881*NTU+0.448; % attenuation coefficient water [m^-1]

rsand=0.19; % reflectance sand
rbark=0.11; % reflectance bark (wood samples)
rconcrete=0.21; % reflectance concrete
rfoliage=0.18; % reflectance foliage

%% losses (reflectance and absorptions/scattering) power (transmittance)
losssurface=((nw-na)/(nw+na))^2; % reflectance at surface
Pairtewater=1-losssurface;
Twater=exp(-uwater(2)*b); % transmittance
Pattarget=Pairtewater*Twater;

%% Power and transmittance for datasets
% sand cloud4, depth=20cm
Twater4=exp(-uwater(2)*Rw4);
Pattarget4=Pairtewater*Twater4;
Pfromtarget4=Pattarget4*rsand;
Pback4=Pfromtarget4.*Twater4-losssurface;

% sand cloud6, depth=10cm
Twater6=exp(-uwater(2)*Rw6);
Pattarget6=Pairtewater*Twater6;
Pfromtarget6=Pattarget6*rsand;
Pback6=Pfromtarget6.*Twater6-losssurface;

% sand cloud7, depth=5cm
Twater7=exp(-uwater(2)*Rw7);
Pattarget7=Pairtewater*Twater7;
Pfromtarget7=Pattarget7*rsand;
Pback7=Pfromtarget7.*Twater7-losssurface;

muP=[mean(Pback4) mean(Pback6) mean(Pback7)];
stdP=[std(Pback4) std(Pback6) std(Pback7)];

% pole cloudp, depth=40cm
Twaterp=exp(-uwater(2)*Rwp);
Pattargetp=Pairtewater*Twaterp;
Pfromtargetp=Pattargetp*rbark;
Pbackp=Pfromtargetp.*Twaterp-losssurface;

% buddha cloudb, depth=40cm
Twaterb=exp(-uwater(2)*Rwb);
Pattargetb=Pairtewater*Twaterb;
Pfromtargetb=Pattargetb*rconcrete;
Pbackb=Pfromtargetb.*Twaterb-losssurface;

```

```

% water plants cloud: At Et Am Em, depth=40cm
TwaterAt=exp(-uwater(1)*RwAt);
PattargetAt=Pairtewater*TwaterAt;
PfromtargetAt=PattargetAt*rfoilage;
PbackAt=PfromtargetAt.*TwaterAt-losssurface;

TwaterEt=exp(-uwater(1)*RwEt);
PattargetEt=Pairtewater*TwaterEt;
PfromtargetEt=PattargetEt*rfoilage;
PbackEt=PfromtargetEt.*TwaterEt-losssurface;

TwaterAm=exp(-uwater(2)*RwAm);
PattargetAm=Pairtewater*TwaterAm;
PfromtargetAm=PattargetAm*rfoilage;
PbackAm=PfromtargetAm.*TwaterAm-losssurface;

TwaterEm=exp(-uwater(2)*RwEm);
PattargetEm=Pairtewater*TwaterEm;
PfromtargetEm=PattargetEm*rfoilage;
PbackEm=PfromtargetEm.*TwaterEm-losssurface;

%% RMSE
% cloud4, depth=20cm
e4=cloud4(:,4)-Pback4;      % residuals
N4=length(e4);             % number of measurements
RMSE4=sqrt((sum(e4.^2)/N4));

% cloud6, depth=10cm
e6=cloud6(:,4)-Pback6;      % residuals
N6=length(e6);             % number of measurements
RMSE6=sqrt((sum(e6.^2)/N6));

% cloud7, depth=5cm
e7=cloud7(:,4)-Pback7;      % residuals
N7=length(e7);             % number of measurements
RMSE7=sqrt((sum(e7.^2)/N7));

RMSE=[RMSE4 RMSE6 RMSE7];

% cloudb, depth=40cm
eb=cloudb(:,4)-Pbackb;      % residuals
Nb=length(eb);             % number of measurements
RMSEb=sqrt((sum(eb.^2)/Nb));

% cloudp, depth=40cm
ep=cloudp(:,4)-Pbackp;      % residuals
Np=length(ep);             % number of measurements
RMSEp=sqrt((sum(ep.^2)/Np));

% water plants
eAt=cloudAt(:,4)-PbackAt;    % residuals
NAt=length(eAt);           % number of measurements
RMSEAt=sqrt((sum(eAt.^2)/NAt));
eEt=cloudEt(:,4)-PbackEt;    % residuals
NEt=length(eEt);           % number of measurements
RMSEEt=sqrt((sum(eEt.^2)/NEt));
eAm=cloudAm(:,4)-PbackAm;    % residuals
NAm=length(eAm);           % number of measurements
RMSEAm=sqrt((sum(eAm.^2)/NAm));
eEm=cloudEm(:,4)-PbackEm;    % residuals
NEm=length(eEm);           % number of measurements
RMSEEm=sqrt((sum(eEm.^2)/NEm));

%% plotting

```

C.6 Matlab function "allfitdist" by Mike Sheppard from Matlab site

The function "allfitdist" can be obtained from the Mathworks file exchange site. The function is created by Mike Sheppard in 2012. It can be accessed from the following link:

<https://nl.mathworks.com/matlabcentral/fileexchange/34943-fit-all-valid-parametric-probability-distributions-to-data/content/allfitdist.m>

The function fits all valid parametric probability distributions to a provided data set. The function has been used to determine which distribution fits best to a data set containing the residuals. The input into function "allfitdist" are the residuals of the computed return signal power and recorded intensity as described in section 4.5.

```
[D PD]=allfitdist(e7, 'PDF')
```

The output of the function gives the distribution that fits best, which in this case is the "tlocation-scale", together with a plot showing the data and the fitted distributions in a probability density plot.

```
D(1)
```

```
ans =
```

```
DistName: 'tlocation-scale'  
NLogL: -1.0748e+06  
BIC: -2.1496e+06  
AIC: -2.1496e+06  
AICc: -2.1496e+06  
ParamNames: {'mu' 'sigma' 'nu'}  
ParamDescription: {'location' 'scale' 'degrees of freedom'}  
Params: [0.0033 0.0059 4.7656]  
Paramci: [2x3 double]  
ParamCov: [3x3 double]  
Support: [1x1 struct]
```

